# CONTENTS — S through Y

**IMPLICATIONS OF $^{26}$Al IN NEBULAR DUST: THE FORMATION OF CHONDRULES BY THE DISRUPTION OF MOLTEN PLANETESIMALS** I. S. Sanders[1] and G. J. Taylor[2], [1]Dept. of Geology, Trinity College, Dublin 2, Ireland (isanders@tcd.ie), [2]Institute of Geophysics and Planetology, University of Hawaii, 2525 Correa Rd, Honolulu HI 96822, USA (gjtaylor@higp.hawaii.edu).

**Introduction:** We explore the idea that chondrules may be frozen droplets of 'splash-ejecta' from collisions between molten planetesimals. Note that in this model impact melting is *not* an issue. Melting had already occurred prior to impact due to radioactive meltdown. Impact served only to disperse existing melt as droplets

**Energy budget and melting:** 4567 Myr ago $^{26}$Al/$^{27}$Al was uniformly 5 $10^{-5}$ in the nebular dust that fed the meteorite parent bodies. This is known because the different initial $^{26}$Al/$^{27}$Al values for various chondrite components (CAIs, chondrules, mineral grains) agree with the Pb-Pb ages of these objects [1]. At that time (t = 0) $^{26}$Al accounted for about 9 kJ of energy per gram of *dry* primitive (nebular) dust. (The decay energy of $^{26}$Al is 4 MeV per atom, and dry dust had about 1.3% by weight of Al.) A further 1.5 kJ/g was probably stored in $^{60}$Fe. Thus >10 kJ/g was available for heating. A mere 1.6 kJ/g is needed to heat cold dust to melting at 1725K. (1725K is roughly the temperature at which the partial melt becomes capable of flow.) Therefore, the insulated interiors of planetesimals that accreted from cold dry dust during the first 2.5 Myr would have melted (Fig. 1). Thermal modeling [2] shows that a planetesimal radius >30 or 40 km will provide enough insulation for substantial melting (Fig 2). Planetesimals with a radius <5 km could never melt.

With accretion at t = 0, meltdown would have occurred by 0.2 Myr. Any planetesimal accreting before about 1.5 Myr would have had abundant 'superheat', well in excess of that needed to cause melting (Fig. 1). This excess energy probably led to turbulent convection in the melt, and caused the volume fraction of melt to increase, leaving a thin shell of solid crust with a high thermal gradient. The inevitable collisions, at low encounter velocity, between these thin-skinned molten orbs during the first 2 or 3 Myr would have produced copious volumes of chondrule spray, and would explain the high efficiency of chondrule production.

**Chondrule ages:** Most chondrules date from between 1.5 and 2.5 Myr after t = 0 [3], yet the model implies that chondrules were made from 0.2 Myr onwards. Why are chondrules older than 1.5 Myr so rare? It seems that chondrules which formed before 1.5 Myr had a poor survival rate. Most would have been destroyed; they would have accreted to planetesimals that were still sufficiently radioactive to melt (Fig. 1). A few older chondrules do exist. A 0.2 Myr chondrule was recently reported from Allende [4]. After 2.5 Myr, with the heat source largely spent, all planetesimals would be cooling fast and acquiring thick, strong outer crusts that only high velocity impacts could disrupt. Chondrules from Gujba are younger than 2.5 Myr. They formed at about 4 Myr, presumably due to a major impact [5].

Chondrite parent bodies obviously accreted after the youngest chondrules within them, i.e. generally after about 2.5 Myr. This age corresponds well with the latest time for melting (Figs 1 and 2). An important, counter-intuitive and widely overlooked implication is that the parent bodies of iron meteorites and other 'igneous' meteorites accreted *before* primitive meteorite parent bodies accreted.

**Chemistry of the melt:** One problem with the model is that the amount of melting would presumably have varied [6]. Melts with igneous compositions, ranging from basaltic to ultrabasic (primitive), might be expected. These are not seen in chondrules. Instead, chondrules mostly have olivine-rich to pyroxene-rich compositions with primitive unfractionated trace elements. Perhaps rapid heating outstripped early separation of partial melt and led to near-total (i.e. unfractionated primitive) melt. This would account for olivine-rich melt compositions. The origin of pyroxene-rich compositions is less clear. Some pyroxene rich types may be linked to olivine crystal settling once convection waned. Pyroxene-rich chondrules do tend to be younger that the others [7]. However, evaporation of melt droplets may also have changed the chemistry. Gravitational separation of metal did occur, and splashing after some metal segregation (possibly around 2 Myr) may explain why some chondritic meteorites, especially the L and LL groups, are short of iron and related (siderophile) elements. We note incidentally that nearly identical $^{182}$W anomalies in iron meteorites and chondritic metal [8] imply that planetesimal disruption and core separation would have occurred at about the same time.

Another problem with the model is that some chondrules are intimate mixtures of metal and silicate [6], so how did these phases get so thoroughly re-mixed on disruption? Perhaps turbulent convection was so vigorous that the whole molten interior was,

for a while, an emulsion of tiny molten metal droplets suspended in molten silicate.

**Textures of chondrules:** Many textural features of chondrules can readily be reconciled with the kind of processes that might occur in a post-impact plume of droplets. Igneous textures imply that chondrule cooling lasted over a period of a few hours, consistent with mutual irradiation of numerous incandescent droplets within an enormous cloud. Occasional cm-sized chondrules would simply be large blobs of melt. An abundance of damaged chondrules would reflect a combination of collision damage in the plume and re-launching of regolith-damaged chondrules from the near-surface zone of the molten planetesimal. Lofted regolith dust might be the source of the fine-grained rims seen on many chondrules. So-called relict grains in chondrules might simply be grains of mineral dust that became wetted and engulfed by the molten droplets. Sintered dust-clumps might be fragments from a deeper level in the planetesimal crust where the temperature was appropriately high. Compound chondrules reflect a high number density of droplets, consistent with a cloud of silicate spray. Near-liquidus temperatures inferred from chondrule textures are consistent with melt temperatures buffered by convection.

**Volatile elements in chondrites:** In some chondrites a complementary relationship exists between volatile-poor chondrules and volatile-rich surroundings (matrix), such that together the average composition is solar (primitive) [9]. Could this elemental separation have resulted from chondrule evaporation in the cloud? Perhaps the vapour condensed during cooling onto the interspersed dust grains that later became the chondrule matrix? Heating of the parent body would then account for volatile-enriched chondrule margins [10]. Also with each disruption event, there would be a net loss of volatile elements to space. Could this account for the varying degrees of volatile depletion in chondritic meteorites?

**Unresolved issues:** The impact splashing model raises new questions and leaves others unanswered. For example, how does it explain the survival of CAIs and pre-solar grains if planetesimal meltdown was so widespread during the first 2 Myr? What can it say about the general lack of mixing between the main chondrite classes? What bearing does it have on the ratios of oxygen isotopes in meteorites? How is size sorting explained? Were all chondrules produced by impact splashing? Were some produced by impact melting or by fire fountaining as has been shown for spherules on the Moon?

**Conclusions:** We have shown that chronological, chemical and textural aspects of chondrules are compatible with an origin for chondrules in the splashing of molten planetesimals, heated by $^{26}$Al and $^{60}$Fe. The model does not yet explain everything about chondrules, but it shows sufficient promise to merit further investigation. In particular the critical transition from of turbulent convection to segregation of metal and olivine invites more detailed analysis.

**References:** [1] Zinner E. et al. (2002) *LPS XXXIII,* Abstract #1204. [2] Woolum D. S. and Cassen P. (1999) *Meteorit. Planet. Sci. 34*, 897–907. [3] Huss G. R. et al. (2001) *Meteorit. Planet. Sci. 36*, 975–997. [4] Lundgaard et al. (2004) *Meteorit. Planet. Sci. 39,* A60. [5] Krot et al. (2004) *Meteorit. Planet. Sci. 39,* A56. [6] Taylor G. J. and Scott E. R. D. *Meteorit. Planet. Sci. 36,* A204. [7] Mostefaoui S. et al. (2002) *Meteorit. Planet. Sci. 37*, 421–438. [8] Halliday A. N. et al. (2001) *Phil. Trans. R. Soc. Lond. A 359*, 2111-2135. [9] Palme H. and Klerner S. (2000) *Meteorit. Planet. Sci. 35*, A124. [10] Nagahara H. et al. (1999) *LPS XXX* Abstract #1342.

**Fig. 1. Al-26 and Fe-60 energy decline in dry primitive dust**

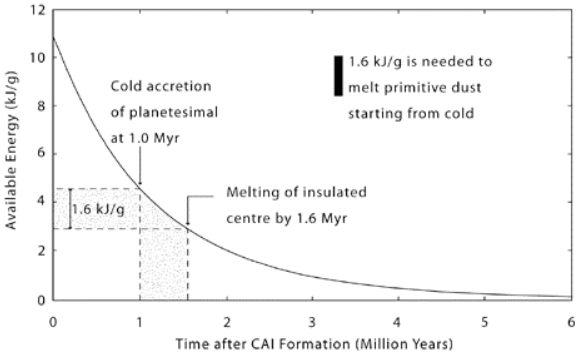


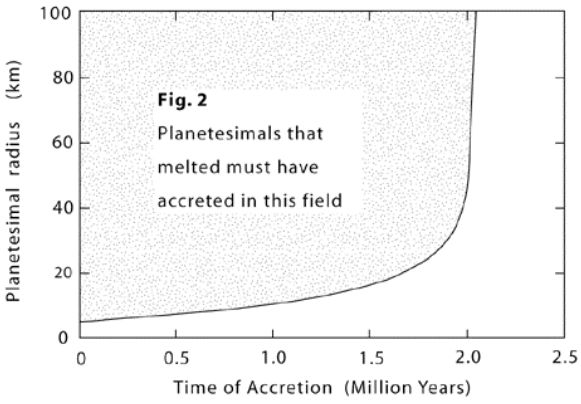

**HIGHLY FRACTIONATED MATERIALS FROM THE INNER SOLAR SYSTEM: EVIDENCE FROM THE EARTH.** G. Schmidt[1,2,3], [1]Institut für Kernchemie, University Mainz, D-55128 Mainz, Germany, gerhard.schmidt@uni-mainz.de, [2]HGF Virtuelles Institut für Struktur der Kerne und Nukleare Astrophysik; http://www.vistars.de, [3]Max Planck Institut für Chemie, Department of Cosmochemistry, D-55020 Mainz, Germany.

**Introduction:** Cosmochemical constraints for the material of planetary processes can be obtained from large samples of the Earth's mantle characterized by a mean Ca/Al atomic ratio of 1.18 ± 0.09 $\sigma_M$ and a mean Ca/Si atomic ratio of 0.10 ± 0.01 $\sigma_M$ [1] overlapping with a mean Ca/Al of 1.069 ± 0.044 $\sigma_M$ and a mean Ca/Si of 0.081 ± 0.023 $\sigma_M$ found in chondrites [2]. The relative abundances of the highly siderophile elements (HSE = Os, Ir, Ru, Rh, Pt, Pd) in pristine lherzolites differ from solar abundance ratios and are several orders of magnitude higher than predicted for equilibrium distribution between metal and silicate (core-mantle). The modest levels of depletion of HSE in the Earth's mantle, their greatly variable partition coefficients, the weak dependence on temperature and the experimentally determined independence of pressure suggest that these elements were added to the accreting Earth by a late bombardment after core formation. Of particular interest for our understanding of the origin of the solar system and processes involved to form planetary bodies is the question of whether HSE are fractionated in the Earth's primitive mantle (PUM).

**Comparison of HSE ratios in Chondrites and PUM**

Distinguishing chondrite groups by refractory HSE-ratios (Os, Ir, Ru) is complex, since the data from different authors on the same chondrite group differ. For example, Kallemeyn and Wasson [3] measured in EH chondrites (N=12) a mean Os/Ir of 1.15 ± 0.07 $\sigma_M$ and a mean Ru/Ir of 1.64 ± 0.16 $\sigma_M$, about 8% higher ratios than those measured by Horan et al. [4]. These authors obtained a mean Os/Ir of 1.09 ± 0.01 $\sigma_M$ and a mean Ru/Ir of 1.52 ± 0.03 $\sigma_M$ on EH chondrites (N=5). On the other hand the compilation of data on eight groups of chondrites by Wasson and Kallemeyn [2] have a mean Ru/Ir ratio of 1.52 ± 0.06 $\sigma_M$ in comparison to a mean Ru/Ir ratio of 1.49 ± 0.10 $\sigma_M$ measured by Horan et al. [4] on 10 groups of chondrites (including the CR group).

Rhodium is not easily determined by INAA, thus the database for Rh is sparse. The Rh data for H, L and LL chondrites are those from McDonald et al. [5]. For the chondrite groups CR, CM, CO, EL, and EH, no Rh data exist.

The Pd/Ir ratio in chondrites and the terrestrial mantle show the largest variations in comparison to other HSE element ratios and is therefore a key issue. Horan et al. [4] obtained Pd/Ir ratios of 1.48 ± 0.18 (1σ) for enstatite chondrites. They noted that EH and EL chondrites also have resolvable Pd/Ir ratios: 1.62 ± 0.10 (N=5) and 1.32 ± 0.09 (N=4), respectively. These new data disagree with the older ones by Hertogen et al. [6]. The Pd/Ir ratio for the EH4 chondrite Adhi Kot from Hertogen et al. [6] is about 56% lower than that measured by Horan et al. [4]. Another problem in determining the HSE by ICP-MS in meteorites is that not all HSE have been measured on a single aliquot as a group and often the elements Rh and Au are missing.

Therefore, the comparison of the HSE pattern from different chondrite groups with the Earth's mantle needs a combination of data from different authors.

The Pd/Ir ratio of the Earth's mantle from this work (Pd/Ir: 2.03 ± 0.47) and others [7,8] show close relations to EH chondrites (EH4 Adhi Kot: Pd/Ir = 1.78) or LL chondrites (LL3 Semarkona: Pd/Ir = 1.46), although even more fractionated. The slightly higher Ru/Ir ratio of EH chondrites in comparison to LL chondrites would be closest to the mantle ratio.

However, the HSE systematics of upper mantle samples do not exactly resemble materials from our meteorite collections.

**Composition of the Late Accreted Material**

The CI-normalized abundance pattern shows decreasing solar system-normalized abundances with increasing condensation temperatures; the abundance of the moderately volatile element Pd is about 2x higher than those in the most refractory siderophiles Ir and Os (Fig. 1).

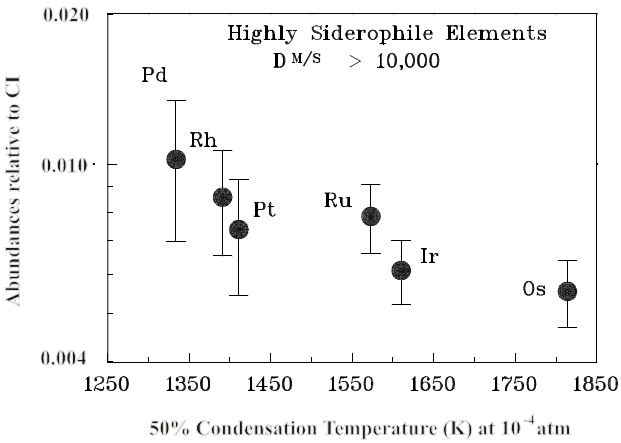


Fig. 1

The HSE systematics of upper mantle samples thus suggest that the late bombardment which added these elements to the accreting Earth resembles materials more closely to highly reduced EH chondrites than carbonaceous chondrites (Fig. 2).

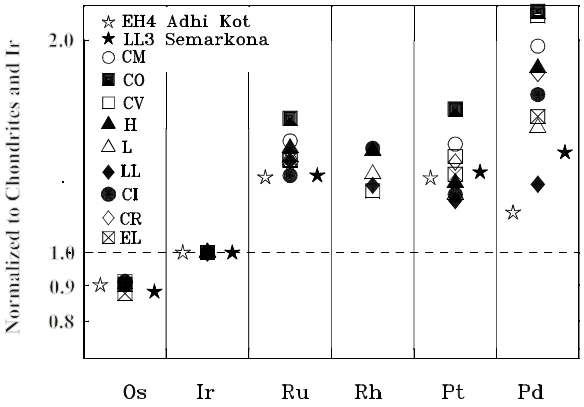


Fig. 2

In fact, the HSE in the Earth mantle are even more fractionated than the enstatite chondrites, an indication that some inner solar system materials were more highly fractionated than enstatite chondrites. An igneous process that can exactly mimic the detailed volatility element pattern as shown in Fig. 1 seems unlikely.

**Formation Location of the Late Veneer Material**

The carbonaceous, ordinary and enstatite chondrites exhibit successively greater degrees of reduction in combination with successively lower contents of refractory elements. Baedecker and Wasson [9] suggested that this is most likely associated with formation at successively smaller radial distances from the Sun in hotter portions of the solar nebula. Based (1) on the oxygen isotope composition that is close to that of the Earth and Moon (i.e., all lie on a single fractionation line) and (2) on the lower FeO and greater depletion of refractories than other meteorites and the Earth, Baedecker and Wasson [9], Clayton et al. [10] and Wasson and Wetherill [11] favored an enstatite formation location in the innermost solar system (perhaps even less than 1 AU from the Sun: possibly in the Mercury-Venus region).

This finding is also consistent with $^{53}$Mn-$^{53}$Cr isotopic systematics in enstatite chondrites and their formation in the inner zones of the solar nebula [12]. Based on the assumtion that the $^{53}$Cr excess of the enstatite chondrites and the observed gradient of radiogenic $^{53}$Cr between the earth-moon system, Mars, and the asteroid Vesta, is considered as a function of the heliocentric distance [12], the formation of the enstatite chondrites would fall at about 1.4 AU or somewhat closer to the Sun (i.e. >1.0-1.4 AU).

However, the HSE in the Earth mantle are even more fractionated than the enstatite chondrites, an indication that some inner solar system materials were more highly fractionated than EH or EL chondrites.

**Uncollected Primitive Planetary Materials?**

Obviously, our meteorite collections with all those different classes of chondrites do not represent the complete set of primitive planetary materials existing in the early solar system, from which the Earth was made. Compositional differences have been shown also for the influx of interplanetary materials onto the lunar surface [13] and the major categories of massive meteorites. Materials from formation regions closer to the sun (Mercury-Venus region), as it is supposed for enstatite chondrites, might be found in future on Earth, Moon or Mars.

**Conclusions**

The abundance distribution of the HSE in the Earth's mantle is remarkably uniform with increasing CI-normalized abundances, with decreasing 50% condensation temperatures. A possible interpretation is that the present upper-mantle noble-metal ratios could have been established in the solar nebula by fractionation processes that resulted in the loss of refractory components. From the HSE systematics it can be shown that none of the known chondrite groups match the mantle pattern excactly. Probably the best agreement of HSE pattern of the Earth's mantle with chondrites are EH chondrites, indicating a reduced environment very different from carbonaceous chondrites. The last material to contribute to the growing Earth is therefore likely to have been derived from the innermost solar system. This scenario is also compatible with inhomogeneous accretion models assuming impacts of large bodies (reducing component of 0.6 ± 0.1 % of the Earth mass [1]) in the late stages of the accretion of the Earth.

**References:** [1] Schmidt G. (2004) *Meteoritics & Planet. Sci.*, submitted. [2] Wasson J. T. and Kallemeyn G. W. (1988) *Phil. Trans. R. Soc. Lond. A 325*, 535-544. [3] Kallemeyn G. W. and Wasson J. T. (1986) *GCA, 50*, 2153-2164. [4] Horan M. et al. (2003) *Chem. Geol. 196*, 5-20. [5] McDonald I. et al. (2001) *GCA, 65*, 299-309. [6] Hertogen J. et al. (1983) *GCA, 47*, 2241-2255. [7] Pattou L. et al. (1996) *Nature 379*, 712-715. [8] Becker H. et al. (2004) *LPS XXXV*, Abstract #1310. [9] Baedecker P. A. and Wasson J. T. (1975) *GCA, 39*, 735-765. [10] Clayton R. N. et al. (1976) *EPSL, 30*, 10-18. [11] Wasson J. T. and Wetherill G. W. (1979) In *Asteroids* (ed. T. Gehrels), 926-974. [12] Shukolyukov A. and Lugmair G. W. (2004) *GCA 68*, 2875-2888. [13] Wasson J. T. et al. (1975) *The Moon 13*, 121-141.

**COSMOCHEMICAL FRACTIONATIONS AND / OR ASTROPHYSICAL EFFECTS IN PLANETARY MATERIALS?** G. Schmidt[1,2,3] and K.-L. Kratz[1,2], [1]Institut für Kernchemie, University Mainz, D-55099 Mainz, Germany, gerhard.schmidt@uni-mainz.de, [2]HGF Virtuelles Institut für Struktur der Kerne und Nukleare Astrophysik; http://www.vistars.de, [3]Max Planck Institut für Chemie, Department of Cosmochemistry, Mainz, D-55020 Mainz, Germany.

**Introduction**

Nucleosynthesis of the heavy elements (beyond Fe) occurs to about 50% each from the two classical neutron-capture processes, i.e. the s- and the r-process (see "$B^2FH$" [1]). As a result of the Galactic chemical evolution over more than 10 Gyr, our present solar-system isotopic and elemental abundance distribution ($N_o$) is a well defined composition of the above two nucleosynthesis processes ($N_o \approx N_{s,o} + N_{r,o}$). Deviations from this $N_o$ pattern may either have their origin in *cosmochemical* or in *astrophysical* effects. Of particular interest for our understanding of the origin of the solar system and the processes involved to form planetary bodies is the question of how the fractionation of the highly siderophile elements (Os, Ir, Ru, Rh, Pt, Pd) in the Earth can be explained.

**Cosmochemical fractionations**

Cosmochemical constraints for the material of planetary processes can be obtained from large samples of the Earth's mantle (see Fig. 1 in Schmidt [2], this volume). The abundance distribution of the highly siderophile elements (HSE) in the Earth's mantle is remarkably uniform with increasing CI-normalized abundances and decreasing 50% condensation temperatures [3]. A possible interpretation is that the present upper-mantle noble metal ratios could have been established in the pre-solar nebula by fractionation processes that resulted in the loss of refractory components. In fact, the HSE in the Earth's mantle are even more fractionated than the enstatite chondrites. This is an indication that some inner solar-system materials were more highly fractionated than enstatite chondrites. An igneous process that can exactly mimic the detailed volatility element pattern seems unlikely.

Based on the assumption that the observed gradient in the abundance of the radiogenic $^{53}Cr$ between planetary bodies is considered as a function of the heliocentric distance [4], the formation of the enstatite chondrites would fall at about 1.4 AU or somewhat closer to the Sun (i.e. >1.0-1.4 AU).

This finding is also consistent with carbonaceous, ordinary and enstatite chondrites exhibiting successively greater degrees of reduction in combination with successively lower contents of refractory elements. This is most likely associated with formation at successively smaller radial distances from the Sun in hotter portions of the solar nebula, as was discussed by Baedecker and Wasson [5]. These authors, as well as Clayton et al. [6] and Wasson and Wetherill [7] favored an enstatite formation location in the innermost solar system; perhaps even less than 1 AU from the Sun: possibly in the Mercury-Venus region.

However, the HSE in the Earth's mantle are even more fractionated than the enstatite chondrites, an indication that some inner solar-system materials were more highly fractionated than EH or EL chondrites.

The last material to contribute to the growing Earth is therefore assumed to have been derived from the innermost solar system.

**Astrophysical Effects**

Pre-solar grains found in primitive meteorites, e.g. silicon carbide, diamonds or CaAl-rich mineral phases, were very likely formed outside the solar system and probably before its birth, and may therefore provide a record of nuclear and chemical processes in stars and in the interstellar medium.

Today, nucleosynthetic enhancement of the one or other neutron-capture process from the early solar system is well known. For example, SiC grains show signatures of s-process enrichments [8] and CaAl-rich meteoritic inclusions (e.g. EK-1-4-1) show signatures of r-process enrichments [9].

**Present observation**

In Table 1, we compare our observed HSE/Ir ratios from the Earth with three different solar-system abundance evaluations [10-12]. Within the given uncertainties the measured element ratios for Os/Ir and Pd/Ir agree well with the recommended solar ratios $N(HSE/Ir)_o$ from Lodders [12]. The measured Pt/Ir ratio is about 30% higher than the mean solar ratio, but it has a large $1\sigma$ standard deviation. Considerable deviations from the solar ratios are, however, observed for Ru/Ir (about 32% lower) and Rh/Ir (about 25% lower). Also the Pd/Ir ratio seems to be slightly lower than solar (about 9%), but still agrees within the rather large $1\sigma$ uncertainty.

**Astrophysical fractionation?**

From the above observations, the question arises whether the non-solar HSE element ratios are correlated with different, non-solar s/r-mixtures? Measurable effects are, however, only expected for element ratios including Ru, Rh and Pd, since only the $N_o$ of these three elements have a sizeable s-process component of about 42%, 21% and 49%, respectively (see

Tab. 1, and Arlandini et al. [13]). The other HSE have only minor s-components between ~7% for Pt, ~11% for Os and 1% for Ir, respectively. Hence, taking Ir for the "element-ratios" is astrophysically justified, because Ir is de facto an "r-only" element [13]. An additional check can be made by regarding the ratio of the sum of the 3 "light" HSE (Ru, Rh and Pd, with a mean s-contribution of about 36%) to the sum of the 3 "heavy" HSE (Os, Ir and Pt, which are to 95% of r-origin).

The Ru/Ir and Rh/Ir ratios are below the solar ratio. This may indicate some r-process enhancement. The Pd/Ir ratio is consistent with the solar ratio within its large 1σ uncertainty. The "light" HSE to the "heavy" HSE ratio is again definitely below the solar ratio of about 1.385 [12] (Earth: 0.97).

In summary, evidence of under-solar yields of the "light" HSE would be astrophysically consistent with a slight enhancement of the $N_{r,o}$ component. On the other hand, one can definitely exclude any s-process enrichment since the "expected" HSE/Ir ratios would be about 6-times Os/Ir, Rh/Ir, and Pt/Ir and about 50-times Ru/Ir and Pd/Ir.

**Conclusions**

A consistent interpretation of possible combined cosmochemical and astrophysical effects of the origin of the observed non-solar HSE/Ir abundance ratios is still missing. It is common belief that a supernova has triggered the formation of our solar system. Primitive meteoritic material contributing to the growing Earth may therefore show non-homogenized isotopic and elemental signatures from this trigger event, e.g. an r-process enhancement. It is therefore the question if the pre-solar signatures of such late accreted material, in our case the HSE, have survived the cosmochemical fractionations, which occured in the solar system, and later the geochemical processing.

**References:** [1] Burbidge E. M. et al. (1957) *Rev. Mod. Phys. 29*, 547-650. [2] Schmidt G. (2004) *Workshop on Chondrites and the Protoplanetary Disk*, this volume. [3] Schmidt G. (2004) *Meteoritics & Planet. Sci.*, submitted. [4] Shukolyukov A. and Lugmair G. W. (2004) *GCA 68*, 2875-2888. [5] Baedecker P. A. and Wasson J. T. (1975) *GCA, 39*, 735-765. [6] Clayton R. N. et al. (1976) *EPSL, 30*, 10-18. [7] Wasson J. T. and Wetherill G. W. (1979) In *Asteroids* (ed. T. Gehrels), 926-974. [8] Hoppe P. and Ott U. (1997) In *Astrophysical Implications of the Laboratory Study of Presolar Materials*, AIP, 27-58. [9] Kratz K.-L. et al. (2001) In *Salting the Early Soup: Trace Nuclei from Stars to the Solar System*, Mem. S. A. It. V72-N.2, 453-466. [10] Anders E. and Grevesse N. (1989) *GCA, 53*, 197-214. [11] Palme H. and Beer H. (1993) In *Landolt-Börnstein, Numerical Data and Functional Relationships in Science and Technology* (ed. H. H. Voigt), 196-202. [12] Lodders K. (2003) *The Astrophysical J. 591*, 1220-1247. [13] Arlandini C. et al. (1999) *The Astrophysical J. 525*, 886-900. [14] Jochum K. P. (1996) *GCA, 60*, 3353-3357.

Tab. 1 Comparison of HSE/Ir ratios from the solar system, Earth and r- and s-Process.

| | A & G [10] | P & B [11] | Lo [12] | Sch [2] | | Arlandini et al. [13] | | | Remarks |
|---|---|---|---|---|---|---|---|---|---|
| | Solar | Solar | Solar | Earth | err. | r-Process[1] | r-Process[2] | s-Process[3] | % r |
| **Os/Ir** | 1.021 | 1.059 | 1.045 | 0.96 | 0.07 | 1.007 | 0.932 | 6.2 | 89 Os |
| **Ru/Ir** | 2.814 | 1.556 | 2.947 | 2.01 | 0.12 | 1.679 | 1.702 | 52.2 | 58 Ru |
| **Rh/Ir** | 0.520 | 0.305* | 0.575 | 0.43 | 0.09 | 0.449 | 0.456 | 5.6 | 79 Rh |
| **Pt/Ir** | 2.027 | 2.166 | 2.105 | 2.74 | 0.54 | 1.920 | 1.947 | 6.3 | 93 Pt |
| **Pd/Ir** | 2.103 | 1.211 | 2.225 | 2.03 | 0.47 | 1.687 | 1.130 | 49.6 | 51 Pd |
| **2./3. peak** | 1.343 | 0.727 | 1.385 | 0.97 | | 0.835 | 0.848 | 10.3 | 61 2. peak |

A & G [10] = Anders and Grevesse (1989)
P & B [11] = Palme and Beer (1993), *Rhodium value from Jochum [14]
Lo [12] = Lodders (2003)
Sch [2] = Schmidt (2004)
[1] = $N(El)_o$ (Anders and Grevesse [10]) / [(100* $N_{r,o}$ (Stell. Mod., Arlandini et al. [13]) / $N(El)_o$ (Anders and Grevesse [10])]
[2] Arlandini et al. (1999), Stellar Model
[3] Average $N_{s,o}$ ratios from the Stellar and Classical Model (Arlandini et al. [13])

**CHONDRITIC METEORITES AND THEIR COMPONENTS**. Edward R.D. Scott and Alexander N. Krot, Hawai'i Institute of Geophysics and Planetology, School of Ocean and Earth Science and Technology, University of Hawai'i, Honolulu, HI 96822, USA (escott@hawaii.edu).

**Chondrites:** Chondrites have bulk compositions close to that of the solar photosphere, neglecting highly volatile elements, and contain chondrules, which are igneous particles that cooled as isolated objects in minutes to hours. Chondrites are divided into 5 classes and 15 groups based on their bulk chemical and oxygen isotopic compositions: enstatite chondrites [abundant enstatite ($MgSiO_3$)] in the EH and EL groups; ordinary (i.e., common): H, L and LL; matrix-rich (CI, CM, CO, CV, CK, CR) and matrix-poor carbonaceous chondrites (CH and CB); and R and K chondrites. Each class is composed of components with distinctive mineralogy, and each group has characteristic proportions and/or sizes of components and comes from one or a few asteroids [1]. The components in chondrites provide an extraordinary record of events during the early evolution of the solar nebula into a disk of planetesimals. This record is preserved in the mineralogy, mineral textures, and chemical and isotopic compositions of the chondritic components.

**Chondritic Components**: Chondrites consist of matrix material surrounding diverse inclusions that formed at high temperatures (>1200 K): refractory inclusions, Al-rich (>10 wt% $Al_2O_3$) chondrules, Fe-Mg chondrules, and metallic Fe,Ni grains. Chondrules are composed largely of olivine ($Mg_{2-x}Fe_xSiO_4$ where $1<x<0$), pyroxene ($Mg_{1-x}Fe_xSiO_3$) and minor metallic Fe-Ni, and are 0.01-10 mm in size. Most chondrules are porphyritic (large crystals in a fine-grained matrix) and can be divided into magnesian ($x<0.05$; Type I) and ferrous ($x>0.05$, Type II). There are two types of refractory inclusions: Ca,Al-rich inclusions (*CAIs*), which are composed largely of Ca, Al, and Ti oxides, and amoeboid olivine aggregates (*AOAs*), which are composed of CAI nuggets surrounded by forsterite ($Mg_2SiO_4$). Matrix material is an aggregate of mineral grains, 10 nm - 5 μm in size that surrounds other components and fills in the interstices between them. Matrix is broadly chondritic in composition on the scale of micrometers, but very heterogeneous on smaller scales. It is made largely of forsterite and enstatite grains and grain aggregates that probably condensed and cooled rapidly like chondrules, and amorphous silicate particles that resemble amorphous rims on lunar regolith grains, which formed by vaporization and radiation damage. Matrix also contains metal-sulfide grains, refractory oxides, carbon-rich material, and a few parts per million of presolar silicate, carbide and oxide grains. Chondrites commonly contain mm-size fragments of early-formed chondritic material. In the outer part of the asteroid belt, water ice also accreted with chondritic components.

Chondritic interplanetary dust particles (*IDPs*), which probably accreted into comets at >5 AU, resemble unaltered matrix material, but are finer grained (sub-μm), and richer in presolar grains (% levels) [2,3] and carbonaceous material.

Except for the presolar grains and an unknown fraction of amorphous particles, all of the silicate, oxide, and metallic grains accreting in the solar system formed in transient high-temperature nebular events.

Most chondritic asteroids were aqueously altered, thermally metamorphosed, and melted, most likely by decay of short-lived radionuclides ($^{26}Al$ and $^{60}Fe$). Only a tiny fraction of chondrites resemble comets in having silicate minerals that were scarecely altered by parent body processing.

**Chemical and Isotopic Compositions of Chondrites and Their Components:** Chemical compositions of chondritic components reflect condensation and evaporation of solids and melts in the solar nebula due to localized and large-scale thermal variations. Chondrites and components are isotopically homogeneous except for (*i*) permil mass-independent variations in isotopic compositions of refractory elements like Ti and Mo that result from partial vaporization of presolar grains; (*ii*) isotopic variations due to decay of short-lived isotopes like $^{26}Al$, $^{60}Fe$ [4]; (*iii*) permil variations in isotopic compositions of Mg and Si in CAIs due to mass-dependent fractionation of isotopes during evaporation [5], and (*iv*) mass-independent O isotopic variations at percent or permil levels [6]. The short-lived isotopes were largely produced in a nearby evolved star, whereas the O isotopic variations probably result from self-shielding during UV photolysis of CO in an initially $^{16}O$-rich molecular cloud or in the nebula [7].

**Tentative Model:** The overall correlation between $^{207}Pb$-$^{206}Pb$ ages and inferred initial $^{26}Al/^{27}Al$ ratios in CAIs, chondrules [8-10], and metamorphic plagioclase in rapidly cooled ordinary (H4) chondrites [11] provides the basis for a chronology for chondrites [12]. Additional chronologic constraints come from O isotopes (as O isotopes in the gaseous nebula became progressively heavier with time), and from petrological inferences from compound objects and relict grains.

CAIs are the oldest solar system components: most CAIs and the closely related AOAs formed from condensates in a brief period of $<10^{4-5}$ years in a $^{16}O$-rich environment [13] with high ambient temperatures (>1100 K at $\sim10^{-5}$ atm). This event could have been triggered by the last major solar flare that vaporized

the innermost part of the disk. A few CAIs with larger stable isotopic anomalies (FUN and FUN-like) formed as evaporative residues in an earlier event, prior to the injection of radioactive isotopes from a nearby supernova. Some CAIs were subsequently melted in $^{16}$O-rich environments. Igneous and non-igneous CAIs developed outer layers of Al-diopside and forsterite ($Mg_2SiO_4$) on cooling. Some CAIs were heated later in $^{16}$O-poor environments during the next few Myr, some during chondrule formation [14].

Most chondrules formed a few Myr after CAIs in diverse $^{16}$O-poor environments at lower ambient temperatures, largely by repeated melting of aggregates and accretion of melt droplets and particles. Type I and Type II chondrules are typically surrounded respectively by magnesian and ferrous igneous silicate (coarse-grained) rims and appear to have formed in different environments [15]. Type I chondrules formed at higher ambient temperatures where ferrous silicates were not stable and reacted with the gas on cooling.

Most matrix materials vaporized and recondensed in an $^{16}$O-poor gaseous environment, probably during chondrule formation. Crystalline matrix silicates, which are largely magnesian, could have condensed at high ambient temperatures, in Type I chondrule-forming regions. Amorphous matrix silicates, which are largely ferrous, may have formed by disequilibrium condensation at low ambient temperatures and could represent the major precursor material for Type II chondrules.

Chondrule formation triggered chondrite accretion, probably by concentration of mm-sized particles between turbulent eddies. Ice-free chondritic asteroids >10 km in size that formed <2 Myr after CAI formation were melted by $^{26}$Al. Fragments of chondritic asteroids were mixed with chondrules, but impact-formed chondrules appear to be rare [cf. 12].

Some chondrites did not form this way. CB chondrules, which formed 4 Myr after CAI formation [9] and have cryptocrystalline and barred textures and unique compositions, appear to have formed in dust-free nebular environments as the first direct gas-liquid condensates in the solar nebula [16]. Associated S-poor and S-rich metal grains condensed as solids and melts respectively [17,18]. CB chondritic components, and a closely related fraction of CH material, formed from nebular gas created by high-speed impact of molten planetesimals [18] or complete vaporization of pre-existing solid particles [17]. Another late-forming chondrite with unique origins, Kaidun, accreted in a dust-poor nebula entirely from mm-sized chondritic fragments [19].

**Major Unresolved Cosmochemical Issues:** These include: *(i)* cause and location of transient heating events that produced CAIs, chondrules, and matrix; *(ii)* origin of short-lived radionuclides and detailed timescales of chondrule and CAI formation: duration of chondrule formation for a single chondrite group; *(iii)* location and timing of accretion of chondrite parent asteroids; *(iv)* understanding the diversity of chondrite groups; *(v)* role of planetesimals in chondrule formation; *(vi)* dynamics of solids in the protoplanetary disk; *(vii)* origin of oxygen isotopic variations; (viii) role of transient vs. global thermal processing in establishing compositions of components. Much progress has been made in the 10 years since the last chondrite workshop, and consensus on many issues is beginning to develop, But inevitably we need fresh synthesis of meteoritic and astronomical observations and astrophysical theories of star formation.

**Conclusions**: Chondrules, CAIs and most other components in chondrites formed by transient heating events at 1-3 AU in the disk during shock heating [20], or <0.1 AU near the protosun [21]. Chondritic components provide the best cosmochemical constraints on the life-time and evolution of the solar nebula and insights into disk evolution around solar-mass stars.

The evolution of a disk depends critically on the star's environment: in isolation in a low-mass region of a molecular cloud, or in a stellar cluster in a high-mass region like the Orion Nebula near a supernova [22]. The latter would better account for the existence of short-lived isotopes, UV photolysis of C$^{17}$O and C$^{18}$O, and the 7° difference between the solar and planetary angular momentum vectors. Disk evolution also depends on how and where Jupiter-sized planets form. Thus, understanding chondrule and CAI formation requires broad astronomical perspectives.

**References:** [1] Scott E.R.D. and Krot A.N. (2003) *Treatise on Geochemistry* (eds, H.D. Holland and K.K. Turekian) *1*, 143. Elsevier. [2] Messenger S. (2003) *Sciencem, 300*, 105. [3] Nguyen A.N., Zinner E. (2004) *MAPS, 39*, A77. [4] Goswami J. et al., this vol. [5] Davis A.M. et al., this vol. [6] McKeegan K.D. et al., this vol. [7] Yurimoto H., Kurimoto K. (2004) *Science*, in press. [8] Amelin Y. et al. (2002) *Science, 271,* 1545. [9] Amelin Y. et al. (2004) *GCA, 68,* A759. [10] Kita N. et al., this vol. [11] Zinner E. et al. (2002) *LPS XXXIII*, #1204. [12] Sanders I. (2004) *MAPS, 39,* A94. [13] Krot A.N. et al. (2002) *Science, 295,* 1051. [14] Krot A.N. et al. (2004) *MAPS, 39,* A56. [15] Connolly H.C., Desch S.J. (2004) *Chem. Erde, 64,* 95. [16] Krot A.N. et al. (2002) *MAPS, 37,* 1451. [17] Meibom A. et al. (2000) *Science, 288,* 839. [18] Campbell A.J. et al. (2002) *GCA, 66,* 647. [19] Scott E.R.D. (2002) In A*steroids III* (W. F. Bottke et al., eds.) 697. Univ. Ariz. [20] Alexander C.M.O'D. et al. (2001) *Science, 293,* 64. [21] Shu F. et al. (1996) *Science, 271,* 1545. [22] Hester J.J. et al. (2004) *Science, 304,* 1116.

**JET FLOWS: FORMATION AND THERMAL PROCESSING OF SOLIDS IN THE PROTOPLANETARY DISK.** F. H. Shu[1], H. Shang[2], and T. Lee[3], [1]National Tsing Hua University, [2]Academia Sinica, Institute of Astronomy and Astrophysics, [3]Academia Sinica, Institute of Earth Science

**Introduction:** We review the processes by which solids near the inner edge of the protoplanetary disk can be thermally processed and experience nuclear transformations by energetic radiation and particle events (diagnosed particularly by X-ray flares) associated with the launch of a magnetocentrifugally driven X-wind. The major advantages of such a picture are a single-source accounting for (1) the sizes, ages, and elemental compositions of CAIs and chondrules; (2) the coexistence of hydrated minerals and unprocessed presolar grains in the matrix of chondrites with the highly processed igneous components represented by CAIs and chondrules; (3) the overall loss of moderate volatiles from the inner solar nebula; (4) the level of remnant magnetism measured in chondrules; (5) a promising mechanistic explanation for the mass-independent fractionation of the oxygen isotopes in various cosmic materials; and (6) the live presence of several short-lived radioisotopes, particularly Be-10 and Be-7, in the early solar system. The theory predicts that thermally annealed (crystalline) dust grains and compact mm- to cm-sized solids should be sprayed over the entire solar system on a time scale (about a million years) characterized by gas accretion onto the central star. The major uncertainty in the model is whether refractory solids can survive by self-shielding at the inferred inner gas edges of protoplanetary disks.

**SPINEL-RICH SPHERULES FROM MURCHISON: A REVIEW AND SOME QUESTIONS.** S. B Simon[1] and L. Grossman[1,2]. [1]Dept. of the Geophysical Sci., 5734 S. Ellis Ave; [2]Enrico Fermi Inst., 5640 S. Ellis Ave., Univ. of Chicago, Chicago, IL 60637. (sbs8@midway.uchicago.edu)

**Introduction.** One way in which we investigate the origin of refractory inclusions is by performing equilibrium condensation calculations for a gas of solar composition and comparing the results to observed assemblages. Although many refractory inclusions have undergone melting, by definition they consist of phases predicted to condense at high temperatures from a gas of solar composition. Bulk compositions of the silicate-rich inclusions from CV3 chondrites, for example, generally follow trajectories of bulk condensate compositions, with an offset probably due to partial evaporative loss of Mg and Si [1]. Spinel-, hibonite-bearing spherules, a major type of inclusion common in CM2 chondrites, however, consist of assemblages of phases that are not predicted by thermodynamic calculations to coexist. Despite updates and additions to the data base over the years condensation calculations [e.g. 2-4] consistently show that melilite should condense after hibonite and before spinel. Spinel-hibonite-melilite inclusions can be found but they are rare. Hibonite-, spinel-bearing inclusions that are melilite-free or melilite-poor are much more abundant, and their origin has puzzled researchers for years. One way to reconcile the observed assemblages with the condensation calculations is if melilite originally present was lost due to evaporation of Ca, Si and Mg during heating of the precursors [5]. If evaporation occurred from partially molten inclusions, then they should be measurably enriched in the heavier isotopes of these elements. Previous studies of Ca [6] and Mg [7] isotopes in Murchison inclusions showed some positive mass-fractionations greater than analytical uncertainty and no large, negative fractionations, providing a hint that Ca and Mg evaporation did take place. We have undertaken a petrologic and ion probe study of a variety of spinel-bearing inclusions from Murchison to see if they are isotopically fractionated and if there are any correlations of isotopic composition with mineral assemblage.

**Petrography.** The first step in this study is a detailed, systematic petrographic classification of spinel-rich spherules. Also known as "blue spherules" [5] or SHIBs [6,7], spinel-rich refractory spherules from CM chondrites actually exhibit a variety of mineral assemblages and textures and should not all be grouped together. The 40 spherules or fragments thereof selected for this study are from Murchison and range from 50 to 200 μm across. They comprise 12 spinel (sp)-hibonite (hib)-perovskite (pv) inclusions; 6 sp-hib-pv-melilite (mel); 8 sp-pv-mel; 2 sp-hib; 2 sp-pyroxene (pyx); 9 sp-pv-pyx; and one sp-mel-anorthite. We found no sp-pv inclusions, although such inclusions have been reported [8]. Some have rims of Fe-bearing phyllosilicate enclosed in an outer rim of aluminous diopside. Most inclusions have many rounded cavities, like those shown in [5, 8] that are commonly lined with mel or pyx, but some have few cavities and may be considered compact. Some spherules have uniform distributions of phases while others have phases that are concentrated in their cores relative to their edges. **Sp-hib-pv inclusions:** Of the nine complete or nearly-complete spherules, four have uniform distributions of phases and four have hibonite-rich cores and spinel-rich edges. The remaining inclusion has a massive outer rim of spinel and a porous core of sp + pv separated by a band of hib + pv. In this group of inclusions, widths of hibonite laths range from just a few μm up to ~25 μm, and their lengths are 10-50 μm. **Sp-hib-pv-mel:** Four of these are spherule fragments. Two appear to have sp-rich rims and hib-rich cores with mel lining cavities in sp. Another fragment is a pie-slice-shaped piece with a hib+sp+pv mantle and a monomineralic melilite core ($Åk_{4-14}$). Another unusual inclusion has a uniform texture of hibonite laths 50 μm long enclosed in melilite and spinel, with grains of perovskite mostly occurring at hib-sp contacts. The remaining two have been described previously [5]. BB-1 has a typical texture, with a hib-rich core and fine mel occurring between

spinel grains. MUM-1, also shown in [5], in contrast is a very melilite-rich fragment that resembles a compact Type A inclusion. Melilite encloses a chain of sp and hib grains. **Sp-hib:** These are SH-5 and SH-6 of [9]. They have fluffy cores of loosely aggregated hibonite laths with no interstitial material, and sp-rich rims. Some of the sp is also lath-shaped. **Sp-pv-mel:** With two exceptions, these inclusions consist almost entirely of cavity-riddled spinel, with small (<~5 μm) blebs of pv and mel. Another inclusion has an elongated mel-rich core enclosed in sp + pv. The remaining inclusion consists of massive melilite enclosing euhedral to rounded sp and fine blebs of pv. **Sp-pyx:** Two inclusions consist of porous spinel with pyroxene inclusions. The pyx in the interiors of these objects is Ti-bearing, so these are not analogous to previously described sp-pyx inclusions [5, 10]. **Sp-pyx-pv:** These spherules are typically dominated by porous to massive spinel with fine, sparse to abundant pyx and pv inclusions. One spectacular inclusion, however, consists of lath-shaped spinel with interstitial pyx and pv throughout. Pore space and pv decrease and pyx increases from core to rim. If SH-6 [9] represents partial pseudomorphic replacement of hibonite by spinel, this object could be the product of that reaction proceeding to completion. **Sp-mel-an:** This unique spherule consists almost entirely of spinel with small inclusions of mel and anorthite.

**Discussion:** Some of the inclusions contain very small amounts of one or more of the phases used to classify them, so some of the categories may reflect non-representative sampling instead of genetic differences. A test of this will be to see if phases in the different groups have characteristic minor element abundances. A lack of mineral-chemical differences among the different inclusion types would imply that they had similar sources. There are trace element and isotopic differences between the major inclusion types used by [11] and within their broadly defined SHIB group, but it is not known if trace element variations correlate with our mineral assemblage types or with texture.

Many of the inclusions upon which this study is based have features, such as interlocking spinel and hibonite grains and hibonite laths that interfered with each other during growth, that suggest that they crystallized from molten droplets. At the temperatures required to keep these objects even partially molten, ~2000ºC, Mg, Si and even Ca should volatilize in a reducing gas. The isotopic compositions of these elements should be strongly fractionated in any spherule that underwent this process. Some questions we will address in the context of our petrographic classification scheme with new mineral-chemical and isotopic data are: Which, if any, of the types of spherules described above underwent evaporative loss of MgO, $SiO_2$ and CaO? Do melilite-free spherules show more evidence for mass-dependent isotopic fractionation than melilite-bearing ones? If inclusions lost Si, Ca and Mg, what were their original bulk compositions, and could they represent equilibrium condensate assemblages?

A lack of isotopic mass-fractionation in the spherules would eliminate evaporation from partially molten assemblages as an explanation for the "missing melilite", but would not rule out evaporation from the solid state [12]. It might support an alternative explanation, also suggested by [5], that when hibonite reacted with the solar nebular gas it formed melilite more slowly than spinel. Complete suppression of melilite condensation does not work, as calculations in which this is done yield absurd phase assemblages [13].

**References:** [1] Grossman L. et al. (2002) *GCA 66*, 145-161. [2] Grossman L. (1972) *GCA 36*, 597-619. [3] Yoneda S. and Grossman L. (1995) *GCA 59*, 3413-3444. [4] Ebel D. S. and Grossman L. (2000) *GCA 64*, 339-366. [5] MacPherson G. J. et al. (1983) *GCA 47*, 823-839. [6] Ireland T. (1990) *GCA 54*, 3219-3237. [7] Ireland T. (1988) *GCA 52*, 2827-2839. [8] Macdougall J. D. (1981) *GRL 8*, 966-969. [9] MacPherson G. J. et al. (1984) *PLPSC 15$^{th}$*, C299-C312. [10] Greenwood R. C. et al. (1994) *GCA 58*, 1913-1935. [11] Ireland T. R. et al. (1988) *GCA 52*, 2841-2854. [12] Davis A. M. et al. (2004) *MAPS 39*, A29. [13] Krot A. N. et al. (2004) *GCA 68*, 2167-2184.

**DISCOVERY OF PRESOLAR CORUNDUM (AND SiC?) IN AN INTERPLANETARY DUST PARTICLE.**

F. J. Stadermann and C. Floss, Laboratory for Space Sciences and Department of Physics, CB 1105, Washington University, 1 Brookings Drive, St. Louis, MO 63130-4899, USA (fjs@wustl.edu).

**Introduction:** This work is part of an ongoing investigation [1-3] of isotopically anomalous phases in interplanetary dust particles (IDPs) on a scale of 100 nm. Previously, such NanoSIMS studies have found sub-micrometer sized, isotopically distinct presolar grains in IDPs at higher abundances than in primitive meteorites [1-5], which demonstrates the unique and primitive nature of IDPs. Although not all presolar grains found so far in IDPs have been chemically or petrographically characterized, the majority appear to be silicate stardust. Conspicuously absent from the presolar grain inventory in IDPs have been other grain types, which are commonly found in primitive meteorites, such as SiC and corundum ($Al_2O_3$).

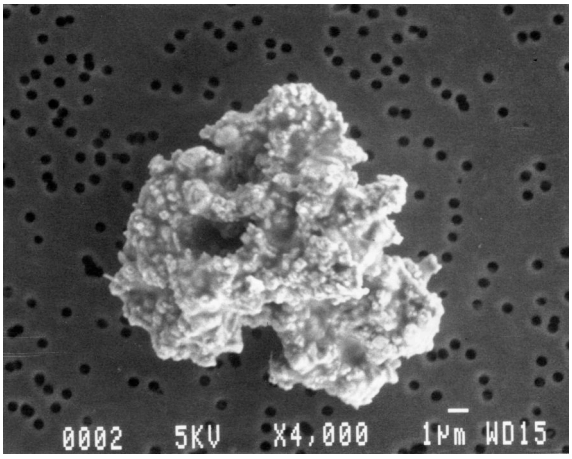


***Figure 1**. SEM microphotograph of IDP TIBERIUS on a nuclepore substrate before mounting for SIMS analyses.*

**Sample and Previous Analyses:** Figure 1 shows particle "TIBERIUS" (u44-m1-5) which is a non-cluster IDP that was originally studied with the Washington University ims3f ion microprobe for bulk isotopic [6] and trace elemental [7] composition. This particle is 15 µm in diameter and has a typical 'chondritic' EDX spectrum. After analysis in the scanning electron microscope, the particle was crushed between quartz plates and portions were pressed into high-purity Au foil and KBr for SIMS and IR measurements, respectively. The IR classification of this particle was not fully conclusive, but hinted at the presence of hydrated phases. Quantitative SIMS measurements of TIBERIUS with the ims3f ion microprobe found roughly chondritic abundances in 25 major and trace elements, including volatile elements. Both H and C isotopic measurements showed normal isotopic compositions in the analyzed fragments of this particle. Oxygen isotopes in TIBERIUS were not measured during the original ims3f study. A N isotopic measurement revealed a slight enrichment in $^{15}N$ with a $\delta^{15}N$ of (53 ± 6)‰. Since the lateral resolution of the ims3f was around 5-10 µm during this study, all of the original SIMS measurement can be thought of as 'bulk' measurements on an IDP size scale. These earlier analyses establish TIBERIUS as a fairly typical IDP with no unusual characteristics other than the bulk N anomaly.

**NanoSIMS Measurements:** Since there was a significant portion of particle TIBERIUS left on the Au foil after the original ims3f measurements, it was possible to perform additional analyses on the same IDP with the high lateral resolution and sensitivity of the Washington University NanoSIMS. These new measurements were done in areas of the sample that were not extensively damaged in the previous study. The NanoSIMS measurements were made in multi-collection imaging mode, as previously described [1-3]. Isotopic measurements of C and O were done with a 100 nm $Cs^+$ primary beam and parallel detection of secondary electrons, $^{12}C^-$, $^{13}C^-$, $^{16}O^-$, $^{17}O^-$, and $^{18}O^-$. A 500 nm $O^-$ primary beam was used for Mg/Al isotope imaging measurements, in which secondary ions of $^{24}Mg^+$, $^{25}Mg^+$, $^{26}Mg^+$, $^{27}Al^+$, and $^{28}Si^+$ (for reference) were detected.

**Results:** Most of the analyzed areas of TIBERIUS (and of 6 other IDPs that were part of this study) contained no detectable isotopic anomalies in C or O. No further measurements were performed on those areas.

*First presolar grain*. One area that clearly stood out in the isotope ratio images of O in TIBERIUS is shown in Figure 2. The isotopic anomaly is clearly correlated with a well-defined individual grain that has a size of 350 nm x 600 nm (see secondary electron image in Figure 2). The composition of this grain is $^{17}O/^{16}O = (1.31 \pm 0.03) \times 10^{-3}$ and $^{18}O/^{16}O = (1.57 \pm 0.03) \times 10^{-3}$, while the terrestrial ratios are $3.81 \times 10^{-4}$ and $2.00 \times 10^{-3}$, respectively. This composition is typical for 'group 1' grains which are thought to be of red giant and AGB star origin [8]. The C isotopic composition of this grain is normal, although the statistical uncertainty is large due to a very low C abundance. The prominent location of

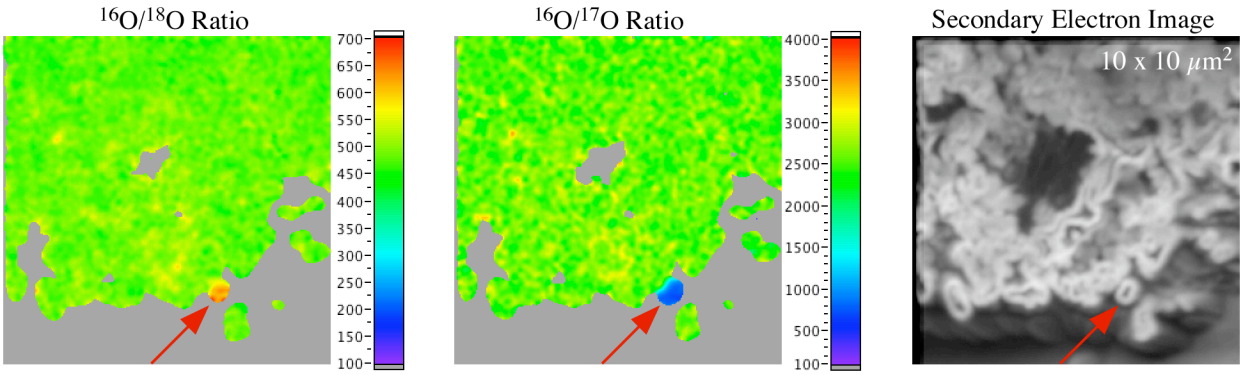


***Figure 2**. NanoSIMS views of IDP TIBERIUS. The false-color images show oxygen isotopic compositions, which are normal ($^{16}O/^{18}O$=499, $^{16}O/^{17}O$=2625) for most of the particle. The isotopically anomalous corundum grain can clearly be identified in the ratio images and in the simultaneously acquired secondary electron image (see arrows).*

this grain on the edge of the main sample mass does not give any indication of its original setting within the IDP, since the internal structure was disrupted when the IDP was crushed and pressed into Au. However, the unique location of this isotopic hotspot simplifies a chemical identification, because it reduces the contribution of neighboring phases in the SEM-EDX spectrum. The major element composition in Figure 3 identifies the anomalous grain as corundum, a presolar grain type that is also found in separates of primitive meteorites [e.g., 8-11]. The mineral corundum is only rarely seen in IDPs [12,13] and this is the first observation of presolar corundum. Subsequent Mg/Al isotopic measurements of this grain found an excess in $^{26}Mg$ corresponding to an initial $^{26}Al/^{27}Al$ of 1.6 x $10^{-3}$.

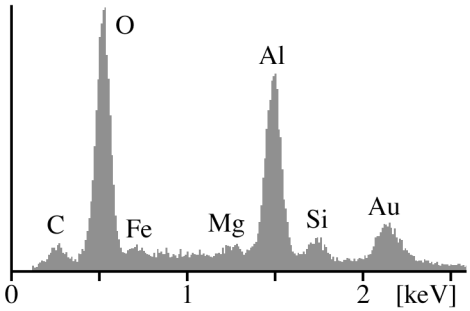


***Figure 3**. SEM-EDX spectrum of the corundum grain. Minor contributions are Au from the sample substrate as well as C, Mg, Si, and Fe from surrounding phases.*

*Second presolar grain*. Another isotopically anomalous region shows up in the C isotopic images of TIBERIUS. This area has a diameter of 150 nm and a $^{12}C/^{13}C$ ratio of 20 ± 2, corresponding to a $\delta^{13}C$ of +3450‰. Isotopic anomalies in C are rarely found in IDPs and the magnitude of this anomaly is unprecedented [*cf.* 2, 3]. The C isotopic composition of this grain, which is C-rich, is similar to those of mainstream SiC from primitive meteorites, raising the possibility that this isotopic hotspot may also be of that type. If that were the case, we would also expect isotopic anomalies in N and Si. Such measurements and a possible FIB extraction (with subsequent TEM analysis) are planned for the near future. The O abundance of this isotopic hotspot was found to be low, with normal $^{17}O/^{16}O$ and $^{18}O/^{16}O$ ratios.

It is important to note that the TIBERIUS has a bulk N anomaly, which is consistent with previous observations that such particles represent a distinct sub-group of IDPs with (relatively) abundant presolar grains [3]. No C or O isotopic hotspots were found in the 6 other IDPs in this study, of which 5 were bulk-isotopically normal in N.

Since the two types of presolar grains in this study are the first such observations in IDPs, it is difficult to determine a meaningful abundance. By dividing the areas of the presolar phases by the total analyzed area of TIBERIUS, we get an abundance of 600 ppm for corundum and 60 ppm for the $^{13}C$-rich phase *in this one IDP*. Normalized to the total area of all previously studied IDPs, the abundances are correspondingly lower.

**References:** [1] Floss C. and Stadermann F. J. (2002) *LPS XXXIII*, #1350. [2] Floss C. et al. (2004) *Science*, *303*, 1355-1358. [3] Floss C. and Stadermann F. J. (2004) *LPS XXXV*, #1281. [4] Messenger S. et al. (2003) *Science*, *300*, 105-108. [5] Messenger S. and Keller L. P. (2004) *Meteoritics & Planet. Sci.*, *39*, A68. [6] Stadermann F. J. et al. (1990) *LPS XXI*, 1190-1191. [7] Stadermann F. J. (1991) *LPS XXII*, 1311-1312. [8] Nittler L. R. (1997) *ApJ*, *483*, 475-495. [9] Huss G. R. et al. (1992) *LPS XXIII*, 563-564. [10] Huss G. R. et al. (1994) *ApJ*, *430*, L81-L84. [11] Hutcheon I. D. et al. (1994) *ApJ*, *425*, L97-L100. [12] Zolensky M. E. (1987) *Science*, *237*, 1466-1468. [13] McKeegan K. D. (1987) *Science*, *237*, 1468-1471.

*This work was supported by NASA grant NNG04GG49G.*

**A SEARCH FOR SOLAR-SYSTEM PROCESSING SIGNATURES IN PRESOLAR GRAINS.** Rhonda M. Stroud[1] and Larry R. Nittler[2], Naval Research Laboratory, 4555 Overlook Ave. SW, Washington, DC 20375, [2] Dept. of Terrestrial Magnetism, Carnegie Institution of Washington, 5241 Broad Branch Road, Washington, DC 20015.

**Introduction:** Presolar grains by definition escaped most of the heavy processing that occurred in the early solar nebula, but limited structural, chemical and isotopic alteration cannot be ruled out. Coordinated isotopic and structural studies of presolar grains, including grains examined *in situ* in the host meteorites or interplanetary dust particles, can provide important information about the degree and type of processing, and possible mechanisms for grain survival and parent body incorporation. For example, some presolar SiC grains may survive exposure to hot oxygen-rich nebular gases through the formation of a protective silica surface layer [1, 2], although definitive evidence for such rims has yet to be reported. Possible processing signatures that could be found include: spatial isotopic heterogeneities, chemically and/or structurally distinct rims, and crystallographic-orientation relationships with surrounding matrix material.

**Methods:** Sections of presolar $Al_2O_3$, SiC, and silicate grains, were prepared for transmission electron microscopy using a FEI FIB200, focused ion beam workstation. The $Al_2O_3$ [3] and silicate grains [4] were identified as presolar on the basis of O isotopic measurements obtained using Cameca ims-6f and NanoSIMS ion microprobes, respectively. Transmission electron microscopy studies of the sections were performed using JEOL 2010F and Philips CM30 microscopes. Spatial distributions of isotopes across sections of SiC X grains were obtained with Cameca Nanosims [5].

**Mainstream SiC:** Structural analyses of the grains reveal a broad range of microstructures [6, 7, present work]. Example micrographs of pristine (non-etched) SiC are shown in Fig. 1. The grain shapes range from strongly faceted to heavily rounded. Of the five grains sectioned to-date, only one exhibits any indication of a rim. Two of the grains contain sub-grains; one containing graphite, and the other containing a Ru-bearing phase tentatively identified as RuC. The orientational relationship with the matrix of the host meteorite was examined for two of the grains, sectioned *in situ*. In both cases, the surrounding material consisted of fine-grained silicates with no orientational relationship to the enclosed SiC.

**Supernova SiC X grains:** The microstructures of two SiC X grains are distinct from the mainstream grain structures. Each X grain was composed of multiple subgrains, approximately 10-nm and densely packed in the one case, and 100-nm and porous in the other (Fig 2). NanoSIMS isotopic maps from these sections showed then to be spatially homogeneous in Si, C and N isotopes.

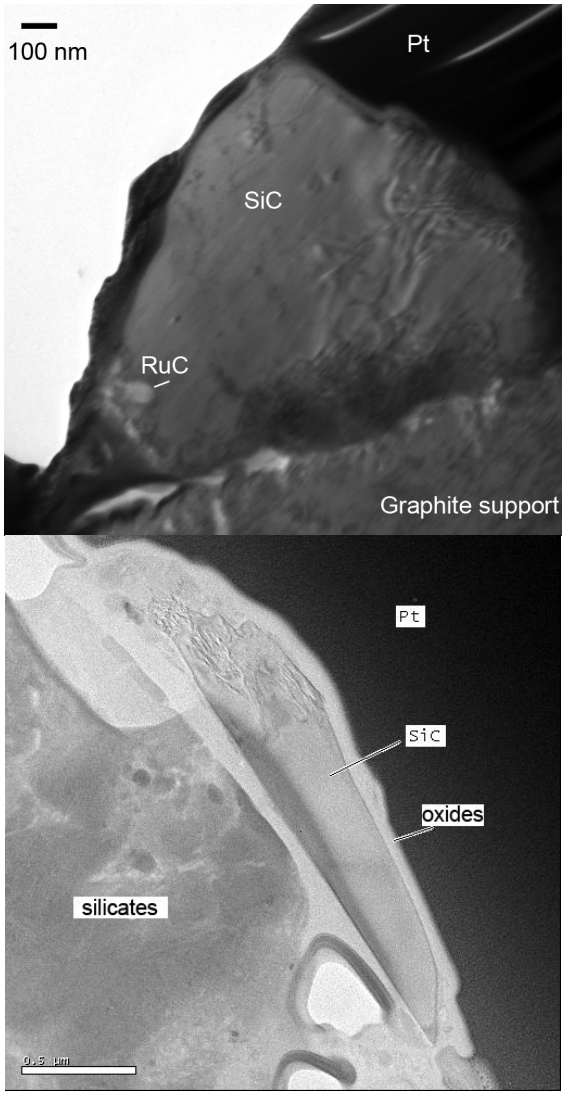


Figure 1. (top) Electron micrograph of a pristine SiC grain. (bottom) Electron micrograph of *in situ* pristine SiC grain. The surrounding oxides are finely nanocrystalline matrix, rather than a reactionary rim.

**$Al_2O_3$:** Two Group 1 grains, believed to have originated in O-rich asymptotic giant branch (AGB) stars, have been examined [3]. One exhibited the co-

rundum structure and the other was amorphous. Neither contained sub-grains.

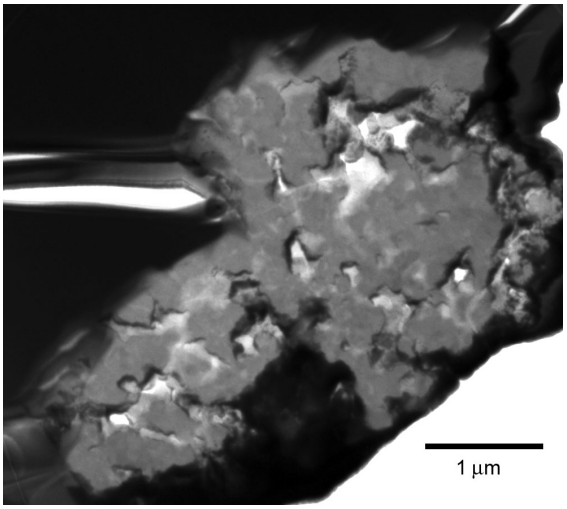


Figure 2. Electron micrograph of a SiC X grain.

**Silicates:** One presolar silicate was examined. The structure of the grain was glassy, with a non-stoichiometric composition. No sub-grains were observed.

**Discussion:** No definitive evidence for nebular or parent body processing signatures, such as rims, spatial isotope heterogeneities, or orientational relationships has yet been observed. Many of the grains exhibit metastable microstructures, i.e., the amorphous $Al_2O_3$ and silicate, and nanocrystalline X grains, incompatible with high-temperature processing. The lack of processing signatures may reflect a selection bias, in that the analyzed grains are generally from very primitive meteorites which do not show evidence for high temperature processing (*e.g.*, pristine SiC from the CM2 chondrites Murchison and Cold Bokkeveld). The presolar $Al_2O_3$ grains are from Tieschitz, which experienced parent-body metamorphism, but not to the ~700°C required to convert amorphous $Al_2O_3$ to corundum. Huss *et al.* [8] showed a correlation between presolar grain abundances and bulk chemistries for different chondrite classes and suggested that this reflects variable high temperature processing in the nebula of chondrite precursor material. The most primitive matrices, formed by the lowest temperature processes, are least likely to cause detectable alteration of the refractory presolar grains. Processing signatures might be more evident in presolar grains identified in meteorites with matrices indicating greater thermal alteration either in the nebula or on parent bodies. For example, CR2 chondrites have depleted volatile element and presolar SiC abundances [8], relative to CI chondrites, suggesting nebular heating. Pristine SiC from such meteorites might thus be expected to show processing signatures (*e.g.,* rims) not yet observed in the CM2 grains. The relative abundance of amorphous and crystalline silicate and $Al_2O_3$ grains should also vary with the degree of thermal processing that meteorites and their parent materials experienced.

**References:**

[1] Mendybaev R. A., Beckett J. R., Grossman L., Stolper E., Cooper R. F. and Bradley J. P. (2002) *Geochim. Cosmochim. Acta, 66,* 661-682.

[2] Bernatowicz T. J., Messenger S., Pravdivtseva O., Swan P. and Walker R. M. (2003) *Geochimica et Cosmochimica Acta, 67,* 4679-4691.

[3] Stroud R. M., Nittler L. R. and Alexander C. M. O'D. (2004) *Science, in press*.

[4] Nguyen A. N. and Zinner E. (2004) *Science, 303,* 1496-1499.

[5] Stroud R. M., Nittler L. R. and Hoppe P. (2004) *Meteorit. Planet. Sci., 39 (supp),* A101 (abstr.).

[6] Stroud R. M., O'Grady M., Nittler L. R. and Alexander C. M., O'D., Transmission electron microscopy of an in situ presolar silicon carbide grain, in: Lunar Planet. Sci. Conf. XXXIII, 2002, Abstract #1785 (CD-ROM).

[7] Stroud R. M., Nittler L. R., Alexander C. M. O'D., Bernatowicz T. J. and Messenger S. R., Transmission electron microscopy of non-etched presolar silicon carbide, in: Lunar Planet. Sci. Conf. XXXIV, 2003, Abstract #1755.

[8] Huss G. R., Meshik A. P., Smith J. B. and Hohenberg C. M. (2003) *Geochimica et Cosmochimica Acta, 67,* 4823-4848.

**DO COMETS HAVE CHONDRULES AND CAIs? CLUES TO THE FORMATION LOCATIONS OF HIGH-TEMPERATURE OBJECTS IN METEORITES.** Timothy D. Swindle[1] and Humberto Campins[2], [1]Lunar and Planetary Laboratory, University of Arizona, Tucson AZ 85721-0092, tswindle@u.arizona.edu, [2]Department of Physics and Astronomy, University of Central Florida, Orlando, FL 32816, hcampins@physics.ucf.edu.

**Introduction:** Chondrules are found in virtually all primitive meteorites, and CAIs are found in many of them. However, there is still no consensus on the origin of either of these types of objects. One problem is that while these objects are common in primitive meteorites, our primitive meteorites probably all come from the Main Asteroid Belt. Much of the rest of the material in the solar system has now been collected either into the Sun or into planets or moons large enough to differentiate and destroy any evidence of the existence of chondrules and CAIs in their precursor material. One category of solar system bodies that has not been processed enough to destroy chondrules and CAIs is the comets. Furthermore, since comets formed at a different location from asteroids, if we could find out whether comets have chondrules and/or CAIs, we would know far more about how ubiquitouos these objects are, and might be able to provide strong evidence for or against certain formation models. Below, we discuss the implications of the presence or absence of these objects in comets, and then discuss various lines of evidence.

**Comets:** There are actually bodies from two different basic locations that can evolve to become observable comets [1]. Low-inclincation, low-eccentricity Jupiter-family comets are most likely derived from the Kuiper Belt, and probably formed in or near the current Kuiper Belt, just beyond the orbits of the planets. Oort Cloud comets, on the other hand, currently approach the inner solar system from virtually random directions, having resided thousands of AU from the Sun during most of their existence. However, they probably formed somewhere in the region between Jupiter and Neptune and were ejected to the Oort Cloud by interactions with the giant planets [1]. Hence the Oort Cloud comets probably formed at a location intermediate between those where asteroids and Jupiter-family comets formed, despite spending most of their existences at much more distant locations.

**Implications for chondrule and CAI formation models:** Most "traditional" chondrule and CAI formation mechanisms posit formation mechanisms that depend on nebular properties such as mass density, number density or effective solar luminosity [2, 3], all of which would be expected to decrease with increasing distance from the Sun. In such models, one would expect chondrules and CAIs to be much rarer, or perhaps even absent, in either type of comet. However, there are some models in which chondrules and/or CAIs were formed at a location remote to that where they were incorporated into asteroids. For example, in the X-wind model [4], chondrules and CAIs are produced near the Sun, and transported outward by the "X-wind." This model explicitly predicts that comets will have chondrules and CAIs. Another case where comets might be expected to have CAIs, or at least their precursors, is that where these objects are created around other stars and transported to the solar nebula [5], although in this case, there might not be chondrules if chondrules were formed locally by one of the more traditional mechanisms. Hence knowing whether or not comets have chondrules and/or CAIs could be diagnostic among some of these models.

**Searching for cometary chondrules and CAIs:** While determining whether cometary material has high-temperature objects would be very valuable, it is also very difficult.

One obvious way would be to study cometary meteorites. Unfortunately, there are no meteorites that are unambiguously cometary [6]. Oort Cloud comets would not be expected to be capable of generating meteorites, because their large inclinations and eccentricities lead to extremely high Earth-encounter velocities, too high for a meteorite to survive. Jupiter-family comets have a better chance, but there would still remain the difficulty of identifying a cometary meteorite [6]. The best identification would be orbital, but only a few meteorites have photographically-determined orbits, and none of those are cometary. A recent analysis of visual observations suggested a cometary orbit for the 1864 fall of (chondrule-free) Orgueil [7], but visual observations are problematic.

Interplanetary dust particles are too small to represent chondrules or CAIs, at least of the size seen in most meteorites. Furthermore, stratospheric collection relies on atmospheric drag slowing the particles enough in the stratosphere for them to have a long residence time there, and objects as compact as chondrules or CAIs are less likely to survive. There have been some suggestions of chondrule fragments in some IDPs [8], but these were believed to be asteroidal particles.

An intriguing possibility is to search through the thousands of recent observations of the Leonid meteors [9], whose source is Oort Cloud comet 55P Tempel-Tuttle. Chondrules or CAIs might show up in several ways in meteor data. In meteorites, chondrule size distributions are sharply peaked, but Leonid size distributions appear to be a uniform power law. Also, chondrule and CAI chemistry is different from the typical carbonaceous meteor, but quantita-

tive chemical composition is hard to obtain, and there is again not much evidence. The most promising technique is to look at light curves – a compact object should have a much different light curve as it ablates and decelerates than should a fluffy collection of smaller particles. There are a few light curves that seem to show some small solid object at the heart of a Leonid [9]. However, the abundances do not seem to be high, and much more modeling and analysis would be needed to quantify the amount of compact material.

Of course, the ultimate answer is likely to come from spacecraft. Stardust has recently completed its flyby of the Jupiter-family (Kuiper Belt) comet Wild 2, and will be bringing back the first certifiably cometary material for laboratory study in early 2006. However, the collectors are incapable of collecting an intact chondrule (although if one passed through the collector, it might leave enough diagnostic fragments to be identified). Furthermore, it is not clear that compact high-temperature objects like chondrules and CAIs would be lofted off a comet as readily as smaller and/or fluffier materials, a problem for both cometary dust collection and meteor analysis.

Hence, the question will probably have to wait until a comet nucleus sample return (or at least landing), presumably in the next decade. However, when we are able to study comet nucleus material in detail, the question of whether or not it contains chondrules, or CAIs, or CAI precursors, or none of the above, will provide some fundamental data for models of the formation of these objects.

**References:**

[1] Weissman P. R. (1999) *Space Sci. Rev.*, *90*, 301-311.

[2] Boss A. P. (1996) in *Chondrules and the Protoplanetary Disk*, p. 257-263.

[3] Jones R. H. et al. (2000) in *Protostars and Planets IV*, p. 927-962.

[4] Shu F. H. et al. (2001) *Astrophys. J.*, *548*, 1029-1050.

[5] Cameron A. G. W. (2004) Submitted to this workshop.

[6] Campins H. and Swindle T. D. (1998) *MAPS*, *33*, 1201-1211.

[7] Gounelle M. et al. (2004) *MAPS*, *39*, A45.

[8] Genge M. J. and Grady M. M. (2000) *MAPS*, *35*, A58-A59.

[9] Swindle T. D. and Campins H. (2004) *MAPS*, *39*, In press.

**INCONGRUENT EVAPORATION OF MINERALS: FORMATION OF POROUS OR COMPACT RESIDUAL LAYER.** S. Tachibana, Department of Earth and Planetary Science (Bldg. 1), University of Tokyo, 7-3-1 Hongo, Tokyo 113-0033, Japan (tachi@eps.s.u-tokyo.ac.jp).

**Introduction:** Evaporation and condensation are major processes for phase changes in low-pressure protoplanetay disks. Many minerals do not evaporate congruently, but react and decompose to form residual solid and gas, of which compositions differ from the original mineral (incongruent evaporation). Thus, incongruent evaporation may have been responsible for chemical fractionation processes that are recorded in chondrites. For instance, sulfur evaporates preferentially from troilite (FeS), and metallic iron is formed as an evaporation residue, resulting in Fe/S fractionation between solid and gas. Incongruent evaporation of enstatite ($MgSiO_3$) can cause Mg/Si fractionation because a residual forsterite layer ($Mg_2SiO_4$) is formed due to evaporation of $SiO_2$ component.

Incongruent evaporation kinetics of troilite and enstatite were studied experimentally by [1, 2] in order to discuss chemical fractionations of major rock-forming elements (Mg, Si, Fe, and S) in protoplanetary disks as time-dependent processes. In the case of incongruent evaporation of troilite, the residual metallic iron layer was porous (Fig. 1a) and a rate-determining process was a chemical reaction on the troilite surface exposed to vacuum or hydrogen gas [1]. On the other hand, a forsterite layer formed by incongruent evaporation of enstatite became compact as evaporation proceeded (Fig. 1b), and the rate-determining process was diffusion through the compact forsterite layer [2].

The surface reaction-controlled evaporation with a "porous" residual layer and the diffusion-controlled evaporation with a "compact" residual layer have different dependences on time: the former proceeds linearly with time, while the latter proceeds linearly with $(\text{time})^{1/2}$. Therefore, the structure of the residual layer affects the time-dependence of chemical fractionation processes. In this study, formation of the residual layer is modeled and the factor that controls the structure of the residual layer is discussed.

**Incongruent evaporation of troilite (FeS):** Evaporation experiments of troilite at 1atm total pressure (partial hydrogen pressure ($p_{H2}$) = 0.2-1.0 atm) and under low $p_{H2}$ conditions ($p_{H2}$ = $10^{-3}$-$10^{-6}$ atm) showed that the thickness of a "porous" metallic iron layer increased linearly with time [1]. The spacing between iron rods ($L$) in the porous residual layer was several microns for samples evaporated at 1 atm total pressure, while $L$ was several tens of microns for samples heated in low $p_{H2}$ conditions [1].

**Incongruent evaporation of enstatite ($MgSiO_3$):** The thickness of the residual forsterite layer ($Z$) increased almost linearly with time in the early stage of evaporation, indicating that the forsterite layer was porous and gases that evaporate from the surface of enstatite could escape through the porous layer. As evaporation proceeded, $Z$ became constant, and further evaporation proceeded with constant $Z$. The constant $Z$ is explained by the balance of diffusion-controlled evaporation of enstatite through the polycrystalline "compact" forsterite layer and evaporation of the residual forsterite layer itself [2].

**Formation model of residual layer:** Incongruent evaporation of a mineral AB is considered here, where a component A evaporates preferentially and a phase B is formed as an evaporation residue. As an analogy to eutectic solidification of a binary system [e.g., 3], a one-dimensional diffusion-controlled model is made for formation of a porous residual layer with some assumptions: (1) No diffusion occurs except in a thin region near the evaporating surface, of which thickness is expressed by $\delta$. (2) The composition of A at the interface between AB and residual B rods is fixed at $C_{A,b}'$. The diffusion equation for A in the thin region near the evaporating surface is expressed by:

$$\frac{\partial C_A'}{\partial t'} = D\frac{\partial^2 C_A'}{\partial x'^2} - \frac{J}{\delta}\frac{C_A'}{C_{A,0}'}, \qquad (1)$$

where $x'$ is the distance along the evaporating surface normal to the rods, $C_A'$ is the concentration of A, $C_{A,0}'$ is the concentration of A in the host phase AB, $D$ is the diffusion coefficient, $J$ is the evaporation flux of A, and $t'$ is time. This equation can be non-dimensionalized by $C_A' = C_{A,0}' C_A$, $x' = L x$, and $t' = (L^2/D)\, t$:

$$\frac{\partial C_A}{\partial t} = \frac{\partial^2 C_A}{\partial x^2} - \frac{JL^2}{\delta C_{A,0}' D} C_A = \frac{\partial^2 C_A}{\partial x^2} - \varepsilon C_A, \quad (2)$$

where $C_A$, $x$, and $t$ are dimensionless concentration of A, distance, and time, respectively, and $\varepsilon$ is a dimensionless number that compares the timescale of chemical reaction (evaporation) to that of transport (diffusion). As evaporation proceeds, $C_A$ decreases with time and then reaches a steady state (Fig. 2)

when evaporation and diffusion are balanced. The profile of $C_A$ at the steady state is expressed by:

$$C_A = C_{A,b}\cosh(\sqrt{\varepsilon}\,x)/\cosh(\sqrt{\varepsilon}/2), \qquad (3)$$

where $C_{A,b} = C_{A,b}'/C_{A,o}'$, with the boundary condition of $C_A(x = \pm 0.5) = C_{A,b}$.

The concentration of A (or B) is minimum (or maximum) at $x = 0$, and nucleation of a phase B may take place if $C_A(x = 0)$ becomes lower than a threshold for nucleation of phase B ($C_{A,Th}$). The spacing $L$ (or $\varepsilon$) decreases until it becomes $L^*$(or $\varepsilon^*$), where $C_A(x = 0)$ at the steady sate becomes equal to $C_{A,Th}$ and no nucleation of B occurs for further evaporation.

If $L^*$ is large enough, it is expected that incongruent evaporation proceeds with keeping a porous residual layer. On the other hand, if $L^*$ is extremely small (e.g., $10^{-8}$-$10^{-9}$ m), the residual layer is considered to be compact and diffusion through the layer controls the evaporation rate.

**Application to evaporation of troilite and enstatite:**

*Troilite.* Difference in sulfur concentrations was observed between the residual Fe-FeS interface and the exposed troilite surface [1]. The back-scattered electron images of evaporated samples show that $\delta$ is probably in the order of $10^{-7}$ m. Because troilite evaporates with keeping the porous metallic iron layer, the observed $L$ (or $\varepsilon$) should be $L^*$ (or $\varepsilon^*$). For samples heated at 1 atm, $\varepsilon^*$ is estimated to be ~0.01 based on the evaporation rate [1], diffusion rate [4], and observed L (several microns). This indicates $C_A(x = 0)/C_{A,b}$ to be ~0.999. Because the evaporation rates for samples heated under low $p_{H2}$ conditions are ~1/100 of those at 1 atm, $L^*$ at low $p_{H2}$ should be ~10 times larger than that at 1 atm to satisfy $\varepsilon^*$ = ~0.01, which is consistent with the observed L for samples heated at low $p_{H2}$ (several tens of microns).

*Enstatite.* If it can be assumed that $\varepsilon^* = 0.01$ and $\delta = 10^{-7}$ m for evaporation of enstatite, $L^*$ is roughly estimated to be in the order of $10^{-8}$ m from the evaporation rate, diffusion rate [5] extrapolated to heating temperatures in experiments. This estimated $L^*$ can be the width of grain boundary of polycrystals. Thus, enstatite cannot continue to evaporate with keeping a porous forsterite layer, but the forsterite layer should become compact as evaporation proceeds as observed in experiments [2].

**References:** [1] Tachibana S. and Tsuchiyama A. (1998) *GCA, 62,* 2005. [2] Tachibana S. et al. (2002) *GCA, 66,* 713. [3] Cahn J. W. (1959) *Acta Metal., 7,* 18. [4] Condit R. H. et al. (1974) *Oxid. Metals, 8,* 409. [5] Schwandt C. S. et al. (1998) *Contrib. Min. Petrol., 130,* 390.

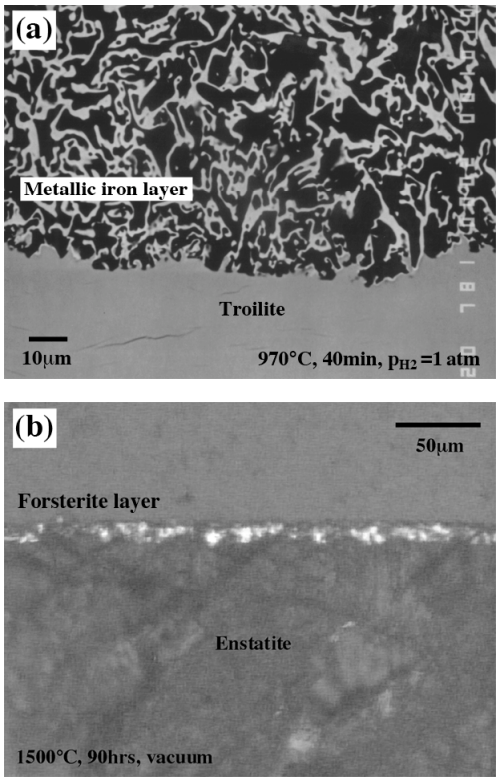


**Fig. 1.** (a) A secondary-electron image of a cross section of troilite evaporated for 40 minutes at 970°C and $p_{H2}$ = 1.0 atm. (b) An optical photomicrograph of a cross section of enstatite evaporated for 90 hours at 1500°C in vacuum.

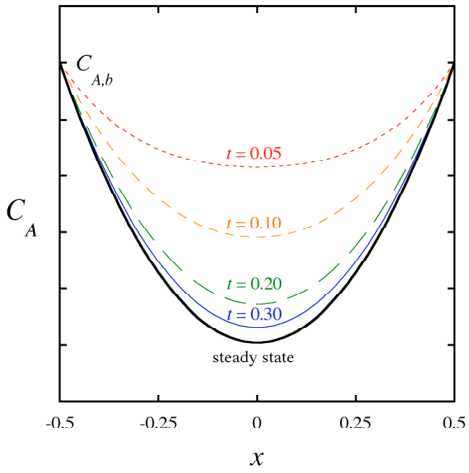


**Fig. 2.** The concentration profile of a component A near the evaporating surface of a mineral AB, from which a component A evaporates preferentially, with different elapsed time. The vertical axis shows an arbitrary concentration of A.

**EXPERIMENTAL STUDY OF IRON METAL CONDENSATION.** K. Tatsumi[1], H. Nagahara,[1] K. Ozawa[1], and S. Tachibana[1], [1]Dept. Earth Planet. Sci., Univ. Tokyo, 7-3-1 Hongo, Bunkyo-ku, Tokyo 113-0033, Japan, chichaneko@eps.s.u-tokyo.ac.jp

**Introduction:** Metallic Fe-Ni is one of the most important constituents of chondrites. Isolated large (>100μm) Fe-Ni metal grains included in CH carbonaceous chondrites are thought to have condensed in the solar nebula on the basis of their chemical compositions that are expected to condense in equilibrium with the solar nebula gas [1]. Some of metal grains in CM [2], CI, and CR chondrites [4] also show Ni-Co positive correlation, and can be condensates from the solar nebula gas [2].

Nickel-iron metal grains in CH chondrites, keeping the compositional zoning during condensation, are expected not to have experienced any thermal alternation [5]. It is also inferred that such metal grains condensed under non-equilibrium kinetic conditions that prevented the zoning profiles from being homogenized. The conditions for condensation of zoned metal grains in the early solar system were discussed based on the growth rate of metallic iron assuming that a condensation coefficient of metallic iron is unity (i.e., all incident iron atoms are incorporated into solid metal without any kinetic hindrances) [5]. However, the condensation coefficient is not necessarily unity and may have dependence on temperature or a degree of supersaturation of iron gas as the evaporation coefficient of Fe metal has dependence on temperature and undersaturation of iron gas [6]. In this study, we have carried out condensation experiments of metallic iron to obtain the condensation coefficient as a function of temperature and supersaturation of iron gas, which will be applied to detailed discussion of condensation of metallic iron in protoplanetary disks.

**Method:** Gaseous iron, produced by heating a metallic iron plate (12 mm x 12 mm) at 1170°C, was condensed on a molybdenum substrate set in a cooler region of a vacuum chamber. The temperature of the substrate varies depending on the distance from the source: 1020, 750, and 415°C for distances of 54, 73, and 88 mm from the source, respectively. Note that, because the incoming flux to the substrate also depends on the distance from the source, we cannot control the substrate temperature and the incoming flux independently at present. The experimental durations were 6-144, 3-48, and 1-48 hours for condensation temperatures of 415, 750, and 1020°C, respectively.

The weight changes of the source and the substrate were converted to evaporation and condensation rates by dividing by the experimental duration and either the surface area of the source or condensable area of the substrate, respectively. Condensates were observed with a field-emission scanning electron microscope (FE-SEM), analyzed with energy-dispersive spectroscopy (EDS) for chemical composition, and with electron-backscattered diffraction (EBSD) for crystallinity and phase identification.

**Results:** Condensates were identified to be crystalline metallic iron under all the experimental conditions. The structure of the condensed layer varies with temperatures of the substrate. A porous layer of granular condensates were formed on the substrate at 415°C, while condensates formed a compact layer at 750°C and 1020°C (Fig. 1). The compact layers at 750°C and 1020°C due to annealing. The surface of the compact condensate layer was granular at 750°C and smooth at 1020°C. The crystal size seen on the top of the condensate layer increased with experimental time at 415°C (Fig. 2). On the other hand, the size change of condensates could not be determined at 1020°C because they formed a compact polycrystalline layer.

The weight of the condensates and the thickness of the condensed layer increased linearly with heating duration, but the basic characteristics of condensates, described above, for each condensation temperature seemed not to change significantly with heating duration.

The iron plate source lost its weight linearly with time, and its evaporation rate was consistent with previous evaporation experiments [6].

**Discussion:**

The condensation coefficient of metallic iron was estimated based on weight gain of the substrate and weight loss of the source with taking geometrical effects of the furnace on incoming flux into account. The condensation coefficients, evaluated as a function of temperature, are shown in Fig. 3. The condensation coefficients have little or no dependence on temperature, which is different from the evaporation coefficient with clear temperature dependence [6]. It should be noted that we cannot control the degree of supersaturation in the present experimental setting and the dependence on supersaturation should be examined in future studies.

The condensation coefficient of ~0.7 irrespective of condensation temperatures does not significantly change the discussion for the origin of zoned metal [5], but makes the growth timescale ~40% longer. Kozasa and Hasegawa [7] has modeled the condensation of

metallic iron in the solar nebula and discussed the growth rates and the kinetic condensation temperature, at which gas species begin to condense, for major refractory condensates ($Al_2O_3$, $CaTiO_3$ $Mg_2SiO_4$, and metallic Fe) in the cooling solar nebula. Although condensation coefficients for all gas species were treated as unity, if the value of ~0.7 is applied to metallic iron, the condensation behavior of metallic iron will be changed. For example, the number density of metallic iron nuclei at the condensation temperature of metallic iron becomes ~0.7 times smaller that the case with the condensation coefficient of unity, resulting in that the mean radius of iron grains becomes 10% larger. Moreover, possible annealing effects seen in experiments at 750°C may suggest rapid coagulation of metal dust particles after nucleation.

In summary, laboratory experimental determination of condensation coefficients of dust species will enable us to make accurate calculations for condensation processes, which include the order of condensation sequence, cooling timescale, and growth rates. Although further experiments are needed, the present study gives an important constraint on the evolution of metallic particle and related silicates.

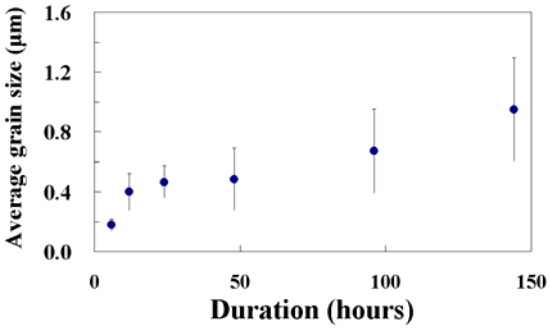


Fig. 2. Change of average crystal size with time, which condensed at 415°C. Vertical bars represent mean standard deviations.

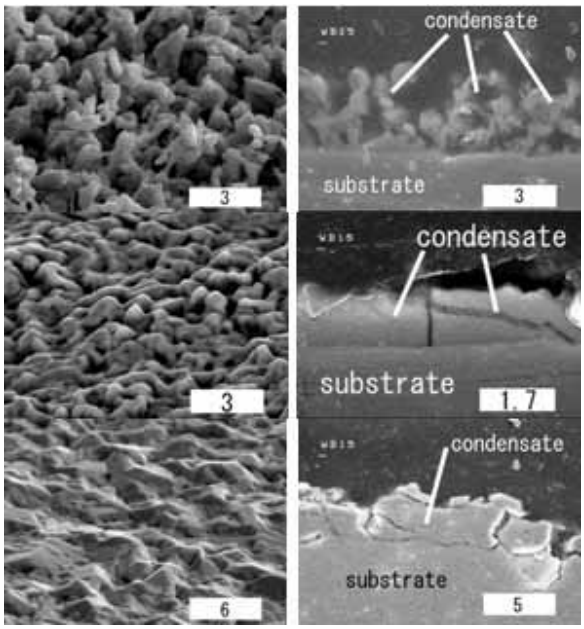


Fig. 1. FE-SEM images of surfaces (left) and cross sections (right) of Fe-metal condensates. Upper panels: 415°C for 96 hours; middle panels: 750°C for 24 hours; bottom panels: 1020°C for 24 hours. White bars with numbers are scale bars (in microns).

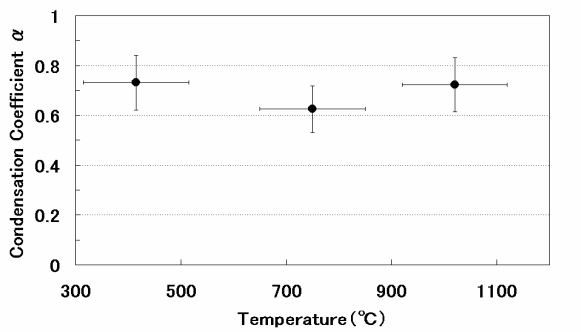


Fig. 3. Condensation coefficients of iron metal as a function of temperature.

**References:** [1] Meibom, A. et al. (1999) *JGR, 104*, 22053. [2] Grossman, L. and Olsen, E. (1974) *GCA, 38*, 173. [3] Anders, E. and Grevesse, N. (1989) *GCA, 53*, 197. [4] Weisberg, M. et al. (1993) *GCA, 57*, 1567. [5] Meibom, A. et al. (2000) *Science, 288*, 839. [6] Tachibana, S. et al. (2001) *LPS XXXII*, abstract #1767. [7] Kozasa, T. and Hasegawa H. (1987) *Prog. Theor. Phys,.77*, 1402.

**$^{26}$Al IN EFREMOVKA CAI E44L – RESOLVED TIME INTERVAL BETWEEN INTERIOR AND RIM FORMATION IN A HIGHLY FRACTIONATED COMPACT TYPE A CAI.** D. J. Taylor[1], K. D. McKeegan[1] and A. N. Krot[2], [1]Dept. of Earth and Space Sciences, UCLA, Los Angeles, CA, 90095, dtaylor @ess.ucla.edu. [2]HIGP/SOEST, University of Hawaii at Manoa, HI 96822.

**Introduction:** The detection of excess $^{26}$Mg* resulting from the *in-situ* decay of the short-lived radionuclide $^{26}$Al (half-life ~0.73 Ma) allows the determination of relative ages among different objects forming within the first few million years of the early solar system if one assumes a homogeneous distribution of $^{26}$Al/$^{27}$Al [1]. However, it may also be possible to discern a time interval between multiple processes occurring within a single solar system object by investigating the initial $^{26}$Al/$^{27}$Al in different petrographic components within that object. Very early forming CAIs, with higher-than canonical ratios of initial $^{26}$Al/$^{27}$Al which later experienced high-temperature event(s) leading to Wark-Lovering rim formation may meet this requirement. In the past it has not been possible to resolve a time difference between interior and rim formation because of the lack of precision and the need to measure high-Al phases. We have identified a very unusual compact type A CAI which is highly fractionated in the interior, but not in the rim, suggesting it may be a FUN inclusion. This inclusion also contains evidence for live $^{26}$Al, and two separate well-correlated internal Al/Mg evolution isochrons can be obtained for the interior and the rim, yielding a high-resolution chronometry for these two solar system events.

**Sample description:** Efremovka E44L is found in the same thin section as the Type B1 inclusion E44. E44L is an oblong, relatively small (~2 mm x 1 mm) compact type A CAI composed primarily of melilite, spinel, hibonite and perovskite (Figure 1). Melilite has a compact, igneous texture and is relatively gehlinitic, ranging from ~Åk$_{31}$ in the interior to Åk$_5$ near the rim. Spinel occurs as subhedral to euhedral grains 10-50 μm in size, heterogeneously enclosed in melilite. Small (~ 2-5 μm) anhedral grains of hibonite are scattered throughout the inclusion, with the largest concentration of hibonite found near and within the Wark-Lovering rim. Perovskite occurs as rounded blobs, some as large as 80 μm across, but most are small ~5 μm grains with a wormy texture, unevenly enclosed in melilite. There are two regions in the CAI where electron probe analyses indicate the presence of high-Ti pyroxene.

E44L is surrounded by a relatively thick Wark-Lovering rim, ranging from 50–150 μm across. The rim sequence consists of three layers: (1) an innermost layer of intergrown clumps of hibonite and spinel with minor perovskite, 50-80 μm thick, (2) a thin (~10 μm) layer of highly gehlinitic melilite, followed by (3) a thick outermost layer of diopside. The outer edge of the diopside rim layer has an irregular and scalloped shape and varies in thickness from 10 to 70 μm. There are two areas where bubbles of complete rim sequence material have broken off and lie immediately adjacent to the CAI. No alteration products are seen in the rim sequence.

**Analysis:** Mg isotopes were measured on the Cameca ims 1270 ion microprobe at UCLA by a multiple-collector method that allows determination of $\Delta^{26}$Mg* with a high precision (better than 0.1‰) in mineral phases with low Al/Mg ratios. Spot size was approximately 20 μm. All Mg isotope data have been normalized to the DSM3 standard [2] by correcting for instrumental mass fractionation using terrestrial standards (Burma spinel, Madagascar hibonite and pyroxene glass). An exponential mass fractionation law was assumed when calculating excess $^{26}$Mg*.

**Mg Isotopes:** E44L was analyzed in two separate sessions, two months apart. Both the interior and rim were measured on both occasions and the data are in very good agreement. A total of 22 spots were measured, 11 in the interior of the inclusion and 11 in the rim. The interior spots included 6 of the largest spinel grains, 3 melilite points, and 2 points in regions which appeared to be high-Ti pyroxene. Four spots located in the rim area are situated in the outer diopside layer, with 2 spots not containing overlap with any phases other than diopside (see Figure 2). Because of the fine-grained nature of the spinel+ hibonite inner rim layer, analyses in this area always overlap more than one mineral phase, with some of the spots also overlapping the middle melilite rim layer. One rim point appeared to be in a region consisting entirely of hibonite, and yielded a relatively high Al/Mg ratio of 14.5.

*Fractionation:* Mineral phases in the interior of E44L contain fractionated Mg favoring the heavy isotopes, on the order of 14-16 ‰ per amu, consistent with (although slightly less than) Mg fractionation seen in most FUN inclusions. Rim phases, however, do not contain isotopically heavy Mg, with $\delta^{25}$Mg ranging from -2 to 0.2 ‰ per amu.

*Radiogenic $^{26}$Mg*:* $\Delta^{26}$Mg* is very well correlated with $^{27}$Al/$^{24}$Mg ratios for all phases (except melilite) in both the interior and the rim of E44L, as long as these two distinct petrographic regions are considered as

separate isotopic systems. Interior spinel and fassaite points, measured on both analysis days, define an isochron with a slope corresponding to an initial $^{26}Al/^{27}Al$ ratio of $6.5\times10^{-5}$, with an intercept = 0.25‰, which is within error of 0. If the fit is forced through the origin, the initial $^{26}Al/^{27}Al$ estimate climbs to $7.7 \pm 0.2\times10^{-5}$ with a reduced $\chi^2$ for this fit of 2.3. A best-fit to the rim phases yields an isochron with an initial $^{26}Al/^{27}Al = (4.9 \pm 0.2)\times10^{-5}$ and an intercept of 0.04, very close to zero (reduced $\chi^2 = 2.3$). If constrained to pass through the origin, the initial $^{26}Al/^{27}Al$ ratio changes only slightly to $(5.0 \pm 0.15)\times10^{-5}$. (Figure 3).

**Implications:** The two distinct, individually well-correlated internal isochrons imply a time interval of approximately 0.44 Ma between the original formation of E44L (through condensation from the nebula) and the high-temperature (possibly flash heating) event [3] resulting in the creation of the Wark-Lovering rim. The high initial $^{26}Al/^{27}Al$ for the interior of E44L is substantially above the classical canonical ratio of $5.0\times10^{-5}$, in agreement with the suggestion by Galy and co-workers [4] for a new solar system initial $^{26}Al$ based on ICPMS analyses of Mg isotopes in bulk CAIs.

**References:** [1] Lee T. and Papanastassiou D.A. (1974) *GRL, 3,* 225-228. [2] Galy et al. (2003) *J Anal. At. Spectrom., 18,* 1352-1356. [3] Wark D. and Boynton W. (2001) *MAPS, 36*, 1135-1166. [4] Galy et al. (2004) *LPS XXXV,* Abstract #1790.

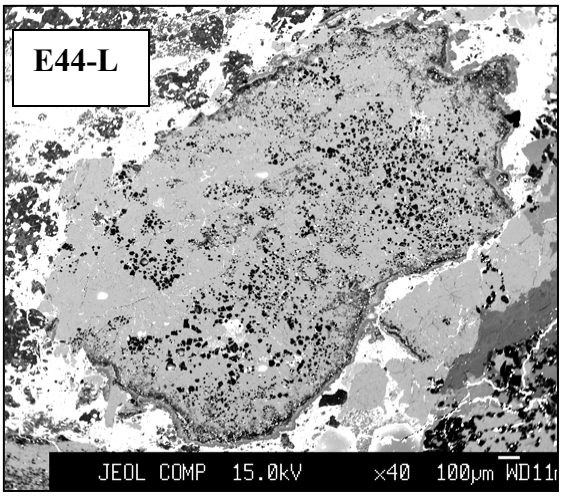


**Fig. 1** BSE image of E44L, a compact type A CAI composed of melilite, spinel, hibonite, perovskite and minor pyroxene.

**Fig 3.** Al/Mg evolution diagrams for E44L (a) Data from the interior points. (b) Data from the Wark-Lovering rim.

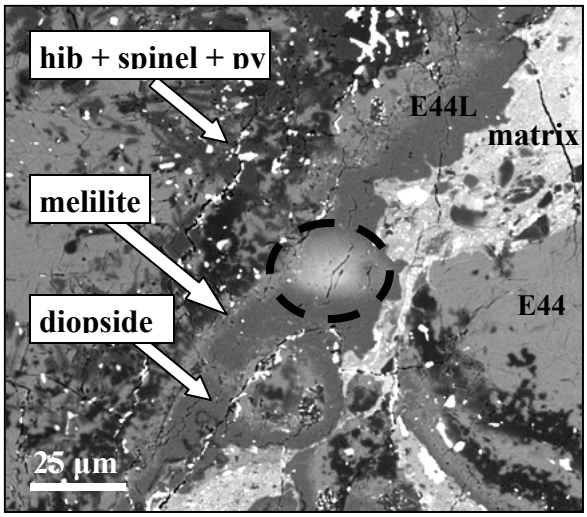


**Fig. 2.** Rim layer sequence, consisting of hibonite + spinel, melilite and diopside. Ionprobe spot lies completely within the rim diopside.

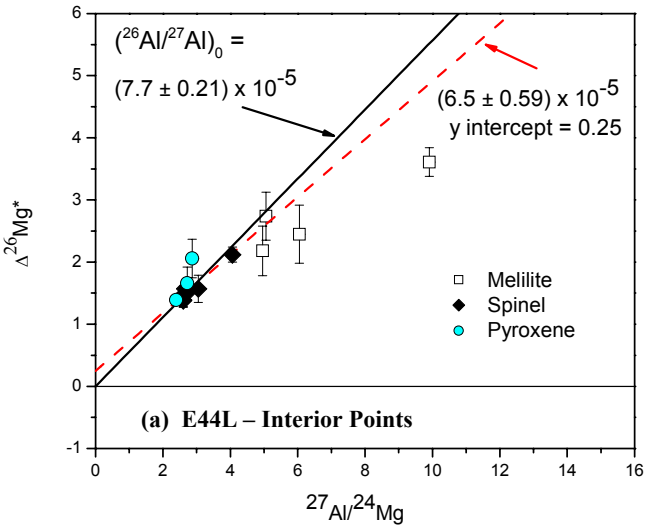


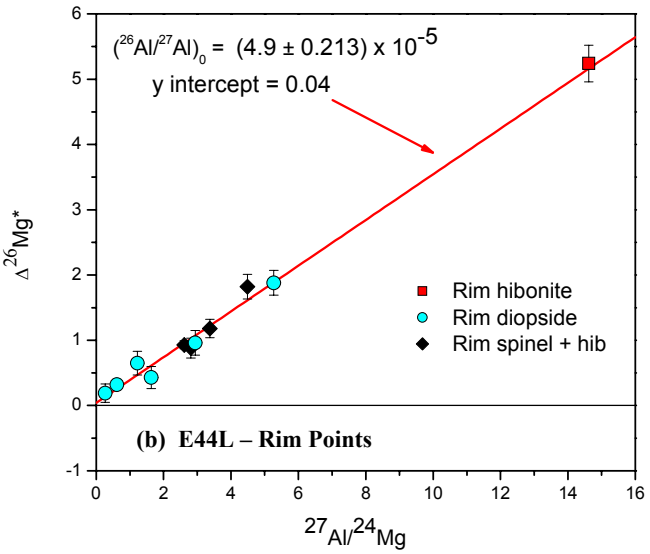

**THE COMPOSITION, ORIGIN AND EVOLUTION OF DUST IN CIRCUMSTELLAR AND INTERSTELLAR ENVIRONMENTS.** Xander Tielens[1] Rens Waters[2], and Tom Bernatowicz[3], [1]Kapteyn Astronomical Institute, Groningen, The Netherlands (tielens@astro.rug.nl), [2] Pannekoek Institute, Amsterdam, The Netherlands, [3]Physics Department, Washington University, St Louis, Missouri, USA.

Astronomical observations and analysis of stardust isolated from meteorites have revealed a highly diverse interstellar and circumstellar grain inventory, including both amorphous materials and highly crystalline compounds (silicates and carbon). In this talk we will review the dust inventory contrasting and comparing both the interstellar and circumstellar reservoirs as also the astronomical and meteoritic evidence. Interstellar dust is highly processed during its sojourn from its birthsite (stellar outflows and explosions) to its incorporation into protoplanetary systems. Of particular importance is processing by cosmic rays in the interstellar medium and by strong shocks due to supernova explosions. The latter leads to rapid destruction due to sputtering by impacting gas ions and shattering due to grain-grain collisions. We will review theoretical calculations describing these processes and the astronomical evidence for their importance. Grains are further processed by the accretion shock upon entering the nebula and also by nebular processes such as lightning. Here, we will focus on the astronomical evidence for such processing.

**NUMERICAL SIMULATION OF THERMAL CONVECTION IN CHONDRITIC PARENT BODIES.**
B. J. Travis[1], and G. Schubert[2], [1]Los Alamos National Laboratory (EES-2/MS T003, Los Alamos NM 87545; bjtravis@lanl.gov). [2]University of California, Los Angeles, Earth & Planetary Sciences Dept., schubert@ucla.edu.

**Introduction:** Chondritic meteorites are so named because they nearly all contain chondrules – small spherules of olivine and pyroxene that apparently condensed and crystallized in the solar nebula and then combined with other material to form a matrix. Their parent bodies did not differentiate, i.e., form a crust and a core. The variation in chemical composition among chondrites reflects the different thermal and chemical environments of their parent bodies, as well as the part of the solar nebula from which they arose. Carbonaceous chondrites (CCs) derived from undifferentiated icy planetesimals. As their name implies, they contain large amounts of carbon, including organic compounds, as well as silicates, oxides, sulfides, large amounts of calcium-aluminum rich inclusions (CAIs) and ice. CCs exhibit liquid water-rock interactions. Asteroids of the inner solar system are probably present-day representatives of the early planetesimals. Planetesimals are categorized in various ways – one classification considers differentiated vs undifferentiated bodies. CCs are the most primitive; their elemental composition probably is similar to the original solar system nebula. There are a number of variants: CI, CM, CV, CO, CH, CR, CK and CB, each representing different proportions of characteristic minerals.

CCs contain small but significant amounts of radiogenic elements. Radiogenic heating (e.g.,from $^{26}$Al) should be sufficient to warm up an initially cold asteroid body, even to the point of melting ice and boiling water. A warming-up phase would last on the order of a million years or so to many millions of years, depending on the size of the body, before eventually cooling back to very cold temperatures. During the warmed-up phase, liquid water would be present, and could evolve into a hydrothermal convective flow, at least for some ranges of parameters. Flowing water will affect the evolution of minerals in an asteroid.

**Previous Work**: Grimm & McSween [1] considered thermal histories of asteroids and CC parent bodies, and carried out a parameterized analysis for convective flow in a porous medium, a reasonable approximation of CC parent bodies. Rigorous stability analyses for porous convection in self-gravitating bodies have appeared recently (e.g., [2]). These demarcate boundaries in parameter space between convecting and non-convecting systems as a function of permeability, radiogenic heating and planetesimal body size.

There is a large body of literature describing numerical solutions of mass flow and energy transport in porous media for terrestrial applications (e.g., [3]); there are many fewer studies that consider flow and transport with water freezing/ice thawing. Travis et al. [4] examined porous media convection with a freezing surface with application to the planet Mars. However, there appear to be no published numerical analyses of the evolution of hydrothermal convection under such conditions as might exist in planetesimals in the early years of the solar system. In this study we have adapted a numerical solution of mass flow and energy and solute transport in porous media (called MAGHNUM) to the study of convection in planetesimals.

This paper considers numerical simulation of thermal evolution and convective motion in planetesimals; our model includes the major factors that control heating history and possible flow, namely: permeability, radiogenic element content, and radius of planetesimal. A detailed analysis is not possible in this short summary; rather, an example is given to illustrate the time course of thermal processes, duration of a convective phase and patterns of flow that might develop, and amount of fluid flow throughout the planetesimals.

**Computational model:** The MAGHNUM code ([4], [5]) can simulate dynamic freezing and thawing and 3-D flow of water and energy in a self-gravitating body such as an asteroid. Governing equations are Darcy's Law (reduced momenta equations), mass conservation, and energy conservation, plus constitutive relations (equation of state for water, and ice and temperature-dependent thermal properties for rock and ice). Equation of state tables [6] provide properties of water (density, internal energy, enthalpy, viscosity) as a function of temperature and pressure. Expressions for the thermal conductivities of ice and liquid water and the heat capacity of ice are taken from Grimm and McSween [1]. We use a volume-weighted average of rock, ice and water values to calculate an effective thermal conductivity. Hence thermal conductivity varies with temperature and ice fraction, and can vary over time at any given location. Local thermal equilibrium among the ice, liquid water and rock is assumed. MAGHNUM can solve the equation set in 1, 2, or 3-D, with time dependence, using an integrated finite difference discretization of the sphere. The version of the code used here differs from the version used in the cited references in that it provides a spherical geometry capability and computes gravity explicitly. The numerical solution has been verified by testing against a 1-D spherical Stefan solution.

**Example Simulation:** For the simulation described here, we use 25 % porosity, 1 darcy permeability (~$10^{-12}$ $m^2$), $3x10^{-8}$ wt fraction of $^{26}$Al (uniformly distributed), solid material density of 3300 kg/$m^3$, specific heat of 700 J/kg/K, body radius of 50 km, solid rock thermal conductivity of 3 W/m/K; an initial temperature of 170 K, and a constant exterior temperature of 170 K with a radiation surface temperature boundary condition.

Figures 1 and 2 summarize the results of this simulation. Figure 1 shows the temperature histories at the center and at a radius of 41 km, which is close to the permanently frozen outer shell of the body. The thickness of the frozen outer region varies in time and with location during the course of the thermal evolution. Radiogenic heating raises temperature eventually to 0 °C, then a short period of no rise occurs due to the latent heat of melting barrier, then the temperatures at the two points begin to rise and diverge. The liquid water phase begins at about 0.6 Myr and lasts over 4 Myr. The center continues to warm until about 2.5 Myr, while the point at 41 km plateaus at about 1.5 Myr and begins to slowly cool. Convection starts at about 2.25 Myr, and the temperature at 41 km then rises sharply due to upwelling of warmer water from the interior. The entire body gradually cools from 2.5 Myr on. At 41 km, re-freezing occurs at about 4.5 Myr. Peak center temperature reaches 165 °C. In this simulation, boiling does not occur, but, for a time, the system is not far from that state.

Figure 2 displays the temperature structure within the planetesimal at 2.67 Myr, near the peak of convective activity. Evident are many upwelling plumes as warm water rises towards the surface and cold water sinks towards the center. The temperature field is not perfectly symmetric; this reflects the random perturbations applied to the initial temperature field, and the fact that the radiogenic heating is decaying over time, and weakens sufficiently by 2.5 – 3 Myr that there is not time for the energy and mass flows to evolve to a symmetric state. The cumulative pore volumes of fluid that pass through any given point in the sphere will vary from point to point, reflecting the heterogeneous but patterned nature of the temperature field. Cumulative pore volumes for most points in the sphere range between 100 and 200 pore volumes, allowing water-rock reactions to proceed further than in a no-convection situation. Future studies will explore sensitivity to major parameters, and eventually include chemical transport and reactions.

**Conclusion:** We have demonstrated through numerical simulations that hydrothermal convection in a self-gravitating, radiogenically heated, permeable planetesimal with a cold exterior should occur for typical parameter values and could last for several millions of years.

**References:** [1] Grimm, R. E. & H. Y. McSween (1989). Icarus 82, 244-280. [2] Young, E. D., K. K. Zhang & G. Schubert (2003). Earth & Planetary Science Letters 213, 249 – 259. [3] Nield, D. A., and A. Bejan, (1992). Convection in Porous Media, 2nd ed. Springer, NY. [4] Travis, B.J., N.D. Rosenberg, J.N. Cuzzi (2003) JGR-Planets, 108, 8040-8054. [5] Dutrow, B. L., B. J. Travis, C. W. Gable, & D. J. Henry (2001). Geochim et Cosmochim. Acta: 65(21), 3749-3767. [6] Johnson, J. W., and D. Norton (1991). Am. J. Sci. 291, 541-648.

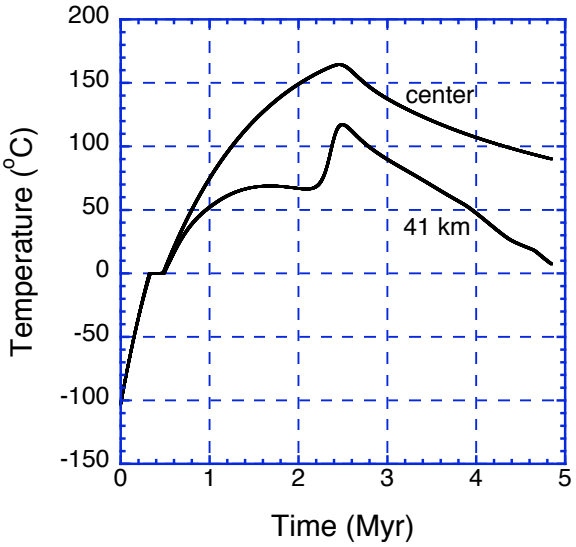


Figure 1. Temperature vs time at the center and at a point at a radius of 41 km for the sample simulation.

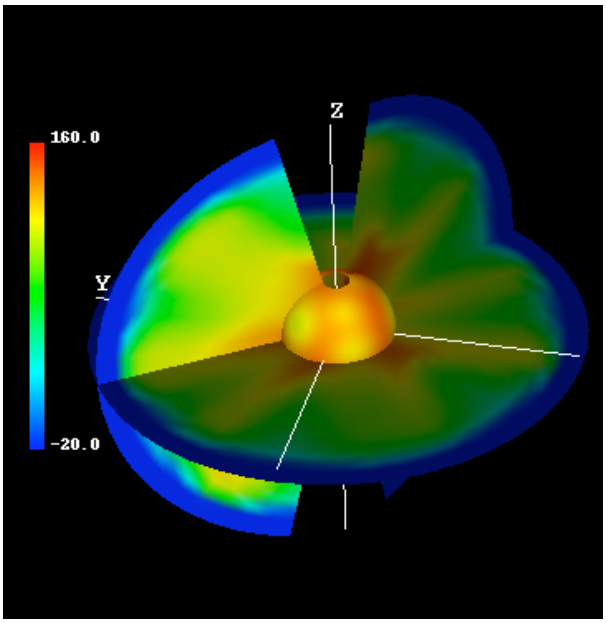


Figure 2. Temperature field on slices through the planetesimal and on a surface at radius of about 10 km, at 2.67 Myr. Blue represents temperatures less than –20 °C, and red represents hottest fluid at 160 °C.

**THREE-DIMENSIONAL SHAPES OF COSMIC SPHERULES AND CHONDRULES: COMPARISON FOR CHONDRULE FORMATION PROCESS.** A. Tsuchiyama[1], T. Yada[2], and T. Noguchi[3], T. Nakano[4] and K. Uesugi[5], [1]Department of Earth and Space Science, Osaka University, 1-1 Machikaneyama-cho, Toyonaka, 560-0043 JAPAN, akira@ess.sci.osaka-u.ac.jp, [2] Laboratory for Space Sciences Physics Department, Washington University, St. Louis, MO 63130-4899, USA, [3]Department of Material Sciences and Biological Sciences, Ibaraki University, 2-1-1 Bunkyo, Mito, 310-8512 JAPAN, [4]Institute of Geoscience, National Institute of Advanced Industrial Science and Technology, Tshukuba, 305-8567 JAPAN, [5]SPring-8, Synchrotron Radiation Research Institute, Mikazuki, 679-5198 JAPAN.

**Introduction:** 3-D structures of chondrules have been studied using X-ray microtomography [1]. It has been proposed from their external shapes and internal structures on the distribution of metal/sulfide grains and voids that chondrules were rotated at high speed (about 100-500 rps) during melting. This high-speed rotation is consistent with a shock wave model for chondrule formation [2]. Cosmic spherules are another type of spherulitic objects, which are formed by shock wave melting during entry into the Earth's atmosphere. In the present study, we examined 3-D structures of cosmic spherules and compared them with those of chondrules to discuss chondrule formation process.

**Experiments:** Fourteen cosmic spherules collected from Antarctica (120-320 μm in size) were imaged with an x-ray microtomographic system (SP-μCT) at beamline BL47XU in SPring-8 [3]. Each sample was held on a fine glass fiber (about 5 μm in diameter) with glycol phthalate. The photon energy was 10 or 13 keV for the imaging. Cross-sectional CT images are reconstructed from sets of 750 projections with a convolution back projection algorithm. The voxel (pixel in 3-D) size of the CT image is 0.5x0.5x0.5 $\mu m^3$, which gives the effective spatial resolution of about 1.5 μm [3]. 3-D structures were reconstructed from about 300-600 slices. After the imaging, two samples were cut and polished sections were made. They were observed under an SEM to compare CT images.

**Results:** Examples of CT images are shown in Figure 1. Textures of the spherules were recognized from their CT and SEM images, such as porphyritic (Fig.1a), barred olivine (Fig.1b,c) and cryptocrystalline textures. Fe-rich grains (probably magnetite) and voids are sometimes seen (Fig.1a). Compound spherules are also found (Fig.1c).

3-D external shapes of the spherules were obtained by binarization of CT images. Examples of the bird's-eye view pictures are shown in Figure 2. Prolate (Fig.2a,b) and oblate shapes (Fig.2c) are recognized. In some prolate spherules, four edges are running from one of the poles (X in Fig.2a,b) towards the equator of each spherule (we call it "edge structure"). The secondary chondrule of Fig.1c is also seen (C in Fig.2b).

The external shapes were approximated as three-axial ellipsoids with a-, b- and c-axes (axial radii are A, B and C ($A \geq B \geq C$), respectively) using the moments of inertia of the spherules, where the rotation axes with the minimum and maximum moments correspond to the a- and c-axes, respectively. The aspect ratio, p, was defined as C/A. The degree of oblate or prolate shape is defined as follows: $C/B=(B/A)^n$ and $\log(n) \rightarrow \infty$ and $-\infty$ for oblate and prolate shapes, respectively. Seven spherules were plotted on a C/B vs. B/A diagram (Fig.3) together with chondrules, which were removed from the Allende meteorite [1]. One compound spherule was also plotted but the other six spherules were not plotted because of their irregular or imperfect shapes. For chondrule shapes, two groups can be recognized: oblate to prolate chondrules with large p of 0.85-0.98 and prolate chondrules with small p of 0.74 to 0.78. The spherule shapes were also plotted onto regions similar to those of the chondrule shapes although the aspect ratios of the oblate spherules are smaller than those of chondrules and some prolate spherules are closer to general three-axial ellipsoids.

**Discussion:** The chondrule shape feature in Figure 3 can be explained by high-speed rotation during melting [1]. A melt droplet becomes oblate by rotation. If rotation rate exceeds a critical value, the shape instability occurs and the melt might become prolate. The rotation rate was estimated by a balance between the centrifugal force and the surface tension of a melt (Fig.4). If the cosmic spherules were also rotating during melting, the rotation rate for the oblate spherule should be about 1000 rps or more.

Cosmic spherules are formed by shock wave melting during their entry into the Earth's atmosphere. The shock wave model has been also proposed for the chondrule formation (e.g., [4]). The similar shape features of spherules and chondrules (Fig.3) might suggest their common formation origin. If this is the case, the both types of spherules, cosmic spherules and chon-

drules, might be formed by shock wave melting with different shock conditions. The presence of compound spherules (e.g., Figs.1c and 2b) suggests that compound chondrules can be formed by shock wave process.

In contrast to the general shape feature (Fig.3) some detailed textural and shape features of the cosmic spherules are different from those of chondrules. Voids seem to be distributed randomly in an oblate spherule (Fig.1a). This is different from chondrule textures, where voids tend to be concentrated near the short axes of oblate chondrules [1]. In the same spherule, Fe-rich objects (magnetite?) is concentrated in one side of the flat surfaces. This may suggest oxidation on this side, which was facing the Earth. The edge structure (Fig.2a,b) is probably formed by abration of spherules with the atmosphere and such structure has not be seen in chondrules. At this moment, we do not know whether the above differences are due to difference of the shock conditions between chondrule and spherule formations or due to different origin of chondrule formation.

**References:** [1] Tsuchiyama A et al. (2003) *LPS XXXIV,* 1271. [2] Susa H. and Nakamoto T. (2002) *Astrophys. J.*, 564, L57-60. [3] Uesugi K. et al. (1999) *Proc. SPIE, 3772,* 214. [4] Connolly H. C. Jr. and Love S. G. (1998) *Science*, 280, 62-67.

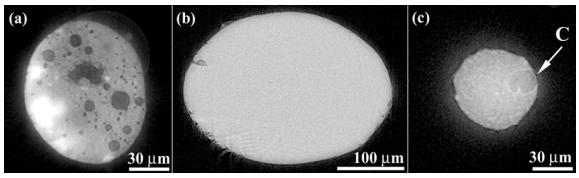


Figure 1. Examples of CT slice images of cosmic spherules. (a) Porphyritic (KW540302). (b) Barred olivine (NM6). (c) Compound (NB5): barred olivine (main part) and cryptocrystalline (secondary spherule marked by C).

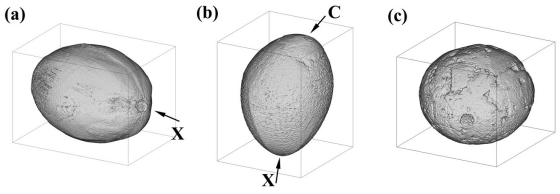


Figure 2. Examples of bird's-eye view pictures. (a) Prolate (NM6: the same sample of Fig.1b). 229 x 230 x 312 μm. (b) Prolate (NB5: the same sample of Fig.1c). 169 x 193 x 229 μm. (c) Oblate (NQ6). 133 x 162 x 164 μm. X and C show the pole of an edge structure and the secondary spherule of a compound spherule, respectively.

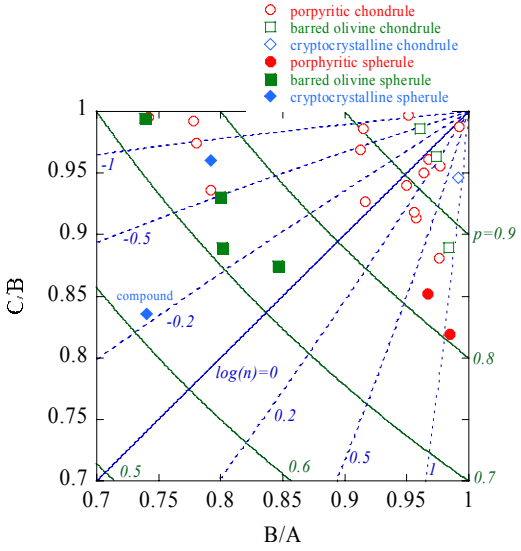


Figure 3. A diagram showing external shapes of cosmic spherules (solid symbols) and chondrules (open symbols) [1]. Spherule and chondrule textures are also shown. See text for details.

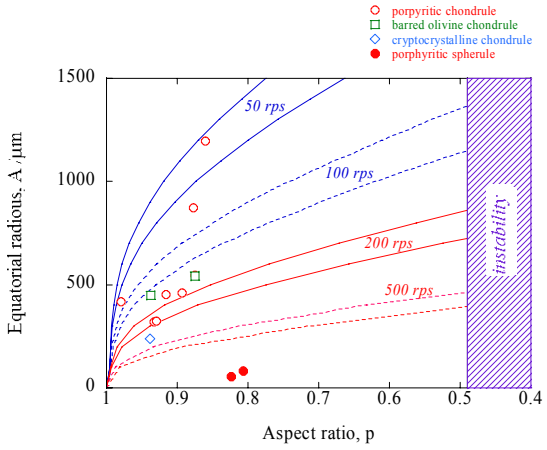


Figure 4. The equatorial radius, A, plotted against the aspect ratio, p, with estimated rotation speeds [1] for oblate spherules and chondrules. If p<0.49, a shape instability occurs.

**Experimental reproduction of relict "dusty" olivine and its implication for paleomagnetic study of chondrules.**

M. Uehara[1] and Nori. Nakamura[2], [1]Department of Geoenvironmental Science, Tohoku University, Sendai, Japan: syok@dges.tohoku.ac.jp, [2]Department of Geoenvironmental Science, Tohoku University, Sendai, Japan: n-naka@mail.tains.tohoku.ac.jp.

**Introduction:** Paleomagnetic study of individual chondrules in carbonaceous chondrites indicated a paleointensity of 0.1~0.7mT [1], which might give a constraint on primitive solar nebular magnetic fields that played a role in the early evolution of the solar system [2, 3]. Previous paleomagnetic studies of carbonaceous chondrites qualitatively recognized that large-dimension chondrules possess a strong and stable remanence, while small-dimension chondrules do a weak and unstable one [4]. Wasilewski and Saralkar [5] interpreted this as a different mineralogy that stable chondrules contain sulfide, while unstable chondrules contain spherical masses of FeNi metal. However, their observation scale is limited on optical microscope responsible for magnetically unstable multidomain state of magnetic minerals.

Recent studies of relict "dusty" olivine (i.e., olivines containing abundant submicron-sized inclusions of Fe-Ni metal) in primitive meteorites have confirmed that dusty olivine can be reproduced by reduction of FeO-rich olivines at high-temperature [6], even though it is considered that "dusty" olivines are remnants of previous chondrule forming events [7]. This suggests the dusty olivines are formed by a high-temperature sub-solidus reduction above Curie temperature. Therefore, the chondrules containing "dusty" olivines are likely to reflect a stable thermal remanence in reducing condition during chondrule formation because of their submicron-sized inclusions. Here, we report an experimental reproduction of "dusty" olivines by dynamic crystallization apparatus to investigate a magnetic stability of these olivines, and propose an alternative interpretation for the origin of stable chondrules, implying a new candidate of remanence carrier in chondrites.

**Techniques:** Dynamic crystallization experiments were conducted in which starting material was reduced in the presence of graphite. The starting material was a crushed olivine (Fo86, $\phi$=10-50μm) from mantle rock fragments of the Ichinomegara volcanic crater, NE Japan. Some of experiments added carbon in the form of graphite powder into olivines. Approximately 10-50mg of the material was placed in a hand-made graphite crucible that is 3.5mm in diameter and 8mm in height, resulting in a reduced condition. It was heated in a fabricated evacuated quartz glass tube furnace under 1-12mT magnetic field by solenoidal coil. The crucible was heated to peak temperature (1140 – 1450°C), held it for 500 to 3000sec, and cooled at 1000-20000°C /hr down to 750°C, then quenched.

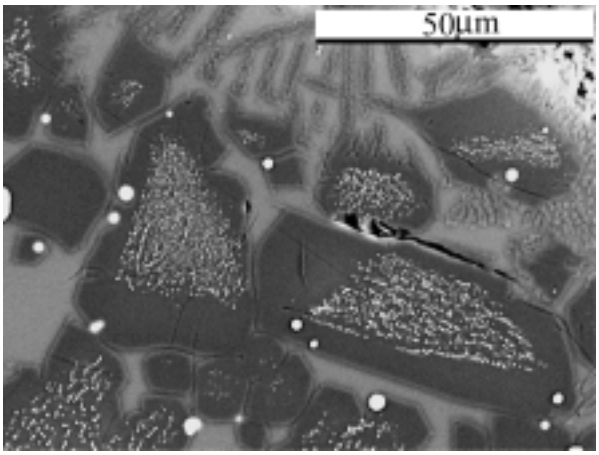


Fig.1 Back-scattered electron image of an assemblage of Fo-rich olivine, silicate glass, and metal in "dusty" olivines produced under reduction experiments (peak temperature 1310°C, rapid cooling). The metallic phases are present as submicron-sized (<1μm) Fe-rich inclusions within olivine grains and micron-sized (1 to 50μm) Fe-Ni globules embedded in the matrix. Submicron-sized Fe-rich inclusions show preferential alignments along the (100) plane of the olivine host.

**Preliminary results:** " Dusty" olivine was reproduced in slowly cooled experiments, even in rapidly cooled ones. " Dusty" olivine is absent in experiments, when the starting material was small in quantity. The synthetic "dusty" olivine specimens were stepwise alternating field (AF) demagnetized to 180mT, and were strongly stable up to 80mT. Back-scattered electron scanning microscopy observation with energy-dispersive X-ray spectrum confirmed that the reduced olivines yielded assemblages of Fo-rich olivine, interstitial glass ($Al_2O_3$, CaO), and metal (Fe-Ni-Cr) (Fig. 1). The metal phase is present either as submicron-sized Fe-Ni inclusions embedded in olivine,

mimicking natural "dusty" olivines, or as micron-sized Fe-Ni-Cr globules (1~50μm) located in the glass matrix at the olivine grain boundaries. This result parallels to the *in situ* reduction experiment [6].

**Implication for paleomagnetic study of chondrules:** AF demagnetization of "dusty" olivines indicates a mean destructive field of up to 80mT, inferring very stable remanence. However, hysteresis measurements of the olivines indicate a multidomain-like behavior despite of the presence of submicron inclusions of Fe-Ni metal. These two observations contradict each other. The behavior can be explained by the stronger signal of micron-sized metal globules (1~50μm) located in the glass matrix than submicron-sized Fe metal inclusions (Fig. 1). Thus, this contradiction suggests that one cannot determine a significance of the remanence from hysteresis properties. Also, the very stable remanence carried by abundant submicron-sized Fe-Ni inclusion within "dusty" olivine might be an alternative origin for stable remanence in large-dimensional chondrules.

Our experimental study suggests that "dusty" olivines is suitable for paleomagnetic studies, because they contain submicron-sized Fe-Ni inclusions within olivines, which is capable of carrying stable, high coercive thermal remanence. Moreover, submicron-sized inclusions may have been "armored" against alteration by rims of clear Mg-rich olivine, such as fine-grained magnetite embedded in a terrestrial submarine basalt glass [8]. Therefore, the existence of pristine, submicron-sized Fe-Ni inclusions in "dusty" olivine of ancient meteorites that have undergone significant alteration implies that such "dusty" olivine chondrules are a good candidate as a reliable recorder for an ambient magnetic field in reducing nebular condition in the early solar system.

**Acknowledgments**: We thank Minoru Funaki for access to the paleomagnetic facilities at National Institute of Polar Research. N.N. was supported by the Ministry of Education, Science, Sports and Culture Grant-in-Aid for Young Scientists (B): 14740290.

**References:** [1] Cisowski, S. M. (1987) In: *Geomagnetism, 2,* 525–560. [2] Shu, F. et al. (2001) *Astrophys. J., 548,* 1029-1050. [3] Nakamoto et al. (2004) *LPS, XXXV*, abst. #1821. [4] Sugiura N. et al. (1979) *PEPI*, *20*, 342-349. [5] Wasilewski, P. and Saralkar, C. (1981), *LPS, XII*, 1161-1163. [6] Leroux, H. et al. (2003) *Meteoritics & Plant. Sci., 38*, 81-94., Connolly et al. (1994) *Nature, 371*, 136-139. [7] Jones, R. H. and Danielson, L. R. (1997) *Meteoritics & Plant. Sci., 32*, 753-760. [8] Zhou, W. et al. (1999) *Geology*, *27*, 1043-1046.

**DIFFICULTIES OF CHONDRULE FORMATION BY NEBULAR SHOCK WAVES.** M. Uesugi[1], T. Akaki[1], M. Sekiya[2], T. Nakamura[2], A. Tsuchiyama[3], T. Nakano[4] and K. Uesugi[5], [1]Department of Earth and Planetary Sciences, Graduate School of Sciences, 33 Kyushu University, [2]Department of Earth and Planetary Sciences, Faculty of Sciences, 33 Kyushu University, [3]Department of Earth and Space Science, Graduate School of Science Osaka University, [4]Geological Survey of Japan, National Institute of Advanced Industrial Science and Technology (AIST), [5]Japan Synchrotron Radiation Research Institute (JASRI/SPring-8).

**Introduction:** Recently, chondrule formation due to nebular shock waves has been examined from viewpoints such as thermal history [1-3] and size distribution of final products [4]. The authors of these studies agree with that chondrule formation due to nebular shock waves is consistent with those natures of chondrules. However, all of these investigations simplified or even ignored the processes during the formation of chondrules, such as melting and resolidification, internal flow of melted chondrules, transportation of the materials inside of chondrules and formation of compound chondrules. We examine two distinctive processes of nebular shock wave heating, transportation of iron-sulfide inclusions by internal flow of molten-silicate and formation of compound chondrules. A recent study has shown that if chondrules are melted by nebular shock waves, a high-speed (~10 cm $s^{-1}$) rotational flow occurs in chondrules during melting [5] and the final distribution of iron-sulfide inclusions in chondrules would be largely affected by the internal flow. And also, if molten or half molten chondrules are collide each other at a suitable range of relative velocity, they would stick and form compound chondrules. In order to investigate whether those microtextures of chondrules can be formed by shockwave heating, detailed two and three dimensional observation was performed on chondrules in some classes of primitive chondrites.

Results of our investigations showed that the distribution of iron-sulfide inclusions in chondrules and formation of compound chondrules are both difficult to be accounted by the nebular shockwave heating.

**Iron-sulfide inclusions inside of chondrules:** In previous studies, we have examined the nebular shock wave model of chondrule formation from the viewpoint of size and distribution of iron-sulfide inclusions in chondrules [6]. Figure 1 shows the X-ray CT image of a chondrule in Y-791717 (CO3) chondrite. As seen in the figure, large iron-sulfide inclusions are often contained inside (do not reach the surface) of chondrules. However, the results of numerical calculations show that the iron-sulfide inclusions must quickly (<< 1 s) reach the surface of chondrules if the radius ratio of the iron-sulfide inclusion to the host chondrule exceeds 0.2, because the high speed internal flow brings them to the surface of the melted chondrule.

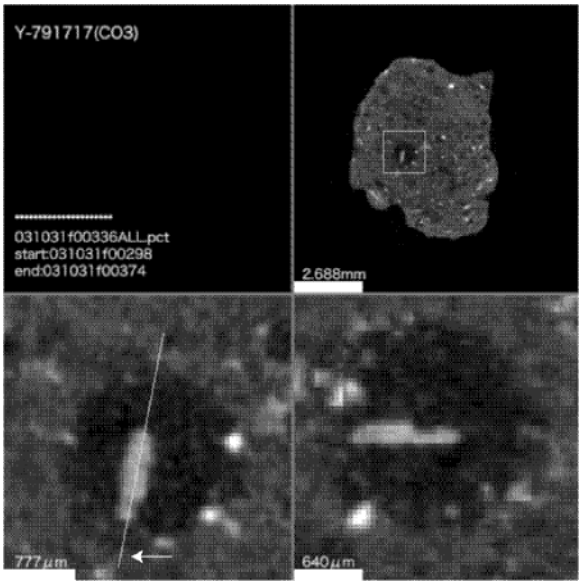


Fig. 1 An X-ray CT image of a chondrule and a large iron-sulfide inclusion in Y-791717 (CO3) chondrite. (Upper right) A whole view of a cross section of the meteorite chip. (Lower left) An enlarged view of the square in upper right part of the image. The dark spherical object is a chondrule and white inclusions inside of the chondrule shows iron and iron-sulfide inclusions. The line of the cross section indicates the direction of cross section. (Lower right) A cross sectional view of the chondrule shown in the lower right image.

The result indicates that the iron-sulfide inclusion that have a radius ratio larger than 0.2 could not remain inside of chondrules, if chondrules were formed by nebular shock waves. However, as shown in Fig. 1, such large iron-sulfide inclusions are included inside of some chondrules. The presence of the off-centered large iron-sulfide inclusions is inconsistent with the chondrule formation by nebular shock waves.

**Formation of compound chondrules:** Here, we show another difficulty of chondrule formation by nebular shock wave heating. Compound chondrules, which consist of two or more chondrules sticking each other, are occasionally found in natural chondrites. When they formed, one of constituent chondrules has already solidified while the other has still molten (Fig. 2). We estimated the probability of sticking of chondrules in the nebular shock wave. In the nebular shock wave, the drag force varies between chondrules depending on their size and chondrules have different relative velocities.

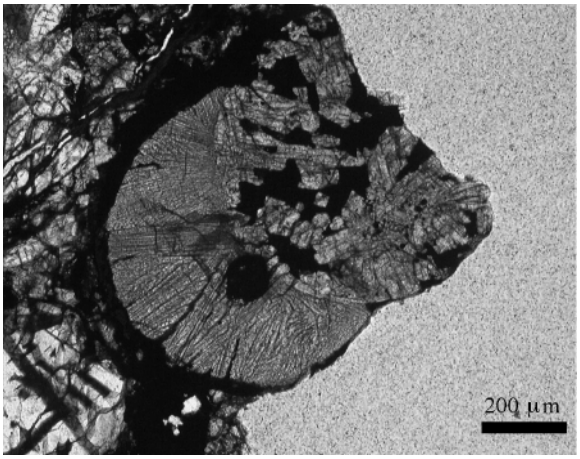


Fig. 2 A transmitted light image of a compound chondrule in ALH-77260 (L3) chondrite. A radial pyroxene chondrule attached on a porphyritic pyroxene chondrule. Dark portions in the chondrules are oxidized iron or iron-sulfide inclusions.

If the relative velocity is sufficiently small, they can stick to each other without disruption. Figure 3 shows that the relative velocity of two different sized chondrules. As seen in Fig. 3, if the radii of chondrules differ by more than 10% at 0.3 mm, the relative velocity becomes very large. This means that nebular shock wave heating could not make the compound chondrules that have radius difference more than 10%, because the collision between those chondrules leads to disruption of them, not leads to sticking. Even the solid chondrules would be disrupted if the relative velocity exceeds 76 m $s^{-1}$ [7]. In the nebular shockwave model, the thermal history and the degree of melting at a certain distance from the shock front strongly depend on the radius of chondrules. If the compound chondrules are formed in the nebular shock wave, their radius, and then their texture must always be similar or same. However, the natural compound chondrules have various combination of their texture [8]. This is the second difficulty of chondrule formation by nebular shock waves.

**Discussion:** We showed two inconsistencies between textures expected from theoretical shock-wave model and those observed in natural chondrules. These results indicate that the chondrule formation by nebular shock waves is considered to be unlikely.

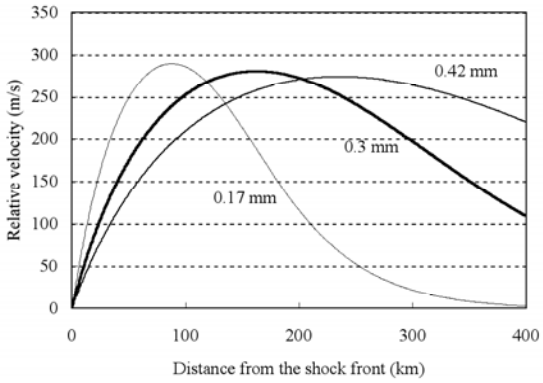


Fig. 3 Relative velocity between two different sized chondrules. Each curve shows that the relative velocity between the chondrules that have radius shown by the captions and that have 10% smaller than the captions.

**References:** [1] Iida A. et al. (2001) *Icarus, 153,* 430-450. [2] Desch S. J. and Connolly H. C. (2002) *Meteorit. Planet. Sci., 37,* 183-207. [3] Ciesla F. J. and Hood L. L. (2002) *Icarus, 158,* 281-293. [4] Miura H. et al. (2002) *Icarus, 160,* 258-270. [5] Uesugi M. et al. (2003) *Earth Planets. Space, 55,* 493-507. [6] Uesugi M. et al. (2004) *submitted*. [7] Ueda T. et al. (2001) *Earth Planets. Space, 53,* 927-935. [8] Akaki T. and Nakamura T. (2004) *submitted*.

**DISTANT EXTRASOLAR PROTOPLANETS IN NURSERY PROPLYDS AND MASS DETERMINATION OF PROTOSTARS.** I. E. Val'tts, S. Yu. Lyubchenko, and V. I. Slysh, Astro Space Center of the Lebedev Physical Institute, Profsoyuznaya Str., 84/32, Moscow 117997, Russia (ivaltts@asc.rssi.ru).

We develop a method of detecting very distant planet-like bodies, based on study of molecular maser emission in the atmosphere of planets situated in the edge-on protoplanetary disks.

Circumstellar, or protoplanetary disks could be very common. Many of them have been detected with the Wide Field Camera of the Hubble Space Telescope (see, for example, [1]). In general a processs prior to the formation of a disk could be described as follows.

Active star formation occurring in the clouds of interstellar gas is observed everywhere in the Galaxy. Star forming regions contain objects at different stages of evolution. High-mass O-stars ionize neutral gas by producing ultra-compact HII regions, and control the formation of nearby stars. Young pre-main sequence stars usually are deeply embedded and show no optical emission. If they have not yet developed an UCHII, they could be surrounded by dust core, contiguous with the boundary of HII region, where content of various molecular species is enchanced due to evaporation of icy grain mantles. The grains may stick together and form large icy solid bodies.

The sublimation of ice composed of a mixture of water and methanol as in the interstellar dust particle ice mantles [2-4] could be a source of gaseous methanol and OH (from $H_2O$ dissociation) in a shell around the solid bodies [5]. OH, water and methanol can emit strong, narrow maser lines in the microwave band.

The ice evaporation could take place from the surface of particles or stones forming rings around the planets, similar to the rings of Saturn. The size of such bodies might be the same as the size of Edgeworth-Kuiper Belt Objects, or rather similar to the size of outer moons of Jupiter - Ganymede and Callisto - with the surface covered by ice.

Among the most widespread interstellar masers are class II methanol masers emitting in the $5_1$-$6_0A^+$ transition at 6.7 GHz, which are formed at the energy levels pumped by far infrared radiation from protostellar cocoon or neighbouring UCHII region [6].

High-resolution images of such masers demonstrate a structure which can be interpreted as the circumstellar disk, with Keplerian motion of the maser spots as protoplanets around central protostellar object (see, for example, [7]). The main goal of our work was to produce a model of methanol maser and thermal emission in the disk and to obtain mass of the central protostar and to evaluate mass of protoplanets.

It was done on the basis of studying of methanol maser spectra and their fine space structure. Masses of 12 protostars were derived as central masses in the protoplanetary disks [8]. The hypothesis was taken into account that class II methanol maser lines are formed in an edge-on Keplerian disk, while the thermal methanol emission and CS lines are formed in a cocoon surrounding protostar. This fact provides an information about protostar velocity and methanol maser condensation velocities relative the disk center - see sketch.

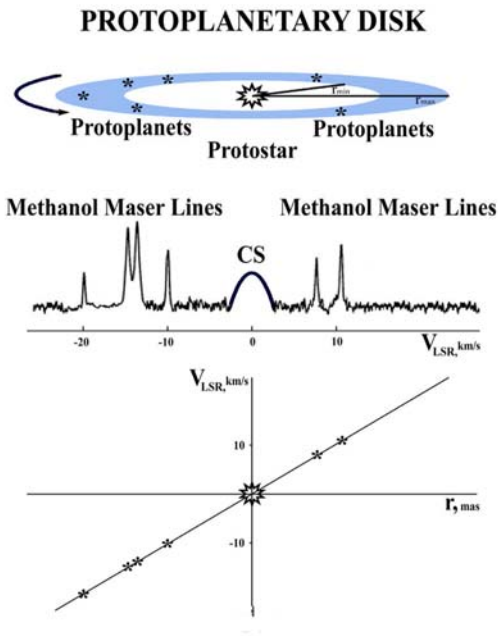


**Sketch:** a model of location of methanol maser condensations (i.e. protoplanets) in protoplanetary disk, and the profile of lines of hypothetical methanol maser source. A cocoon providing thermal radiation in CS line and thermal methanol lines is not pictured. In lower part of the figure is shown respective V(r) diagram if a Keplerian disk is observed.

**References:**

[1] O'Dell C.R. et al. (1993) *ApJ*, *410*, 696.

[2] Allamandola L. J. et al. (1992) *ApJ*, *399*, 134.

[3] Skinner C. J. et al. (1992) *ApJ*, *399*, L79.

[4] Bockellée-Morvan D. et al. (1994) *A&A*, *287*, 647.

[5] Slysh V. I. et al. (1999) *Ast. Rep*., *43*, 657.

[6] Menten K. M. et al. (1986) *A&A*, *157*, 318.

[7] Norris R. P. et al. (1998) *ApJ*, *508*, 275.

[8] Val'tts I. E. and Lyubchenko S. Yu. (2004) *Ast. Rep*., *48*, 210.

**CAI REFRACTORY RIMS: DISTINGUISHING BETWEEN FORMATION BY FLASH HEATING OR REVERSE CONDENSATION.** D.A. Wark[1,2], [1]Earth Sciences, University of Melbourne, Parkville 3010, Australia; [2]Physics & Materials Engineering, Monash University, Clayton 3800, Australia. (davidwark@ozemail.com.au)

**Introduction:** In CV chondrite CAI's, the concentrations of ultra-refractory elements in the Wark-Lovering (WL) rims are several times higher than in the underlying CAI's [1,2] and were derived from the CAI's, as the rims and CAI's have identical ultra-refractory element *patterns*. The conclusion that the ultra-refractory rim elements are not condensates onto the CAI's but were derived from the CAI's is particularly compelling in Type B1 CAI's whose rims have Rare Earth patterns parallel to those of the underlying, *igneously fractionated* melilite mantle*s* and not to the patterns of the bulk CAI's.

In order to produce the ultra-refractory rim, the more volatile major elements Mg, Si & Ca in the original outer CAI must have been removed to leave a residue of ultra-refractory elements (Al, Ti, Zr, REE, Ir, Pt, etc). Two competing models, Flash Heating and Reverse Condensation, have been proposed to account for the removal of volatiles. This work suggests experiments for testing each model.

Note: Since the *present* WL rims consist mainly of spinel, melilite & pyroxene layers, some Mg, Si (& Ca) must have re-entered the initial ultra-refractory residue. This work is concerned only with how the ultra-refractory rim residue was created, not with how the present layers were produced from it.

**The Flash Heating Model:** Flash Heating envisages removal of volatiles during an intense, brief volatilization event [2]. Boynton has calculated [3] that ~300 J/cm$^2$ is required to volatilize a 200 m thick outer layer of CAI and leave a typical 5-fold ultra-refractory enriched rim residue. The energy must be deposited within ~1 sec to allow only a thin surface layer to be melted and to prevent the interior from being melted by inwardly conducted heat. The absence of melting below the rim of 'fluffy' Type A (FTA) CAI's is the key constraint on the duration of Flash Heating, which would also require surface volatilization temperatures >2500K [4].

The difficulties that such extreme requirements pose for astrophysical models, and the failure so far of laser experiments [5] to produce the required volatilization without deep melting, lead us to a re-examination of the rationale for Flash Heating.

**Key requirements for refractory rims:** (1) The outer CAI was volatilized to leave an ultra-refractory residue, and (2) the underlying CAI did not melt. These requirements could be met, and the stringent time constraint avoided, if volatilization occurred without melting i.e. *subsolidus*. This is the basis of the Reverse Condensation model.

**The Reverse Condensation Model:** FTA CAI's [6], and many other precursor materials in melted 'compact' Type A (CTA) and type B CAI's, are solid condensates for which Grossman [7] calculated the equilibrium condensation sequence in cooling nebular gas: corundum, hibonite, melilite, spinel, pyroxene, etc. Palme [8] calculated the analogous condensation sequence for metals.

What would happen to a solid condensate if the falling temperature reversed and rose again (or, equivalently, if pressure fell) ? The solids that had condensed would begin to volatilize, the most volatile first and the ultra-refractories last, reversing the condensation sequence.

Davis has reported [9] subsolidus 'reverse condensation' experiments in which ultra-refractory hibonite was produced at the surface of solid synthetic CAI's heated in hydrogen at 1 atm pressure. Volatile elements lost from the outer layer were replaced so slowly by diffusion from the underlying solid that a refractory residue, expected to contain minimal heavy isotope enrichment, was formed at the rim.

Reverse Condensation thus appears to be a potential mechanism for producing ultra-refractory rims on CAI's. Most importantly, it would occur slowly at temperatures comparable to those at which CAI's condensed, and would relieve the astrophysical modelling difficulties posed by intense, rapid Flash Heating.

**Isotopic measurements to distinguish Flash Heating from Reverse Condensation:** Reverse Condensation would probably produce minimal isotopic mass-dependent fractionation in Mg, Si, Ca & O in the refractory residue, as noted above. On the other hand, volatilization from a Flash Heated melt could produce significant mass-dependent fractionation and an isotopically 'heavy' residue, *provided* that the rates of volatilization and diffusion in the melt were comparable, and also that the element was not completely volatilized.

Hence, the discovery of isotopically 'heavy' element compositions in rims would be *prima facie* evidence for volatilization from a melt. The absence of an isotopically 'heavy' rim would not, however, prove Reverse Condensation or disprove Flash Heating, which might have occurred too fast for isotopic fractionation to take place.

**Unsuitable elements and samples:** Type B1 and CTA CAI's mantles are likely to contain isotopically 'heavy' Mg and Si as a result of the melting and volatilization [10] that they underwent prior to the rimming event. Some of this 'heavy' Mg and Si in the mantle would have entered even rims formed by Reverse Condensation. The finding of 'heavy' Mg or Si in such rims would therefore not be proof of Flash Heating. The finding of isotopically 'normal' Mg or Si in such rims would also not disprove Flash Heating, since 'normal' Mg and Si (needed to make the spinel, pyroxene, etc layers) re-entered the refractory residues, which could well have been almost devoid of volatile Mg & Si immediately after Flash Heating. Thus, Mg & Si isotopic measurements in Type B1 or CTA rims will not indicate how refractory rims formed.

**Suitable elements and samples:** Unmelted condensate 'fluffy' Type A (FTA) CAI's are expected to have isotopically 'normal' or 'light' compositions. If an FTA rim were isotopically 'heavier' than the interior, that would be evidence for melting and volatilization during the rim-forming process i.e. for Flash Heating. However, absence of an isotopically 'heavier' rim would not disprove Flash Heating which might have been too rapid for isotopic fractionation to occur. The absence of 'heavier' Mg or Ca in the rim of an FTA would leave the question open as to whether the rim formed by Flash heating or Reverse Condensation.

In contrast to the situation for Mg & Si in Type B1 and CTA's discussed in the previous paragraph, the presence of 'heavy' Ca in the rim of a Type B1, CTA or FTA would be evidence for 'Flash Heating'. This is so because there was probably little volatilization loss, and little isotopic mass fractionation, of the rather refractory Ca during mantle formation prior to rimming. (No evidence for Ca mass-fractionation differences between a Type B1 CAI core & mantle was found by SHRIMP II ion microprobe at the ANU [11]).

However, Ca probably did experience significant volatilization during the rim-forming process because Eu (of similar volatility to Ca) is heavily depleted in rims. If the volatilization were due to Flash Heating (with melting) then the residual Ca is likely to be isotopically 'heavy'. Hence 'heavy' Ca in the rim of a Type B1, CTA or FTA would suggest Flash Heating, while the presence of 'normal' Ca in the rim would be inconclusive.

**Isotopic Analyses in Progress:** The isotopic compositions of the rims on two CAI's are being analysed with the aim of presenting evidence at the Conference on whether refractory rims were formed by Flash Heating or by Reverse Condensation. The first sample is Allende FTA 20A,J which has rare unaltered melilite in the rim, plus spinel and perovskite, whose Mg & Ca isotopic mass-fractionations can be compared with those of the same phases in the interior.

The second sample is Leoville CTA #1. Its rim has unusually thick hibonite, plus melilite, perovskite and diopside whose Ca mass-fractionation can be compared with that of melilite and perovskite in the interior.

**Conclusions:** The discovery in the above rims of 'heavy' Ca &/or Mg would strongly suggest that Flash Heating caused the ultra-refractory enrichment in rims. If isotopically 'heavy' rims were not found it would, however, leave the question unanswered as to whether Flash Heating or Reverse Condensation (or some other process) were responsible.

This is an important question to answer because the requirements of Flash Heating are so extreme. If Flash Heating is a myth, then it may severely and needlessly deform astrophysical models. On the other hand, if Flash Heating is true, then it offers a unique window into some of the extreme conditions in the early solar nebula.

**References:** [1] Boynton W.V. and Wark D.A. (1984) *Meteoritics, 19,* 195–197. [2] Wark D. A. and Boynton W.V. (2001) *Meteoritics & Planet. Sci., 36,* 1135-1166. [3] Boynton W.V. (1988) *Meteoritics, 23*, 259. [4] Wark D. A. and Sun S. (2001) *Metsoc.Conf., Rome,* Abstract #5431. [5] Wark D.A. and Brandt M. (2004) unpubl.data. [6] MacPherson G.J. and Grossman L.A. (1984) *Geochim. Cosmochim. Acta, 48,* 29-46. [7] Grossman L.A. (1972) *Geochim.Cosmochim.Acta, 36,* 597-619. [8] Palme H. and Wlotzka F. (1976) *EPSL,33,* 45-60. [9] Davis A.M. *et al.* (2004*) Meteoritics & Planet. Sci. Suppl. 39*, A 29. [10] Grossman L.A. *et al.* (2000) *Geochim. Cosmochim. Acta, 64,* 2879-2894. [11] Holden P *et al.* (2004) unpubl. data.

**Petrographic Evidence for Rapid Heating and Cooling during Chondrule Formation.** J. T. Wasson, Institute of Geophysics and Planetary Physics, University of California, Los Angeles 90095-1567 USA.

**Introduction**. The chondrule cooling rates used in most chondrule-formation models appear to be too low. Recent petrographic evidence [1] indicates that the amount of crystal (especially olivine) growth that occurred after the last melting event was about 30× smaller than the grain sizes simulated in order to estimate cooling rates. The smaller amount of growth leads to an upwards revision of cooling rates by about a factor of 1000.

Most chondrules are porphyritic. They consist of large and small crystals of olivine and, less commonly, pyroxene immersed in a mesostasis having a plagioclase-rich composition. In the most primitive chondrites the mesostasis is often vitreous.

Because the large majority of chondrules contain FeS, it is clear that the nebula had cooled below the FeS condensation temperature (ca. 650 K) before chondrule formation occurred. The high FeO/(FeO+MgO) ratios of some chondrules require still lower nebular temperatures (<500 K) [2].

The traditional view has been that porphyritic chondrules formed in a single heating/cooling event and many laboratory experiments have been carried out in various kinds of kinds of furnaces to try to simulate the formation of chondrules textures in a single heating/cooling cycle [3, 4]. These furnace experiments have been used to infer the cooling rates of chondrules during the temperature range at which olivine crystallized from the melt. Most of these inferred values are in the range 0.01-1 K $s^{-1}$ [5].

These low cooling rates are problematical because there is no long-term nebular environment that yields such values. In transparent regions chondrules would cool at rates orders of magnitude higher, whereas in an opaque nebular disk the cooling rates would be many orders of magnitude lower. And these latter conditions are not suitable locations for chondrule formation because such high temperatures would cause the complete evaporation of chondrules (which have melting temperatures about 600 K higher than their evaporation temperatures) [2].

During the last several years several kinds of petrographic evidence indicating rapid chondrule cooling have been recognized. These include thin overgrowths on relict grains, clusters of small crystals that grew following the most recent melting event, and fragments preserving shard-like shapes that would have been hidden had several tens of micrometers of new growth occurred following the last melting event. And there are other indications of rapid cooling including the preservation of volatiles such as FeS and one case where the modeling of O-isotopic and FeO/(FeO+MgO) gradients indicated a high cooling rate [6].

**Petrographic evidence**. Because aqueous alteration can confuse the evidence in chondrites showing appreciable effects (such as such as CR, CM and CV) we have limited our studies to LL3.0 Semarkona, CO3.0 Yamato 81020, and the ungrouped type-3.0 carbonaceous chondrite Acfer 094.

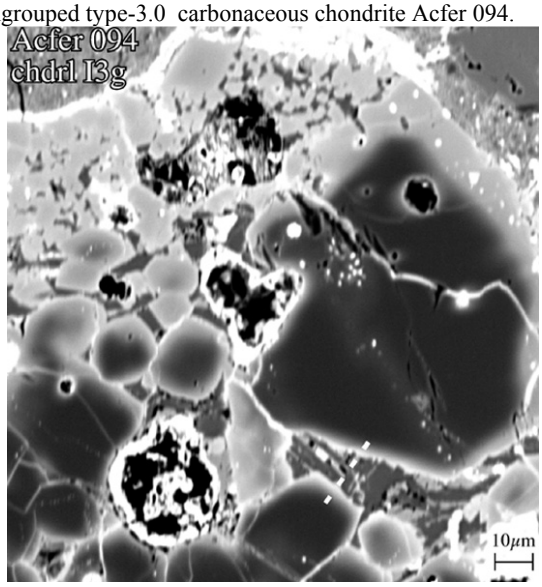


Fig 1. Cluster of relict olivines in Acfer 094 chondrule I3g. At the dashed line overgrowth thickness is ~4 μm.

The most telling evidence for rapid cooling consists of overgrowths on relict grains; these form in melting events in which the mesostasis melts and phenocrysts remain as largely intact substrates for the overgrowths. Wasson and Rubin (2003) surveyed and discussed high-FeO overgrowths on low-FeO olivine grains in Y81020 and observed that more than 90% of the high-FeO (type-I structured) chondrules contain low-FeO relicts with thin overgrowths adjacent to mesostasis (necessary to allow unimpeded growth during cooling). The apparent thickness of overgrowths oblique to the plane of the section are too high; after allowance for this it appears that all overgrowth thicknesses are in the range 4-5 μm. This is the property that needs to be reproduced. The high-FeO chondrules in Acfer 094 show similar features; in Fig. 1 the dashed line marks a position where low-FeO olivine grains on opposite sides of a patch of mesostasis each show high-FeO overgrowths about 4 μm thick. Similar overgrowth thicknesses are observed on phenocrysts in ordinary-chondrite chondrules. Fig. 2 shows a shard-like low-FeO fragment from Semarkona with an FeO-rich overgrowth that is about 4 μm thick in the narrowest regions. In some high-FeO pyroxene-rich chondrules in Semarkona up to four successive 4-5 μm growth layers are observed; these are preserved because cation diffusion is much slower in pyroxene compared to olivine. we interpret these to reflect successive melting events in which the melt fraction was largely confined to the mesostasis. Although it is more difficult to recognize overgrowths on phenocrysts in low-FeO chondrules, they are visible on the surfaces of olivine grains that contain clouds of dusty metal in their interi-

ors, where they are observed to have the canonical thickness of 5-10 μm [7]. Olivine precipitates at higher temperatures in low-FeO chondrules, thus overgrowths are expected to be slightly thicker .

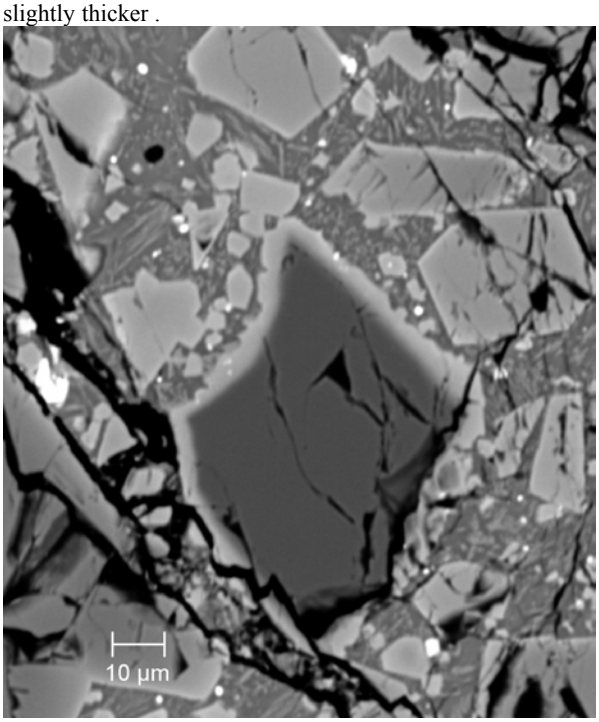


Fig. 2 Semarkona chondrule Q8b. The high-FeO overgrowth on this olivine shard is about 4 μm thick.

**Constraints on chondrule formation models**. Thus 4-5 μm overgrowths are the feature that needs to be reproduced in laboratory simulations, not the gross porphyritic structures of the chondrules. The impact these thin growth layers have on inferred cooling rates can be readily modeled.. Olivine has higher Fe and Mg and lower Si contents than the mesostasis melt. A reasonable assumption is that olivine growth requires the diffusion through the melt of Fe and Mg towards and Si away from the growing surface, and that growth stops when the temperature drops to a value below which negligible additional growth occurs. This "blocking" temperature will depend on the cooling rate but, because diffusion coefficients vary exponentially with temperature, the actual values will probably differ by only a few tens of degrees. We will define $\Delta t$ to be the interval between the maximum temperature reached by the melt and the blocking temperature. Because most growth occurs in the high portion of this range, the difference in blocking temperature is negligible for the purposes of this approximation. It thus follows that where D, the mean diffusion coefficient during the growth period, should be independent of the cooling rate.

If the growth rate is limited by the diffusion of constituents through the mesostasis melt, the thickness X of the overgrowth is given by:

$$X = \left(D \cdot \Delta t\right)^{0.5}$$

We will assume that the 4-5 μm overgrowth thickness is 30× smaller than the half-thickness of the phenocrysts that led to an estimated cooling rate of 1 K/s in published furnace simulations. It then follows that the correct cooling rate is about $10^3$ K/s. This cooling rate applies at the olivine liquidus temperature for the individual chondrule, probably generally in the range 1600-1800 K.

A cooling rate of $10^3$ K/s is an order-magnitude lower tha cooling rates estimated for chondrules cooling in a transparent nebula in which allowance is made for latent heat of crystallization (Wasson, 1996). Although this difference is probably not outside errors of estimation, it is important to keep in mind that chondrule formation occurred in the dusty and thus somewhat opaque midplane, and cooling models need to include allowance for the slower rates of heat transport away from the small (1-10 $m^3$) scale regions associated with chondrule melting events.

**Acknowledgements**: I am greatly indebted to Alan Rubin for data and extensive discussions. This research mainly supported by NASA grant NAG5-12887.

**References**:

[1] Wasson J. T. and Rubin A. E. (2003) *Geochim. Cosmochim. Acta* **67**, 2239-2250.

[2]Wasson J. T. (1996) In *Chondrules and the Protoplanetary Nebula* (Hewins R.H., Jones R. and Scott E. R. D., eds.), Cambridge, 45-54.

[3] Lofgren G. E. (1989) *Geochim. Cosmochim. Acta* **53**, 461-470.

[4] Radomsky and Hewins R. H. (1990) *Geochim. Cosmochim. Acta* **54**, 3537-3558.

[5] Lofgren M. (1996) In *Chondrules and the Protoplanetary Nebula* (Hewins R.H., Jones R. and Scott E. R. D., eds.), Cambridge, 187-196.

[6]Yurimoto H. and Wasson J. T. (2002) *Geochim. Cosmochim. Acta* **66**, 4355-4363.

[7] Rubin A. E. and Wasson J T.. (2004) *Geochim. Cosmochim. Acta* **68,** in press.

**ARE PRISTINE NEBULAR CONDENSATES PRESENT IN THE METEORITE RECORD?** M. K. Weisberg[1,2] and D. S. Ebel[2]. [1]Department of Physical Sciences, Kingsborough College of the City University of New York, Brooklyn, NY 10314. [2]Department of Earth and Planetary Sciences, American Museum of Natural History, New York, NY 10024.

**Introduction:** Astrophysical models of the early solar system predict a fairly homogenized gaseous nebula that evolves into a disk that is above the silicate boiling temperature from 0 to 3 AU and progressively cools to temperatures at which solids precipitate. Thermodynamic calculations grounded in experiment can predict the order in which minerals condense as a gas of solar composition cools in both equilibrium and non-equilibrium cases [e.g., 1, 2, 3]. However, little is known about the physical nature of the earliest condensates. Were they amorphous, submicron to dust-size minerals, or did condensation produce mm-size mineral grains? Are these materials present in the most primitive unequilibrated (Type 2 and 3) chondrites? Unequilibrated chondrites contain micron-size grains with isotopic anomalies that are interpreted to be ABG star and supernova ejecta that survived interstellar processing, heating in the early solar nebula, accretion into chondrite parent bodies and later aqueous alteration, impacts, lithification and thermal metamorphism on the parent bodies [e.g., 4]. Therefore, we would expect that some nebular condensates have also survived. A number of chondrite components have been interpreted to be primary nebular condensates. However, interpretation of objects as nebular condensates is highly controversial. Here we consider several components of chondrites that have been interpreted to be nebular condensates.

**Calcium, Aluminum-rich Inclusions (CAIs):** Some of the objects in chondrites consist of minerals that are rich in refractory elements and are among the highest temperature phases predicted to condense from a gas of solar composition [1]. Of these objects many have been melted, however, the CAIs that have highly irregular shapes, fluffy/porous textures and minerals organized in discrete layers have been interpreted to be aggregates of sequential condensates that may have been coarsened by sintering or were melted to very low degrees following their formation . These include Fluffy Type A (FTA) inclusions and Spinel-Pyroxene Aggregates (SPA). (See MacPherson [5] and Brearley and Jones [6] for reviews of refractory inclusions and interpretations of their origins.) The FTA and SPA inclusions are irregularly shaped aggregates of nodular assemblies; in FTA inclusions the nodules are dominantly melilite, while in the SPA inclusions spinel is the major mineral. In both types of inclusions the nodules are surrounded by concentric rim layers. Absent from these inclusions are features indicative of melting, such as glassy mesostasis or porphyritic, cryptocrystalline or barred textures, as found in fluid-drop chondrules. The highly irregular, lobate shapes of the nodules also suggest that they are not melt droplets that would have formed a stable spherical shape (e.g., a chondrule). The minerals in FTA inclusions in Allende [7] and Murchison [8] have been interpreted to be nebular condensates. SPA's in CM chondrites have been interpreted to be direct nebular condensates [8], while equivalent inclusions in Allende (CV) have been interpreted as vaporization residues [9]. MacPherson et al. [8] suggested that these inclusions formed by condensation and heterogeneous nucleation of spinel onto pre-existing dust, followed by condensation of diopside onto the spinel. Kornacki and Wood [9] suggested that these inclusions are better interpreted as fractionated distillation residues that lost a Ca,Si-rich partial melt. However, the Mg isotopic compositions of spinel-rich inclusions in the Mighei CM chondrite suggest that they are not evaporation residues because they lack enrichment in the heavier isotope [10].

**Amoeboid Olivine Aggregates (AOAs):** Amoeboid Olivine Aggregates (AOAs) are fine-grained aggregates of olivine and Ca, Al-rich minerals. The AOAs in CV chondrites have been interpreted to be aggregates of solid nebular condensates (e.g., 11) and the AOAs in the CR chondrites have similar characteristics that

suggest they too did not crystallize from liquids (12, 13). AOAs have highly irregular shapes that differ from the spherical to semi-spherical once-molten chondrules. They do not appear to contain glassy mesostasis like that found in many chondrules, and they contain porosity suggesting they formed from aggregation of solids. They appear to be aggregates of nodules with some nodules having a concentrically layered mineralogy of perovskite and spinel surrounded by anorthite surrounded by Ca-pyroxene, followed by olivine. The diversity of nodules within a single AOA also attests to the aggregational, unmelted character of the AOAs. Olivine in AOAs in CR chondrites is $^{16}$O-rich similar to unmelted CAIs, whereas in igneous CAIs some minerals are $^{16}$O-poor, because they experienced isotopic exchange with the $^{16}$O-poor reservoir during melting [12].

**Metal in CB and CH Chondrites:** The metal in CB and CH chondrites has an approximate solar Ni/Co ratio, and zoning patterns in some metal grains with Ni-rich cores argue for a primitive origin [e.g., 14]. The occurrence of asymmetrical zoning in fragmental metal surfaces indicates that the zoning predated incorporation into the meteorite [15]. The heterogeneity and preservation of primary zoning indicates that these grains cooled rapidly to below 500˚C and were not reheated above this temperature. Further, the occurrence of high (up to 14%) Ni in the cores of some zoned metal suggests that these grains are metastable and would likely have decomposed to plessite structures if they were only mildly heated (above 300˚C) during thermal metamorphism. There is an enrichment in refractory PGEs in the cores of the zoned metal grains in the QUE 94411 CB chondrite, and Pd, which has a volatility similar to Fe, shows no zoning relative to Fe in the zoned metal grains. This indicates that the metal compositions are the result of a volatility-controlled process, supporting a direct nebular condensation origin for the metal [16].

**Isolated Olivine:** The origin of isolated olivine grains in chondrite matrices remains unresolved. They have been interpreted to be nebular condensates [e.g., 17, 18, 19] or chondrules fragments [20]. They have a number of intriguing characteristics that remain unexplained including (1) some have $^{16}$O-rich compositions in the range of -30 to -40, similar to minerals in refractory inclusions and unlike most chondrules olivine, (2) CL properties that differ from most olivine in chondrules [19], (3) in some cases they are as large as the chondrules in their host meteorite. It is unlikely that these olivine grains crystallized from chondrules presently found in the meteorite record. However, the process in which such large olivine crystals grow directly from a gas in the solar disk is unknown.

**Chondrite Matrix:** The matrix of some chondrites has been interpreted to be primitive nebular condensate. The matrix in the Kakangari chondrite has been interpreted to have formed through high temperature annealing of fine-grained dust and amorphous or poorly crystalline nebular condensate [21]. The matrix and chondrule rims in the ALHA 77307 CO chondrite consists of Si- and Fe-rich amorphous material, olivine, pyroxene, metal, and oxide and sulfide phases. It has been interpreted to have formed by disequilibrium condensation as amorphous dust and the amorphous material currently in the matrix is thought to be a remnant of the primary condensate material [22].

**References:** [1] Grossman (1972) *GCA* 36, 597-619. [2] Larimer (1967) *GCA* **31**, 1215-1238. [3] Ebel and Grossman (2000) *GCA* 64, 339-366. [4] Zinner (1996) in *Astrophysical Implication Laboratory Studies of Presolar Materials*, AIP Conf. Proc. 402, 3-26. [5] MacPherson et al. (1989) in *Meteorites and the Early Solar System*, 746-087. [6] Brearley and Jones (1998) *Planetary Materials*, Rev. Mineralogy vol. 36, 3-1-398. [7] MacPherson and Grossman (1984) *GCA* 48, 29-46. [8] MacPherson et al. (1983) *GCA* 47, 823-839. [9] Kornacki and Wood (1985) *GCA* 49, 1219-1237. [10] Davis and MacPherson (1992) *Meteoritics* 27, 212-213. [11] Grossman and Steele (1976) *GCA* 40, 149-155. [12] Aléon et al. *MAPS* 37, 1729-1755. [13] Weisberg et al. (2004) MAPS 39, in press. [14] Miebom et al. (1999) *JGR* 104, 22 053 - 22 059. [15] Weisberg et al. (2001) MAPS 36, 401-418. [16] Campbell et al. (2001) *GCA* 65, 163-180. [17] Olsen and Grossman (1978) *EPSL* 41, 111-127. [18] Kurat et al. (1989) *Meteoritics* 24, 35-42. [19] Steele (1995) *Amer. Min.* 80, 823-832. [20] McSween (1977) *GCA* 41, 411-418. [21] Brearley (1989) *GCA* 53, 2395-2411. [22] Brearley (1993) *GCA* 57, 1521-1550.

**OVER WHAT PERIOD OF TIME DID CHONDRULE FORMATION OCCUR?.** J. A. Whitby Physikalisches Institut, University of Bern, Sidlerstrasse 5, CH-3012 Bern Switzerland. email: James.Whitby@phim.unibe.ch

**Introduction:** There have been many suggestions for the nature of the chondrule forming event(s) including lightning, impacts, X-winds and shocks e.g. [1]. Models of chondrule formation which invoke shock-heating agree well with constraints inferred from petrographic and chemical observation of chondrules [2], however, the location of chondrule formation and the origin of the shocks remain uncertain. suggestions for the origin of the shocks include planetary bow-shocks...Whatever the origin of the heating event that produced chondrules, its seems likely that information about the frequency of occurence, and about the period of time over which chondrules were formed, is likely to provide constraints on proposed mechanisms.

**Chondrule ages:** Individual chondrule ages have been determined by the I-Xe, Pb-Pb and Al-Mg radiometric dating techniques. The majority of data comes from the I-Xe system which is known to readily respond to parent-body processes such as aqueous alteration, or thermal events. The interpretation of radiometric ages from chondrules relies on a petrographic assessment of the sample for textures or minerals that may be attributable to secondary events. Where textures and compositions (e.g. the continuing presence of glassy phases) are consistent with rapid cooling from a melt, it is assumed that a measured radiometric age reflects that event. In the case of the I-Xe system, this assumption can be further checked by the use of step-heating when performing the analysis – the presence of iodine bearing phases which degas at low temperatures suggests chemical reactions in the parent body, especially if the inferred $^{129}I/^{127}I$ ratio varies with temperature.

Radiometric age determinations of individual chondrules remain technically challenging due to the small amounts of material involved, and scientifically challenging due to the difficulties in proving that no disturbance of the radiometric isotope system has occurred subsequent to the chondrule forming event. The available dataset is thus rather small.

*I-Xe ages.* The high sensitivity and low background of noble-gas mass spectrometers, together with the simple sample preperation mean not just that many more I-Xe chondrules ages are available than for Pb-Pb or Al-Mg, but also, as noted above, isochrons for individual chondrules with many datapoints are the norm. Fig. 1 is a summary of most available chondrule data, after (Whitby and Gilmour, 2001); only chondrules with simple isochrons have been selected. (In some cases, a chondrule may appear to have recorded two events which can be thermally separated).

I-Xe ages for chondrules generally cluster close to the reference values of Bjurbole and Shallowater (which are only ~ 0.6Myr different). Ages of chondrules from Chainpur scatter over a much larger extent, attributed to shock processing [3]. For the remaining data, well-determined I-Xe ages believed to reflect closure to diffusion after chondrule formation, cover at least 2.5 Myr from any single meteorite. This is a significantly larger range than the uncertainties due to the experimental technique.

The poster presentation will compare the spread in I-Xe ages to the smaller range of values observed using other isotopic systems, and discuss the significance of an extended period of chondrule formation.

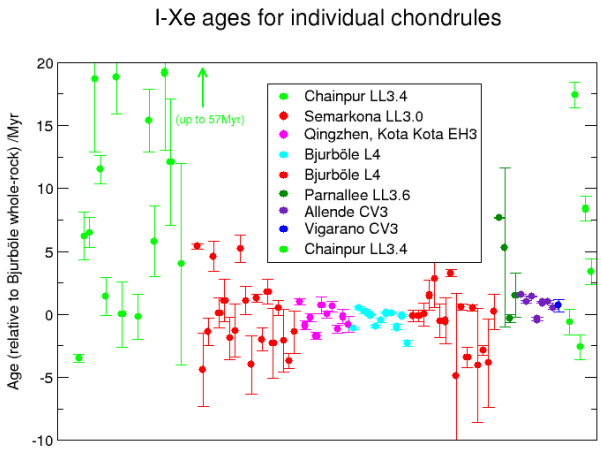


**Figure 1.** Selected I-Xe ages for individual chondrules [3-13]

**References:** [1] Whipple *Science,* 153, p54 (1966); Wood *Earth Planet. Sci. Lett.*,70, p11 (1984); Shu et al. *Science*, 271, p1545(1996); Kieffer *Science*, 189, p333 (1975) [2] Desch and Connolly *Meteoritic. Planet. Sci.*, 37, p183 (2002) [3] Swindle et al. *Geochim. Cosmochim. Acta*, 55, p861 (1991) [4] Whitby and Gilmour *Meteoritic. Planet. Sci.* 36 A224 (2001) [5] Swindle et al. *Geochim. Cosmochim Acta*, 55, p3723 (1991) [6] Whitby et al. *Meteoritic. Planet. Sci.* p347 (2002) [7] Gilmour et al. *Meteoritics*, 30, p405

(1995) [8] Gilmour et al. *Meteoritic. Planet. Sci.* 35 p445 (2000) [9] Caffee et al. JGR 87 A303 (1982) [10] Swindle et al. Geochim. Cosmochim. Acta 47 p2157 (1983) [11] Nichols et al. *Lunar Planet. Sci. Conf.*, 21, p879 (1990) [12] Whitby et al. *Meteoritic. Planet. Sci.,* 39, p1387 (2004) [13] Busfield et al. *Goldschmidt Conference abstracts* A112 (2002)

**THE CHONDRITE TYPES AND THEIR ORIGINS.** John A. Wood, Harvard-Smithsonian Center for Astrophysics, 60 Garden Street, Cambridge MA 02138, USA. jwood@cfa.harvard.edu

**Introduction:** In an earlier paper [1] the author placed his bet on the origin of CAIs. This paper discusses aspects of the origin of chondrules, matrix, and bulk chondrites. Important results have appeared recently, especially the $^{26}$Al and U-Pb ages found for chondrules in apparently pristine chondrites [2 - 10] and consideration of the behavior of presolar condensed organic compounds in the nebula [11 - 13], that begin to bring into focus a plausible model for the origin of the several types of chondritic meteorites.

**Ages of Chondrules:** [2 - 10] have found that chondrule formation extended over several million years, and requires efficient mixing of the chondrules produced, in the nebula prior to accretion or in parent body regoliths or (more probably) both. This is a new ingredient in the chondrite-formation picture; it is the opposite of the rapid chondrule-formation-and-accretion events the author has always pictured [14], and it is also inconsistent with the idea of compositional complementarity of chondrules and matrix [15]. [8, 10] find chondrule ages extending all the way back to $t_0$ (the age of CAIs). [2 - 7] find ages ≥~1 Myr younger than $t_0$, but older chondrules may simply have been missing from the small suites of chondrules they studied.

**Formation of Chondrules:** The inner edge of the nebula, where [1] holds CAIs were formed, was too hot to be consistent with the brief heating and rapid cooling histories of chondrules. Conventional wisdom says these must have formed farther out in the nebula, probably by the agency of shock heating [16]. Presolar condensed organic compounds in the nebula may have played a key role in the formation of chondrules. In this connection [11 - 13] discuss three radial distance and temperature regimes in the nebula: >~3 AU, where abundant organic compounds (and ice) from the solar system's parent molecular cloud could survive; ~2.2 - ~3 AU, where only less-abundant and more-refractory organics from the diffuse interstellar medium that predated the molecular cloud survived; and <~2.2 AU, where organics were largely pyrolyzed. These organics may have been the "glue" that bound chondrule precursors together. The qualitative difference between Type I and Type II chondrules may stem from formation of the former in the >3 AU zone, where abundant molecular-cloud organics in the precursors served as an internal reducing agent [17], while Type II chondrules formed in the warmer zone inside 3 AU from precursors that contained only less-abundant diffuse-cloud organics. The Type I chondrules formed in this fashion were a major ingredient of C and CR chondrites that accreted outside ~3 AU, but a fraction of them also diffused inside 3 AU and were incorporated in OC that accreted there, along with the abundant Type II chondrules which formed in that zone.

**Ordinary Chondrites:** The most prominent compositional property of OC (though not the only one) is their depletion in Fe: Fe/Si is 10% (H) to 50% (LL) smaller than the solar ratio. Since there are correlated Ni and Co depletions [18], it is clear that a loss of metal phase occurred before accretion. This may have occurred during a protracted early period when chondrules of various ages were mixed as they remained dispersed by turbulence in the nebula. During this time the larger and denser solid objects were most disposed to sink to the midplane against the buoying effect of turbulent gas, and these were probably metal-rich. Near the midplane they were eligible for aggregation into meter-sized objects (again, sticky organic coatings they had acquired may have been important; an old idea [19]), after which they were promptly subtracted from the system by gas-drag spiralling. The OC parent bodies formed, out of residual solid particles depleted to varying degrees in metal, only after dissipation of gas made the nebula so thin that gas drag became ineffective in removing accretions.

**Carbonaceous Chondrites:** Because of the C and $H_2O$ content of C chondrites, and the localization of spectral C asteroids beyond ~2.3 AU in the asteroid belt [20], it has always been clear that this chondrite class formed at greater radial distances in the nebula than O chondrites. A rationalization of the disparate textural properties of the various C chondrite classes has not become apparent. The territory beyond 2.3 AU is probably large enough that each class can be representive of a particular radial interval which was not blended with neighboring zones by turbulent diffusion. The fragmentary data on chondrule ages is consistent with CV chondrites (*i.e*, Allende [8, 10]) forming earlier than CO [7] and CR [6, 8] chondrites, and this is also consistent with the greater abundance of CAIs in CV chondrites (if, as [1] argues, CAIs formed early at the inner margin of the nebula and were transported to the asteroid belt by an x-wind or by turbulent diffusion).

**Enstatite Chondrites:** The formation of E chondrites has always been particularly enigmatic. Accounting for the reduced minerals they contain requires more than physically fractionating the nebula's solid ingredients; the bulk chemistry of the system they formed from must be made radically non-solar (*e.g.*, [21]). [13] has suggested these conditions were created by shock-vaporization of dust-enriched systems,contemporaneous with chondrule-formation, in a radial distance range cold enough for the dust to include organic compounds (increasing C in the system) but not cold enough for the dust to include ice (which would also increase O). [13] accomplishes the necessary increase of sytem C/O near the midplane at ~2.4 AU, outside their formation zone for OC. (However, this does not square with the observed localization of E asteroids at ~2 AU, inside the mean distances of most S asteroids, presumably the source of OC [20]). If E chondrites were formed by this or a related scheme, it would have to happen early, because repeated shock heatings would irreversibly remove C from the dust in the nebula and leave it in the gas

phase, meaning that dust-enrichment no longer offered an opportunity to increase C/O. The near-absence of CAIs in E chondrites also needs to be explained.

**Source of Chondrule-Forming Shocks:** [22] attributed chondrule-forming shock waves in the nebula to the development of spiral density waves in a gravitationally-unstable disk. However, the protracted period of chondrule formation revealed by recent radiometric studies is inconsistent with this mechanism. The solar nebula could have been gravitationally unstable for only a very short time, 0.1 Myr or less, and during the remaining millions of years when chondrules were being formed the disk mass was a few percent of the solar mass, too small for gravitational instability. Another, longer-lasting, source of shocks in the nebula must be sought. Larson [23] has noted that most if not all stars probably form in binary or multiple systems, meaning that tidal interactions with early companion stars could have been the source of energetic shocks in the solar nebula until the cluster dispersed.

**References:**

[1] Wood, J. A. (2004) *Geochim. Cosmochim. Acta,* in press. [2] McKeegan K. D. et al. (2000) *LPS XXXI,* Abstract #2009. [3] Kita N. T. et al. (2000) *Geochim. Cosmochim. Acta 64,* 3913-3922. [4] Hutcheon I. D. et al. (2000) *LPS XXXI*, Abstract #1869. [5] Mostefaoui S. et al. (2002) *Meteoritics & Plan. Sci. 37,* 421-438. [6] Amelin Y. et al. (2002) *Science 297,* 1678-1683. [7] Kurahashi E. et al. (2004) *LPS XXXV,* Abstract #1476. [8] Amelin Y. et al. (2004) *Geochim. Cosmochim. Acta 68,* Suppl. 1, A759. [9] Rudraswami N. G. et al. (2004) *LPS XXXV,* Abstract #1236. [10] Bizarro M. et al. (2004) *Nature,* in press. [11] Kouchi, A. et al. (2002) *Astrophys. J. 566,* L121-L124. [12] Kudo, T. et al. (2002) *Meteoritics & Plan. Sci. 37,* 1975-1983. [13] Nakano, H. et al. (2003) *Astrophys. J. 592,* 1252-1262. [14] Wood, J. A. (1985) In *Protostars and Planets II* (eds. D. C. Black & M. S. Matthews), 687-702, Univ. Arizona Press. [15] Klerner, S. and Palme, H. (1999) *LPS XXX,* Abstact #1272. [16] Desch, S. J. and Connolly, H. C. Jr. (2002) *Meteoritics & Plan. Sci. 37,* 183-207. [17] Connolly, H. C. Jr. et al. (1994) *Nature 371,* 136-139. [18] Urey, H. C. and Craig, H. (1953) *Geochim. Cosmochim. Acta 4,* 36-82. [19] Hoyle, F. (1955) *Frontiers of Astronomy,* p. 93. Harper & Bros. [20] Gradie, J. and Tedesco, E. (1982) *Science 216,* 1405-1407. [21] Wood, J. A. and Hashimoto, A. (1993) Geochim. Cosmochim. Acta 57, 2377-2388. [22] Wood, J. A. (1996) *Meteoritics & Plan. Sci. 31,* 641-645. [23] Larson, R. B. (2002) *Mon. Not. R. Astron. Soc. 332,* 155-164.

**HIGH SILICATE CRYSTALLINE-TO-AMORPHOUS RATIOS IN COMETS C/2001 Q4 (NEAT) AND HALE-BOPP.** D. H. Wooden[1], D. E. Harker[2], and C. E. Wodward[3], [1]NASA Ames Research Center, MS 245-3, Moffett Field, CA 94035-1000, wooden@delphinus.arc.nasa.gov, [2]CASS/UCSD, 9600 Gilman Dr. Dept. 0424, La Jolla, CA 92093-0424, harker@talos.ucsd.edu, [2]Dept. of Astronomy, 116 Church St., SE, Univ. of Minnesota, Minneapolis, MN 55455, chelsea@astro.umn.edu.

**Introduction:** Crystalline silicates, by their apparent absence in the ISM [1], are dust grains that experienced high temperatures in the solar nebula. Mg-rich crystalline silicates formed either by condensation [2] from hot nebular gases (1450 K) or by the annealing [3, 4] of Mg-rich amorphous silicates (~1000 K) in shocks in the 5—10AU region [5] or by radial transport into and out of the hot inner zones, e.g., $T_d$>1000K at $r_h$<5AU, $10^{-6}$ –$10^{-5}$ $M_O$ $yr^{-1}$, $\alpha=10^{-4}$ [6] of the early solar nebula [7]. Mg-rich crystalline silicates are found in interplanetary dust particles (IDPs) [8] and produce IR spectral features in many Oort cloud comets [9,10,11]. In May 2004, we discovered strong crystalline silicate features in the dynamically new Oort cloud comet C/2001 Q4 (NEAT). Thermal emission modeling of comets Q4 and C/1995 O1 (Hale-Bopp) demonstrate that both these comets have similar, high silicate crystalline-to-amorphous ratios of 2.4 [12] and 2.1 [13], respectively, indicating that these icy planetesimals aggregated from similar reservoirs of material or that crystalline silicates were widely distributed within the comet-forming zone. This argues for efficient annealing mechanisms and radial mixing [14].

**Cometary Silicate Crystalline-to-Amorphous Ratios:** Primitive grains released from cometary muclei into their comae during perihelion passage reveal the conditions in the solar nebula during the regime of icy planetesimal formation. The relative abundance of silicate crystals to amorphous silicates deduced for cometary comae can be used to constrain high-temperature processes in protoplanetary disks, as the silicate crystalline-to-amorphous ratio probes the combination of the relative masses of grains that reached temperatures above 1000 K versus those that did not and the degree of radial mixing of the high-temperature processed materials with cooler materials.

Constraining the relative abundances of mineral grains from IR spectra of comets requires fitting thermal emission models to cometary spectral energy distributions (SEDs). Computing thermal emission models requires solving for the radiative equilibrium temperatures of discrete mineral grains characterized by a radius $a$ and whose relative number are defined by a size distribution $n(a)$. Size distributions are either power-law or modified power law such as the Hanner size distribution $n(a) = (1-a_o/a)^m \ (a_o/a_p)^n$ where $a_o$=0.1μm and $a_p$ is the grain radius at which the size distribution peaks. The radiative equilibrium temperatures of grains of a given radius of different mineral composition will differ because of their absorptivity or emissivity at visible to near-IR wavelengths and mid- to far-IR wavelengths. Specifically, at the same heliocentric distance, Mg-rich crystalline silicates are cooler than Fe-bearing amorphous silicates because Mg-rich crystals absorb sunlight significantly less efficiently than Fe-bearing amorphous silicates. The temperatures, and hence the optical properties, of Fe-bearing amorphous silicates are confirmed by fitting the relative fluxes of the 10 and 20μm features in the cometary SEDs [10]. The detection of Mg-rich crystalline silicates is confirmed by the wavelengths of their resonant peaks [9, 11, 15, 16] and their optical properties are confirmed by fitting thermal emission models to the ISO SWS spectrum of comet Hale-Bopp at 2.8 AU [10].

In order for any silicate feature to be detected in a comet's SED, there must be a preponderance of submicron silicate grains in the coma. Grain aggregates with submicron grain constituents may show features if porous enough [10, 17, 18]. Solid (non-porous) grains larger than ~1μm produce weak emission within the spectral resonance wavelength range in contrast to emission at wavelengths outside their resonances. For the sharp resonant peaks of Mg-rich silicate crystals to be detected in contrast to the strong broad spectral resonances of amorphous silicates, the crystals must be as or more abundant than the amorphous grains: their cooler temperatures mean they produce less flux and their relative numbers need to be greater in order to be detected in constrast to the warmer amorphous silicates.

Comets Q4 and Hale-Bopp had silicate features with remarkably similar shapes as shown in Fig. 1. Fitting thermal emission models to comet Q4 [12] and Hale-Bopp [13] constrains their relative mineral abundances. The silicate crystalline-to-amorphous ratios derived for comets Q4 and Hale-Bopp are 2.4 and 2.1 respectively.

**Constraints on High Temperature Processes in the Solar Nebula Provided by Comets Hale-Bopp and Q4 :** Hale-Bopp was observed to have the largest

contrast silicate feature to date and is deduced to have a grain size distribution that peaks at 0.2μm [10]. The structure of Hale-Bopp's coma was also dominated by jet activity. We hypothesize that small pristine grains, grains minimally altered since their formation and aggregation as grains and their incorporation into the nucleus, were dredged up from the subsurface layers of the nucleus and expelled into the coma via jets and/or that pristine grains fragmented in the coma [10,12]. Comet Q4 has a parabolic orbit and also has strong jet activity close to perihelion [19]. Comet Q4 has not suffered the nuclear surface processing that occurs through repeated perihelion passages [20] that leads to the loss of volatiles from the near-surface layers of the nucleus and potentially decreases the fragility of grain aggregates and decreases the silicate-to-amorphous carbon ratio though the carbonization [21,22] of the organic "glue" [23] that holds grain aggregates together. Probably both comets Q4 and Hale-Bopp are releasing primitive grains into their comae through their strong jet activity. Thus, their high silicate crystalline-to-amorphous ratios provide strong constraints on high temperature processes in the early solar nebula and on the radial mixing of grains processed at high temperatures (>1000K) into the Jupiter–Saturn region [24] and to some extent into the trans-Neptunian region [25]. A silicate crystalline-to-amorphous ratio of 0.5 is predicted by radial diffusion models of the early solar nebula, given a warm nebula model and rapid (300,000 yr) radial diffusion of annealed silicate grains from the hot inner regions to throughout the disk [7]. The high silicate-to-amorphous ratios deduced for comets Q4 and Hale-Bopp of 2.4 and 2.1 indicate efficient annealing mechanisms such as heating in shocks [5] and efficient radial mixing [14].

**References:**

[1] Kemper F. et al. (2004) ApJ, 609, 826. [2] Grossman L. (1972) GCA, 36, 597. [3] Rietmeijer F. J. M. et al. (2002) Icarus, 156, 269. [4] Brucato J. R. et al. (1999) A&A, 348, 1012. [5] Harker D. E. and Desch S. P. (2002) ApJ, 565, L109. [6] Bell K. R. et al. (2000) in Protostars and Planets IV, ed. V. Mannings et al. (Tucson: Univ. Arizona Press), 897. [7] Bockelee-Morvan D. et al. (2002) A&A, 384, 1107. [8] Bradley, J. P. et al. (1999) in In Solid Interstellar Matter: The ISO Revolution, ed. L. d'Hendecourt et al. (Les Ullis: EDP Sciences), 297. [9] Wooden, D. H. (2002) EMP, 89, 247. [10] Harker D. E. et al. (2002) ApJ, 580, 579. [11] Wooden, D. H. et al. (1999) ApJ, 517, 1034. [12] Wooden D. H. et al. (2004) ApJ, 612, L77.[13] Harker D. E. et al. (2004) ApJ, 615, in press. [14] Boss A. P. (2004) ApJ, in press. [15] Crovisier J. et al. (1997) Science, 275, 1904. [16] Hanner M. S. et al. (1994) ApJ, 425, 274. [17] Bradley J. P. et al. (1999) Science, 285, 1716. [18] Xing Z. and Hanner M. S. (1997) A&A, 324, 805. [19] Lecacheux J. and Frappa E. (2004) IAU Circ. No. 8349. [20] Meech K. J. and Svoren J. (2004) in Comets II, ed. M. C. Festou (Tucson: Univ. Ariz. Press), in press. [21] Moroz L. V. et al. (2004) Icarus, 170, 214. [22] Moroz L. V. et al (2004) Icarus, submitted. [23] Boehnhardt H. et al. (1990) A&A, 231, 543. [24] Fernandez J. A. and Ip. W.-H. (1981) Icarus, 47, 470. [25] Morbidelli A. and Levison H. F. (2003) Nature, 422, 30.

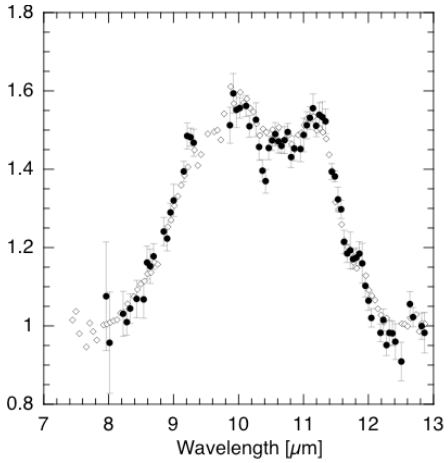


**Figure 1:** The silicate feature strength (flux-to-continuum ratio) derived from two HIFOGS spectra of comet C/2001 Q4 (NEAT) on 2004 May 11.30 UT (*solid circles*) [12] compared with the scaled (0.3) silicate feature derived from the HIFOGS spectrum of comet C/1995 O1 (Hale-Bopp) on 1997 February 15 UT (*open diamonds*) [11]. The flux-to-continuum ratios for Q4 (NEAT) are derived by dividing the HIFOGS flux spectra by a blackbody fitted to $\lambda \leq 8.4\mu m$ and $\lambda \geq 12.4\mu m$ and characterized by $T_{bb}$=310±4 K and $F_\lambda$=1.19±0.01E-16 W cm$^{-2}$ μm$^{-1}$.

**FIRST PRESOLAR SILICATE DISCOVERED IN AN ANTARCTIC MICROMETEORITE.**
T. Yada[1,2], F. J. Stadermann[1], C. Floss[1], E. Zinner[1], and C. T. Olinger[1,3], [1]Lab. for Space Sci., Phys. Depart., CB 1105, Washington Univ., 1 Brookings Dr., St. Louis, MO 63130-4899, USA. [2]Depart. Earth Planet. Sci., Grad. Sch. Sci., Univ. Tokyo, 7-3-1 Hongo, Bunkyo-ku, Tokyo 113-0033, Japan. [3]*Current address:* Los Alamos Nat. Lab., MS E541, BO Box 1663, Los Alamos, NM, 87545, USA. E-mail: tyada@physics.wustl.edu

**Introduction:** The study of presolar grains has given important information about the isotopic compositions of stellar matter which has become a building block of our solar system. Recently, presolar silicates have been discovered in interplanetary dust particles (IDPs) [1, 2] and meteorites [3, 4]. Micrometeorites, which are the most dominant extraterrestrial materials on Earth [5-7], have previously been searched for presolar grains [8-10], but no presolar grains have been discovered yet. Here, we report a newly discovered presolar silicate phase from an Antarctic micrometeorite (AMM).

**Samples and Methods:** AMMs analyzed in this study were collected at Cap-Prudhomme, west Antarctica in 1988 [11]. Seven AMMs, AWU01-3, 9, 11, 14, 16, 24, and 25, were crushed and fragments were pressed into Au foil for study with the ims3f ion microprobe [12]. Other fragments of the same AMMs were analyzed for Ne isotopes by noble gas mass spectrometry [13]. NanoSIMS, a newly developed ion microprobe for investigating sub-µm isotopic distribution, is now available, and we re-analyzed the samples that were left after the ims3f measurements. For the NanoSIMS analysis, a ~1pA $Cs^+$ primary ion beam was accelerated to 16kV and rastered over the samples. The primary beam diameter was ~200nm. Negatively-charged secondary ions were extracted with 8kV to go through a double focusing mass spectrometer and be detected by a multi-collector system. Mass resolution power was set around 6,000. $^{12}C^-$, $^{13}C^-$, $^{16}O^-$, $^{17}O^-$, and $^{18}O^-$ were simultaneously detected by five electron multipliers. The AMMs were analyzed in isotopic imaging mode with repeated scans over a 20x20µm area for each analysis.

**Results:** In total, a 8000µm$^2$ area of the pressed surfaces of seven AMMs was analyzed with the NanoSIMS in 38 individual imaging measurements. Almost all analyzed areas were isotopically normal in C and O on a 200nm scale. The only exception was found in AWU01-16, which contains an isotopically anomalous area of ~5x3µm (Fig. 1). Its isotopic ratio is $1.41\pm0.05\times10^{-3}$ in $^{17}O/^{16}O$ and $2.42\pm0.03\times10^{-3}$ in $^{18}O/^{16}O$ (Fig. 2). The observed +2700‰ enrichment of $^{17}O$ indicates a presolar origin of this phase. After the isotopic analysis of this presolar phase, the area was investigated by SEM-EDS and FE-SEM. The presolar phase was identified as silicate, but was chemically indistinguishable from the surrounding isotopically normal material (Fig. 3, 4). This phase was also analyzed for Mg isotopes with the NanoSIMS, but no $^{26}Mg$ excess was observed.

**Discussion:** As seen in Figure 2, the presolar silicate phase has an oxygen isotopic composition similar to that of group 1 presolar oxides. The lack of a $^{26}Mg$ excess in group 1 grains indicates that it formed in the early stage of an asymptotic giant branch (AGB) star [14]. The most striking feature of this presolar silicate phase is its size. It is larger than any presolar silicates found in IDPs and meteorites, which range in size from 200-940nm [1-4]. A secondary electron image (Fig. 3) of the isotopically anomalous area shows that it is not a single grain but an aggregate of 10-20 grains. These grains may originally have formed a single larger grain in the AMM which was then crushed during sample preparation. The pressing into the Au foil may have led to a flattening of the fragmented presolar phase, which may have increased its apparent size. Based on a simple calculation, its original size may have been 1-2µm.

The Ne isotopic composition of AWU01-16 is distinctly different from that of other AMMs in this study. AWU01-16 is enriched in the solar wind (SW) component, whereas the solar energetic particle (SEP) component is dominant in other AWU01 AMMs (Fig. 5). The SW component penetrates only several tens of nm near the surface of material exposed to interplanetary space [15], whereas SEP is penetrating to a few tens of µm from the surface because of its higher energy than normal solar wind [16]. Thus, the high SW concentration in AWU01-16 indicates that this particle experienced significantly less heating during its atmospheric entry and/or that it had a highly porous structure before atmospheric entry.

Based on the possibly inflated two-dimensional size of this presolar phase, the abundance of presolar material in AMMs from this study is calculated to be ~1300ppm. Although the statistics is limited, this value is higher than that of meteorites (~40ppm) [3,4], but comparable to that of IDPs (~800ppm) [2]. Further studies of presolar grains in AMMs are necessary for a better understanding of their characteristics.

**Acknowledgement:** The AMMs were graciously provided by Michel Maurette, CSNSM, Orsay, France.

**References:** [1] Messenger S. *et al.* (2003) *Science, 300,* 105. [2] Floss C. and Stadermann F. J. (2004) *LPS XXXV,* #1281. [3] Nguyen A. N. and Zinner E. (2004) *Science, 303,* 1496. [4] Nagashima K. *et al.* (2004) *Nature, 428,* 921. [5] Love S. G. and Brownlee D. E. (1993) *Science, 262,* 550. [6] Taylor S. *et al.* (1998) *Nature, 392,* 899. [7] Yada T. *et al.* (2004) *Earth Planet Space, 56,* 823. [8] Prombo C. A. *et al.* (1990) *LPS XXII,* 1103. [9] Yates P. D. (1993) *LPS XXIV,* 1559. [10] Strebel R. *et al.* (1998) *MAPS, 33,* A151. [11] Maurette M. *et al.* (1991) *Nature, 351,* 44. [12] Stadermann F. J. and Olinger C. T. (1992) *Meteoritics, 27,* 291. [13] Olinger C. T. *et al.* (1989) *EPSL, 100,* 77. [14] Nittler L. R. *et al.* (1997) *ApJ, 483,* 475. [15] Benkert J. -P. *et al.* (1993) *JGR, 98,* 13147. [16] Wieler R. *et al.* (1987) *LPS XVIII,* 1080.

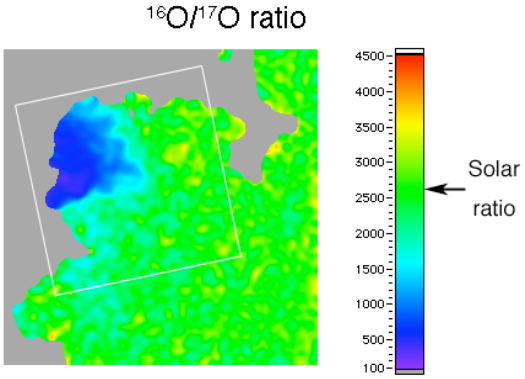


Fig. 1. $^{16}O/^{17}O$ ratio image of presolar silicate phase discovered in AWU01-16. The isotopically anomalous area is ~5x3μm. The size of the image is 20x20μm. The white square indicates the area shown in Fig. 3.

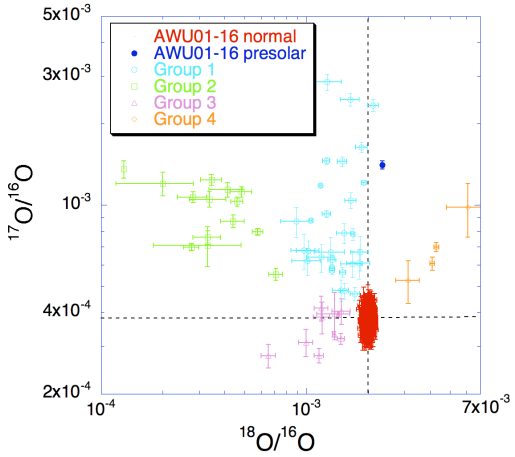


Fig. 2. Oxygen three isotope plot of presolar oxides. Data of group 1-4 presolar oxides are from [14]. The presolar phase discovered in this study is similar to group 1 presolar oxides. Dashed lines express solar isotopic ratios. Errors are 1σ.

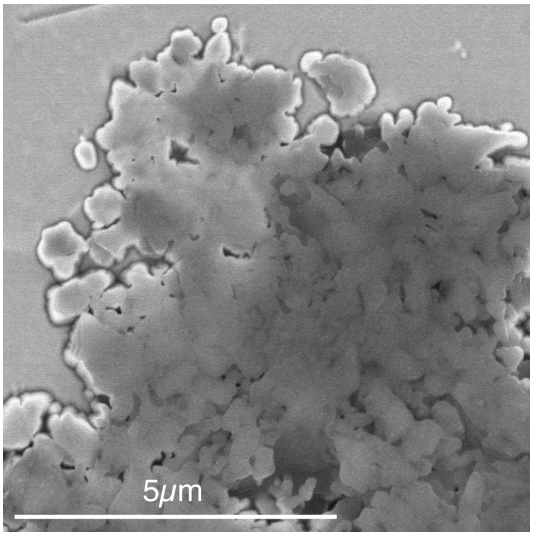


Fig. 3. FE-SEM image of the presolar silicate phase.

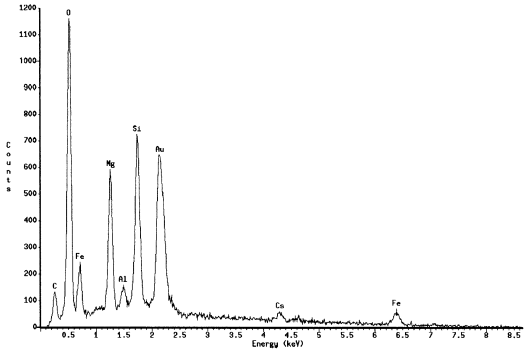


Fig. 4. EDS spectrum of the presolar silicate phase. Its pattern is similar to that of low-Ca pyroxene.

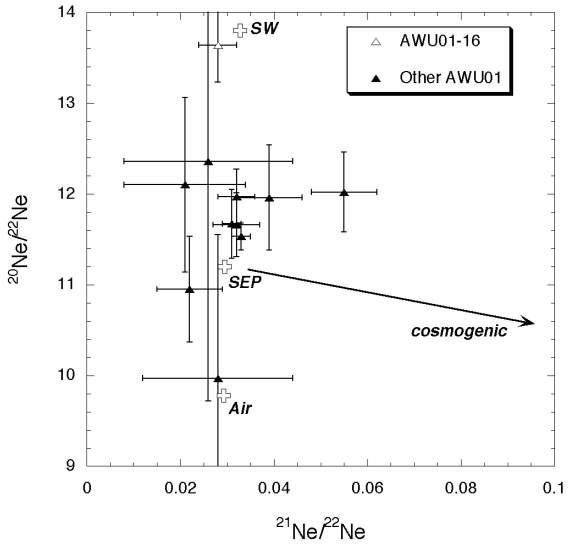


Fig. 5. Neon three isotope plot of AWU01 AMMs. Data are from [13]. AWU01-16 is more enriched in the SW component than other AWU01 AMMs.

**Rare Earth and Trace Elements Abundances of Refractory Inclusions in Ningqiang Meteorites.** A. Yamakawa[1], H. Hiyagon[1], Y. Lin[2] and M. Kimura[3], [1]Department of Earth & Planetary Science, Graduate School of Science, The University of Tokyo, Tokyo 113-0033, Japan. y-akane@eps.s.u-tokyo.ac.jp. [2]Institute of Geology and Geophysics, Chinese Academy of Science, P.O.Box 9825, Beijing 100029, China. [3]Faculty of Ibaraki University, Mito 310, Japan.

**Introduction:** The relationship between bulk chemical compositions and rare earth element (REE) abundance patterns remains poorly constrained for refractory inclusions (Ca-Al-rich inclusions, CAIs) and amoeboid olivine aggregates (AOAs). Lin and Kimura [1] observed bulk chemical compositions of refractory inclusions and AOAs in Ningqiang carbonaceous chondrite, and suggested that they vary along the condensation trajectory on the anorthite-gehlenite-forsterite plane in the order: hibonite-bearing Type As, hibonite-free Type As, spinel-pyroxene inclusions, and AOAs from high to low temperatures. As a part of the systematic study of the Ningqiang meteorite, we analyzed abundances and distribution of REEs and other trace elements in the Ningqiang CAIs and AOAs, and investigate the correlation between the bulk chemical composition and REE abundance for better understanding of the formation processes of CAIs.

**Techniques:** Samples were measured using a CAMECA ims-6f ion microprobe at the University of Tokyo. We used an energy filtering method for determining REE abundances.

REE analyses were performed using a $^{16}O^-$ primary beam at -12.5keV with a ~1nA beam intensity. Positive secondary ions from the sample were accelerated at 10keV and analyzed at a low mass resolution of ~300. A 60V energy offset with an energy window of 30eV was applied to eliminate complex molecular interferences to the peaks of REEs [2].

**Sample:** We analyzed so far ten inclusions: a hibonite-bearing fluffy Type A (FTA) (NQJ3-3-4), two hibonite-bearing compact Type A (CTA) (NQJ3-3-1.4), a hibonite-free CTA (NQJ3-5-9), three hibonite-free FTA (NQW1-1, NQW1-16 and NQL2-3-3) and a spinel-pyroxene-rich inclusion (NQW1-5). Most inclusions consist of melilite and spinel as major phases, anorthite, diopside and perovskite as minor phases, and nephelite and hedenbergite as altered phases.

**Results and Discussions:** Almost all inclusions we analyzed show flat REE patterns with Eu, and sometimes Yb, anomalies. Most perovskite and some fassaite show negative Eu anomaly, while melilite shows positive Eu anomaly.

Since Eu and Yb are more volatile than the other REEs (under relatively oxidizing conditions), Eu and Yb would condense only partially at a certain temperature while other REEs have condensed almost completely. If condensation stopped at this temperature (possibly due to separation of the inclusion from the gas), negative Eu and Yb anomalies would be produced. The remaining gas would become enriched in Eu and Yb. If an inclusion with relatively flat REE pattern acquires excess Eu and Yb from the remaining gas at lower temperatures, positive Eu and Yb anomalies would be produced.

Only NQW1-16 show a Group II pattern, in which heavy REE (Gd to Er and Lu) are depleted relative to light REE (La to Sm). It may form from the gas left behind after an ultra-refractory component was removed from the gas [3]. The bulk chemical composition of this inclusion is in the middle of the condensation trajectory, and hence, there seems to be no correlation between the REE pattern (flat vs Group II) and bulk composition. Although it has been reported that fine-grained inclusions tend to show Group II REE pattern[4], we observed so far only one Group II inclusion in Ningqiang meteorite. The reason for this is not clear at present, but may be due to limited number of analyses.

An interesting observation is that some inclusions with compositions of lower temperature condensates (NQW1-16, NQW1-5, NQW3-1) show positive anomalies in Ce, Yb and Eu. Celium may become as volatite as Eu and Yb under an oxidizing condition, because it exists in the form of $CeO_2$ as well as CeO in the gas phase. Hence, positive anomalies of Ce, Yb and Eu may be interpreted as enrichment of the most volatile REEs. This also implies that these inclusions fromed in a relatively oxidizing condition.

At present, we have not yet observed clear correlation between REE patterns and bulk chemical composition or texture of the refractory inclusions in Ningqiang meteorite, probably due to limited number of analyses. We will carry out more analyses to better understanding condensation conditions as well as later alteration processes (e.g. melting) of CAIs.

**References:** [1] Lin Y. and Kimura M. (2003) *Geochim. Cosmichim. Acta 67,* 2251-2267. [2] Fahey A. (1988) *PhD Thesis, Washington University.* [3] Boynton W. V. (1983) *Rare Earth Element Geochemistry. Developments in Geochemistry, 2ed.* 63-114. [4] Tanaka T. and Masuda A. (1973) *Icarus* 19, 523-530.

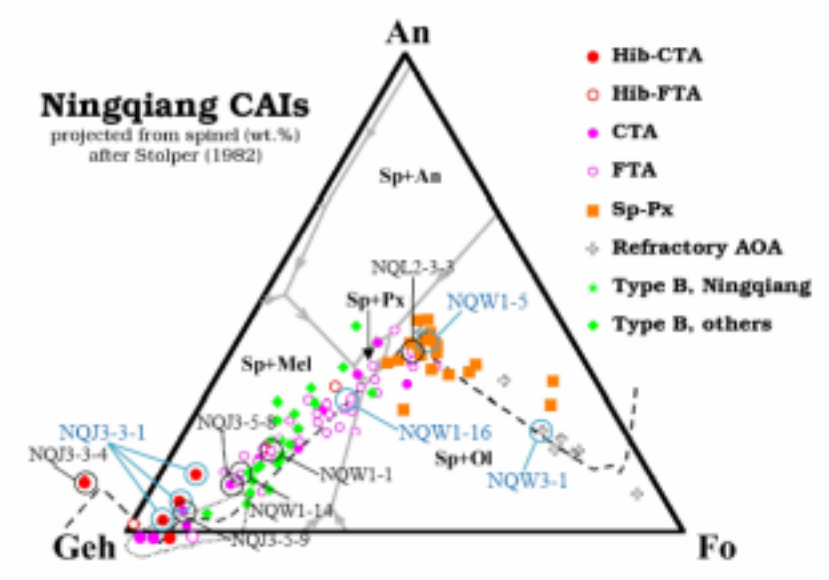


**Figure 1:** Bulk chemical compositions of the Ningqiang CAIs projected from spinel onto anorthite-gehlenite-forsterite ternary plane [1].

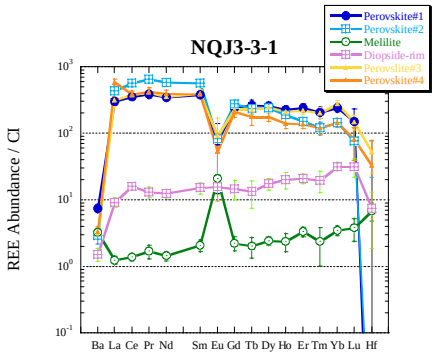


**Figure 2:** REE patterns of different phases in a hibonite-bearing CTA, NQJ3-3-1.4.

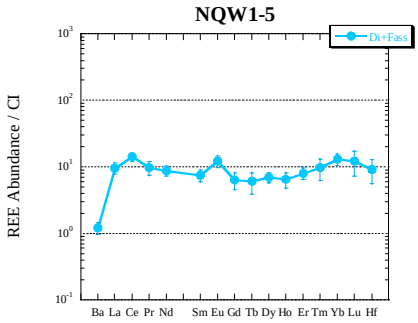


**Figure 4:** REE pattern of a spinel-pyroxene rich inclusion, NQW1-5.

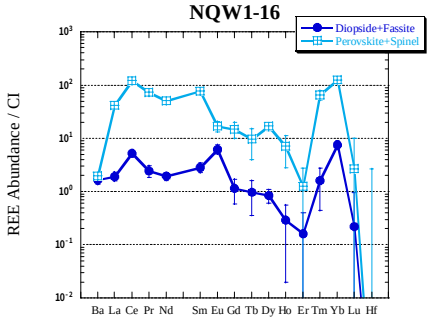


**Figure 3:** REE patterns of two analysis spots in a hibonite-free FTA, NQW1-16.

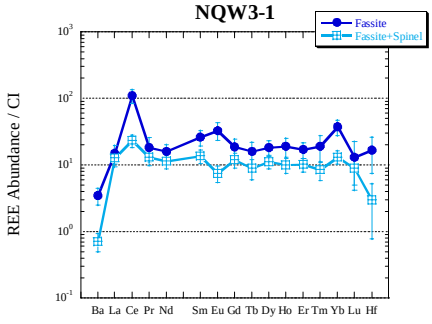


**Figure 5:** REE patterns of two analysis spots in a AOA, NQW3-1.

**FROM DUST TO PLANETS: THE TALE TOLD BY MODERATELY VOLATILE ELEMENT DEPLETION (*MOVED*).** Qing-zhu Yin, Department of Geology, University of California at Davis, One Shields Avenue, Davis, CA 95616, USA. yin@geology.ucdavis.edu

**Introduction:** The pronounced depletion of *m*oderately *v*olatile *e*lements (MOVE, that condense or evaporate at temperatures in the range 1350-650K) relative to the average solar composition is a characteristic feature in most primitive chondrites and bulk terrestrial planets (Fig. 1a). It differs from the composition of the Sun and from the materials further away from the Sun (CI chondrites). None of the remaining planets or even meteorites shows an enrichment of volatile elements that would balance the depletion in the inner Solar System. Whether this depletion occurred in solar nebular stage or in planetary formation stage has been the subject of long lasting debate. The search for "mysterite" initiated in 1973 [1] continues today "in search of lost planets"[2]. Here I show that the MOVED patterns demonstrate a clear connection between the rocky materials of the inner solar system and the interstellar dust. The inheritance of interstellar materials by the solar system is not only documented by the presence of presolar grains, various isotopic anomalies, but also expressed in the chemical element distribution in the inner solar system.

**Data:** The most widely used method in astronomy to study the chemical composition of interstellar dust grains has been to determine the gas-phase elemental abundances from the elemental absorption-line in the line of sight of stars, adopt a reference cosmic composition for the interstellar medium (ISM), which normally uses average solar composition, and then assume that what is depleted from the gas must be in the dust. The method covers a wide range of elements, including refractory and volatile elements, and it refers to the bulk composition of the grains rather than just the surface composition [3]. The absorption lines of most atoms and molecules found in the ISM occur at ultraviolet (UV) wavelengths, which requires their detection above the Earth's atmosphere. The Goddard High-Resolution Spectrograph (GHRS) aboard the *Hubble Space Telescope* (HST) has yielded the most precise abundance results for a range of interstellar environments, including gases in the local medium, in the warm neutral medium, in cold diffuse clouds, and in distant halo clouds. Plotted in Fig. 1b are three examples of such data [4.5]. Analyses of other diffuse-cloud lines of sight have shown that the pattern of depletion is nearly invariant from cloud to cloud.

When compared to meteoritic data in Fig 1a, the most obvious and striking feature is that the interstellar gas abundance is complemented by the meteorite data. Note that the complementarity of the MOVE seen in Fig. 1 is independent of condensation temperature. Complementarity holds even if elements are arranged in random order. Fig. 2 shows the ISM gas is anti-correlated with the primitive meteorite composition, independent of condensation temperature. Dust composition is calculated using $(X/H)_{dust}=(X/H)_{solar}-(X/H)_{gas}$, which is positively correlated with meteorite composition for MOVE (Fig. 3).

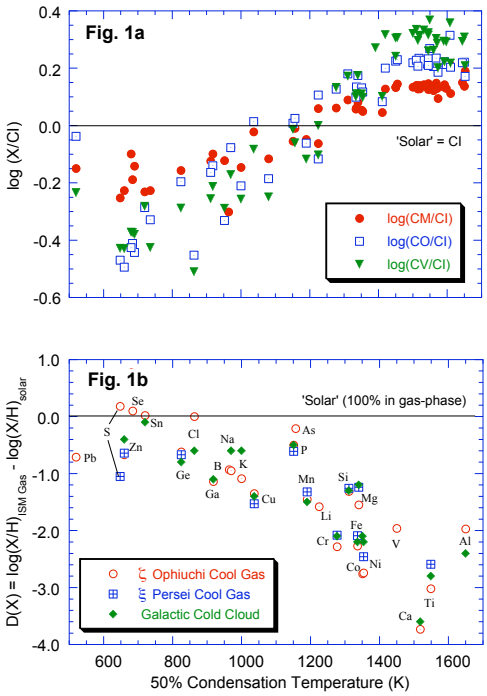


Fig. 1 (a) Elemental abundance data of primitive meteorites normalized to CI versus their 50% condensation temperature [6,7]. Only three carbonaceous chondrite groups are plotted for illustration purpose. The patterns for other groups of primitive chondrites and bulk terrestrial planets compositions are broadly similar. (b) Interstellar gas phase abundances relative to solar (CI) abundances vs. condensation temperature in Fig. 1b. The data sources are [4,5]. For MOVE, interstellar gas phase data is mirror imaged by the meteorite data

It is apparent from Fig. 1a and 1b that some of the MOVE (500-1100K) are depleted in both chondrites ($\log(X/CI)<0$) as well as in the interstellar gas ($D(X)<0$]). This is also shown in Fig. 2 where the negative correlation between the ISM gas and the meteorite composition passes below zero, which represents the solar composition. This may be due to the fact that we used our Sun (=CI) as representative of "cosmic" abundance. There is growing evidence that our Sun is overabundant in most heavy elements by a factor of 1.6 compared to other representative stars in our Galactic neighborhood [3]. If the new standard reference value is adjusted to 0.6 solar level, elements with condensation temperatures between 500-1000K will not show significant depletion in

both carbonaceous chondrites as well as in interstellar gas.

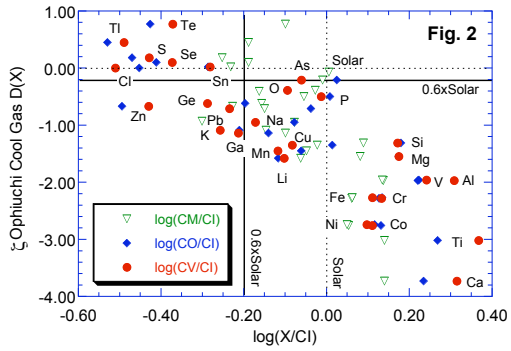


Fig. 2. For moderately volatile elements, the primitive meteorite composition (CM, CO, and CV groups are used as an example) is anti-correlated with the interstellar gas composition (ζ Ophiuchi Cool Gas is shown as an example).

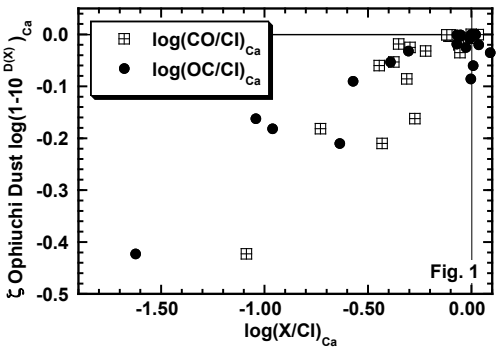


Fig. 3 ISM dust composition that is positively correlated with that of primitive meteorites for moderately volatile elements (CO and ordinary chondrite, OC, are used as examples). Dust composition is calculated from the observed ISM gas composition. ζ Ophiuchi Cool Gas is used as an example. Both data sets are normalized to CI and Ca.

**Discussions:** The solar nebula was formed by the collapse of rotating interstellar matter (gas and dust). The complementarity in Fig. 1 and the correlations in Fig. 2 and 3 lend themselves to a simple hypothesis that the fine dust from the ISM, *in cosmic proportion to gas*, makes up canonical solar composition in samples as large as the Sun and as small as the CI meteorite hand specimen. On the other hand, most rocky bodies of the inner solar system (between 0.38-5.2 AU) inherited the dust composition of ISM through coagulation, thermal annealing, and accretion of dust grains of interstellar origin which accumulated into bodies large enough (diameter>1km) to de-couple from the gas (without coalescing into the star) eventually evolving into planetesimals and planets. Evidences are mounting that the rapid grain growth occurs both during the molecular cloud stage as well as the solar nebula stage (e.g. [8, 9]). This implies reduced surface area and removing them from contact with the full volatile complements in the gas phase, increasing the possibilities to preserve the ISM chemistry in the dust aggregates.

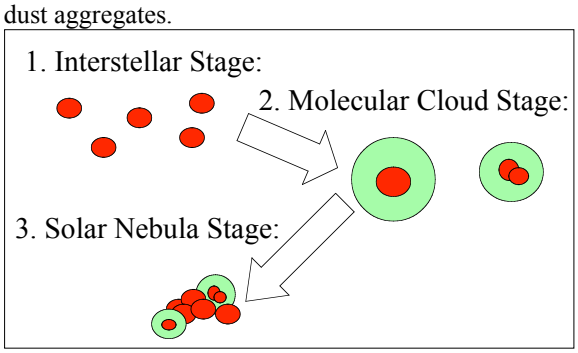


Fig. 4. The schematics of the inheritance model. (1) In the interstellar stage, the volatile elements are in hot ionized gas phase (not shown), while the refractory elements are locked in the dust grains (red); (2) In the cold and dense molecular cloud stage, the gas phase consists of H and He only. Organic-rich icy mantle (green) condenses with all the volatile elements on to the refractory core (red); (3) In the solar nebula stage, adiabatic compression or passage through a shock wave takes off the icy mantle. It is shown that the silicate core survives the entry into the solar nebula while the icy mantle with organics and other volatiles is largely destroyed [10], consistent with the primary mineralogy of chondrites being anhydrous. Progressive accretion of primary solids (ISM dust grains) as well as secondary solids (further processing of the primary solids within solar nebula, such as molten chondrules, condensates, evaporation residue, etc) lead all the way to planetesimals and planets. Proportion of green and red in stage 3 reflects the degree of moderately volatile element deletion. The model *does not* argue for massive survival of physical identities of presolar grains, but instead argue for discernible chemical links between the ISM dust and primitive chondrites (and terrestrial planets).

**Acknowledgments:** Supported by NASA's Cosmochemistry and Origin of Solar System programs. Scholarly discussions with Al Cameron are sincerely acknowledged.

**References:** [1] Higuchi H. et al. (1977) *GCA, 41,* 843-852. [2] Halliday A. and Porcelli D. (2001) *EPSL, 192,* 545-559. [3] Snow P.T. (2000) *JGR, 105,* 10239-10248. [4] Savage B. and Sembach K.R. (1996) *Annu. Rev. Astron. Astrophys. 34*, 279-329. [5] Welty D.E. et al. *ApJ Supp. 124*, 465-501. [6] Wasson J.T. and Kallemeyn G.W. (1988) *Phil. Trans. R. Soc. Lond. A325*, 535-544. [7] Wasson J.T. (1985) *Meteorites: their record of early solar system history* (W.H. Freeman & Co. NY). [8] Throop J. B. et al. (2001) *Science*, 292, 1686-1689. [9] Blum J. et al. (2002) *Adv. Space Rev.* 29, 497-503. [10] Cassen P. & Chick K. M. (1997) in *AIP Conf. Proceedings 402* (eds. Bernatowicz T. J. and Zinner E.), 697-719.

**OXYGEN ISOTOPIC DISTRIBUTIONS AMONG CHONDRULES IN ACFER 214, CH CHONDRITE.** M. Yoshitake and H. Yurimoto, Department of Earth and Planetary sciences, Tokyo Institute of Technology (2-12-1, Ookayama, Meguro, Tokyo 152-8551, Japan. E-mail: miwa@geo.titech.ac.jp; yuri@geo.titech.ac.jp).

**Introduction:** Chondrules are major constituents of chondrites. Among carbonaceous chondrites the O isotopic distributions of chondrules well have been studied for Allende CV3 meteorite. The O isotopic distributions of Allende chondrules are about from –10 to 4‰ ($\delta^{18}O$) along CCAM line (e.g., [2, 3]). The distribution suggests that O isotopes exchange between a $^{16}O$-rich solid precursor and a $^{16}O$-poor nebular gas during chondrule formation (e.g., [2, 4]). The range and frequency of the distribution reflect the degree of equilibrium of the exchange or O isotopic composition of nebula gas at chondrule fraction.

Recently a chondrule having extreme $^{16}O$-rich composition ($\delta^{18,17}O$ = –75‰) was found the CH chondrite, Acfer 214 [5]. Therefore it is expected O isotopic distribution of CH chondrules is wider than that of Allende chondrules.

In this study, we compared O isotopic compositions among chondrules in CH chondrite with CV chondrite, Allende meteorite.

**Analytical Techniques:** O isotopic compositions of 153 chondrules in a thin section of the Acfer 214 CH carbonaceous chondrite were determined by secondary ion mass spectrometry (SIMS). Before the O isotope measurements the mineralogy and petrology were studied by scanning electron microscope (JEOL JSM-5310LV) equipped with energy dispersive X-ray spectrometer (Oxford LINK ISIS).

O isotopes were measured *in situ* using multi-collection mode of the TiTech CAMECA IMS-1270. A $Cs^+$ primary beam (20 keV, 0.2 - 0.5 n A) of 10 - 15 μm diameter was used. Both $^{16}O^-$ and $^{18}O^-$ were measured using off-axis Faraday cups at mass resolution power (MRP) ~ 2000, while $^{17}O^-$ was measured on the axial electron multiplier at MRP ~ 4500, sufficient to separate interfering $^{16}OH^-$. Measurements of background noises of Faraday cups were made and signals of $^{16}O^-$ and $^{18}O^-$ were corrected. In order to correct instrumental mass fractionation, one big chondrule in the thin section was used as a standard for other chondrule. The O isotopic composition of the standard chondrule ($\delta^{18,17}O$ = –1.0‰, 2.5‰ relative to SMOW) was determined using a San Carlos olivine standard. The reproducibility within one analysis sequence of the standard chondrule (1σ) were ~ 1.6‰ for $\delta^{17}O$ and ~ 1.9‰ for $\delta^{18}O$, while the internal precision ($1\sigma_{mean}$) for each spot were typically ~ 0.3‰ and ~ 0.5‰, respectively. The error of reproducibility within one analysis sequence is larger than he internal precision and probably mainly depends on variable surface condition of spot by spot and sensitivity change of electron multiplier through the analysis. The reproducibility among independent analysis sequences of the standard chondrule (1σ) of were ~ 1.5‰ for $\delta^{17}O$ and ~ 2.3‰ for $\delta^{18}O$. Therefore, we estimate that accuracy of the measurement were ~ 1.5‰ for $\delta^{17}O$ and ~ 2.0‰ for $\delta^{18}O$, respectively, in 1σ.

**Sample:** Acfer 214 is a CH carbonaceous chondrite and is paired as Acfer 182 and 207. The size distributions of the chondrules analyzed were about 30 - 200 μm in apparent diameter. The lower limit of the size distribution (30 μm) is controlled by the primary beam size (15 μm). Chondrule types of the 153 samples are porphyritic chondrule (PC) (51%), cryptocrystalline chondrule (CC) (33%), granular olivine pyroxene chondrule (GOP) (5%), radial pyroxene chondrule (RPC) (0.5%), barred olivine chondrule (BOC) (2%), and other types (8.5%). The abundance ratios among chondritic types is consistent to those reported by [6].

*PCs.* Most PCs over 120μm in diameter are fragmented. Therefore, average size is larger than 100 μm. This size distribution of PCs in Acfer 214 seems to be consistent with Acfer 182 [6]. The fragmentation indicates Acfer 214 is probably more brecciated than the case of Acfer 182. Type II (Fe-rich) PCs are rare (2 of 78 PCs).

*CCs.* The average size of CCs is about 80 μm. The sizes of CCs are smaller than PCs. This distribution is consistent with CCs in Acfer 182 [6].

*BOCs, RPS and GOPs.* All BOCs and RPC were fragmented. The sizes of GOPs are less than 100 μm.

The relative abundance between PCs and CCs are consistent with [6] in the smaller size than 200 μm.

**Results and discussion:** Fig. 1 shows O isotopic compositions of isotopically homogeneous 153 chondrules in Acfer 214. The chondrule having $\delta^{18,17}O = -70, -75‰$ is re-analysis of the same chondrule as a006 in [5]. We have not been uncovered other chondrules having such extremely anomalous oxygen isotopic composition. O isotopic compositions among chondrules in Acfer 214 are concentrated over the range from –2.5 to 15‰ ($\delta^{18}O$). Small amount of chondrules have the O isotopic compositions < –2.5‰ ($\delta^{18}O$). The light end of this range (–2.5‰) is consistent to the distribution of Allende chondrules but the heavy end (15‰) exceeds the distribution of Allende chondrules. This result is consistent that bulk oxygen composition of Acfer 182 (this is paired chondrite of Acfer 214; $\delta^{18,17}O$ = 5.47, 1.29) is heaver than that of Allende ($\delta^{18,17}O$ = 1.51, –2.73) [7]. The heavy end of O isotopic composition suggests that chondrules of CH chondrite formed in more $^{16}O$-depleted nebula gas than the case of Allende chondrule.

The O isotopic compositions of 4 CCs (8% of 51 CCs) and a PC (about 1% of 77 PCs) were distributed from –20 to –12‰ ($\delta^{18}O$). These 5 chondrules can be distinguished from the most chondrules by 2σ.

Fig. 2 is O isotopic compositions of 3 chondrules in Acfer 214. They have heterogeneous O isotopic compositions distinguishable by 2σ. The proportion of chondrule having heterogeneous O isotopic composition is about 2% (3 of 153). This result indicates that a few chondrules have heterogeneous O isotopic composition.

The distribution of O isotopic compositions of CCs expands around –20‰ ($\delta^{18}O$). CCs experienced very high temperature and complete melting on dynamic crystallization model [8]. These matter indicate that the precursors of CCs in Acfer 214 had more $^{16}O$-rich compositions than –20‰ ($\delta^{18}O$).

The distributions among CH chondrules have more variation than Allende chondrule. In other words, CH chondrite contains chondrules having various O isotopic compositions. They might form in various O isotopic compositions environments.

**References:** [1] Clayton R. N. et al., (1983) In *Chondrules and their Origins* (ed. E. A. King) Lunar Planet. Inst., pp. 37-43. [2] Clayton R. N. (1993) *Annu. Rev. Earth Planet. Sci., 21,* 115-149. [3] Hiyagon H. (1997) *Antarct. Meteorite Res., 10,* 249-274. [4] McSween H. Y. Jr. (1985) *Meteoritics, 20,* 523-539. [5] Kobayashi S. et al., (2003) *Geochem. J., 37,* 663-669. [6] Bischoff A. et al., (1993) *Geochim. Cosmochim. Acta 57,* 2631-2648. [7] Clayton R. N. and Mayeda, T. K. (1999) *Geochim. Cosmochim. Acta 63,* 2089-2104. [8] Lofgren G. E. (1996) In *Chondrules and the Protoplanetary Disk* (eds. R. H. Jones and E. R. D. Scott) Cambridge Univ. Press, Cambridge. pp. 187-196.

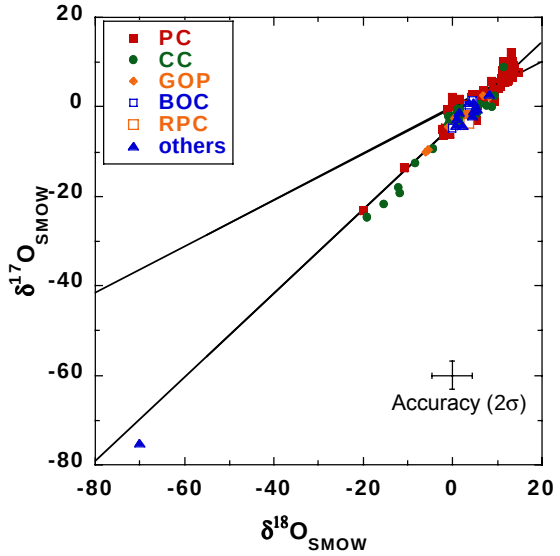


Fig. 1. O isotopic compositions of 150 individual chondrules in the Acfer 214. PC: porphyritic chondrule, BOC: Barred olivine chondrule, RPC: radial pyroxene chondrule, CC: cryptocrystalline chondrule, GOP: Granular olivine pyroxene chondrule, and other types chondrule. Typical accuracy (2σ) is calculated by repeated analyses of the standard chondrule.

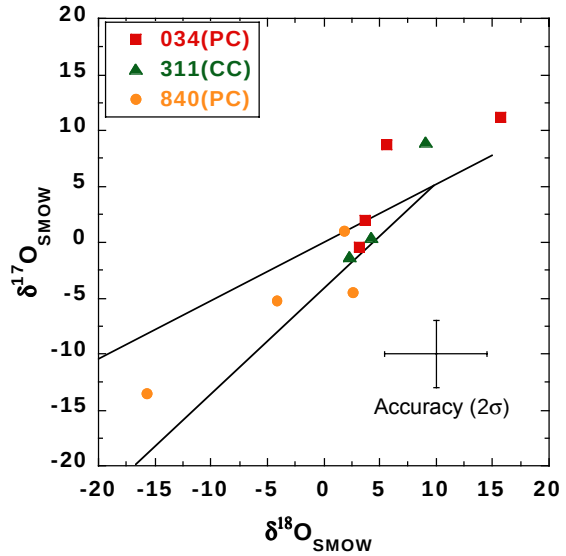


Fig. 2. O isotopic compositions of chondrules having isotopic heterogeneity in the Acfer 214. Each symbol corresponds to individual chondrules. Abbreviations are the same as Fig. 1.

**MOLECULAR CLOUD ORIGIN FOR THE OXYGEN ISOTOPE HETEROGENEITY IN THE SOLAR SYSTEM.** H. Yurimoto[1] and K. Kuramoto[2], [1]Department of Earth and Planetary Sciences, Tokyo Institute of Technology, Meguro, Tokyo 152-8551 Japan (yuri@geo.titech.ac.jp), [2]Division of Earth and Planetary Sciences, Hokkaido University, Sapporo, Hokkaido 060-0810 Japan.

**Introduction:** Oxygen is the most abundant element in the solid phases that formed early in the solar system and has three stable isotopes of mass numbers 16, 17 and 18. On a three-oxygen isotope diagram, $^{18}O/^{16}O$ and $^{17}O/^{16}O$ abundance ratios of most terrestrial material constitute a line with slope of ~1/2, called the terrestrial fractionation (TF) line. This slope is due to the isotope fractionation processes dependent on the mass difference between each pair of isotopes. In contrast, most meteorites have oxygen isotopic compositions diverging from the TF line [1]. Refractory inclusions and some chondrules in primitive meteorites have the most $^{16}O$-enriched isotope compositions shifted from TF line with magnitudes of several percent in $^{17 \text{ and } 18}O/^{16}O$ ratios. Non-radiogenic effects in the other major elements (e.g., Mg, Si) in these meteorite components have isotope compositions close to the terrestrial compositions, and their small deviations can be explained by the isotope fractionation due to thermal processes, e.g. evaporation, condensation, aqueous alteration, and low temperature chemical reaction.

The origin of mass independent fractionation of oxygen isotopes and the lack of such fractionation in other major elements in meteorites remain poorly understood. It cannot be due to nucleosynthetic processes or nuclear reactions involving energetic particles from the sun or from galactic cosmic rays because these processes would also change the isotopic compositions of the other elements. In addition, presolar grains enriched in $^{16}O$ are rare in meteorites. Although some types of gas molecule reactions have been found to induce such mass independent isotope fractionation in oxygen, they are observed among gas species (e.g., $O_3$, $O_2$, $CO_2$) which are minor in the solar nebula. Furthermore, even if such fractionation occurs, no plausible mechanism has been proposed for trapping the fractionated products into chondrite components. Oxygen isotope effects due to selective ultraviolet (UV) dissociation of molecules in the solar nebula gas has been proposed, however a mechanism for transferring these effects to the chondritic components has not been identified.

**Self-shielding in molecular cloud:** Recently, variations in $C^{16}O/C^{18}O$ ratio have been directly observed in diffuse molecular clouds. These variations are explained by selective predissociation of $C^{18}O$ by UV radiation. In the environment of molecular clouds, predissociation due to line spectrum absorptions of UV photons is the dominant mechanism for photodissociation of CO. UV intensity at the wavelengths of dissociation lines for abundant $C^{16}O$ rapidly attenuates in the surface layer of molecular cloud because of its UV self-shielding. For less abundant $C^{17}O$ and $C^{18}O$, which have shifted absorption lines due to difference in vibrational-rotational energy levels, the attenuation is much slower. As a result, $C^{17}O$ and $C^{18}O$ are dissociated by UV photons even in a deep molecular cloud interior. This process results in selective enrichment of CO in $^{16}O$ and enrichment of atomic oxygen in $^{17}O$ and $^{18}O$.

Because CO and atomic oxygen are the dominant oxygen-bearing gas species in molecular clouds, their isotopic fractionation may propagate to other oxygen-bearing species. Water ice is the dominant oxygen-bearing species among ices in molecular clouds, where it nucleates and grows on silicate dust grains by surface hydrogenation reactions between atomic oxygen and hydrogen. Therefore, oxygen isotope compositions of $H_2O$ ice should be close to those of gaseous atomic oxygen enriched in $^{17}O$ and $^{18}O$. Water ice is observed in molecular clouds of total visual extinctions $A_V$ >3.2 mag; its abundance increases with the $A_V$ value. As a molecular cloud becomes dense, most of the atomic oxygen reacts to form $H_2O$ ice, and CO becomes the most dominant gas species within $10^5$ years. Thus oxygen isotope composition of gas in dense molecular cloud becomes enriched in $^{16}O$ with time.

Low-mass (<2$M_\odot$) stars form by collapse of individual cores or clumps in a cold, dark molecular cloud with densities $n_{H2}=10^4$-$10^5$ cm$^{-3}$, $A_V$= 5-25 mag, and temperatures as low as ~10 K. According to the model simulating photochemical isotope fractionation in a molecular cloud, under these typical cloud parameters, the isotopic compositions of ice and gas are expected to be in the ranges $\delta^{18}O_{MC}$ = +100 to +250‰ and $\delta^{18}O_{MC}$ = -60 to -400‰, respectively, where $\delta^{18}O_{MC} \equiv [\{(^{18}O/^{16}O)/(^{18}O/^{16}O)_{MC}\} - 1] \times 1000$; $(^{18}O/^{16}O)$ and $(^{18}O/^{16}O)_{MC}$ are the isotope abundance ratios of corresponding chemical species and bulk molecular cloud, respectively. The degrees of fractionation for calculated $^{18}O/^{16}O$ ratios are consistent with astronomical observations. Although the lack of laboratory experimental data for $C^{17}O$ predissociation prevents us from a detailed analysis of $^{17}O/^{16}O$ fractionation, its degree is likely near that for $^{18}O/^{16}O$ because the absorption lines of these minor isotope species are unsaturated at least over

several tens of $A_V$. Such expected similarity has been recently observed for diffuse interstellar gas.

In denser and more evolved cold molecular cloud cores, most CO may become frozen onto dust grains. Because of the low temperature, oxygen isotope exchange between CO and $H_2O$ ices is inefficient and the original isotope fractionation of oxygen is preserved in each phases. Transient external heating by shock waves or by other mechanisms would cause vaporization of both $H_2O$ and CO ices and a local homogenization in such cloud. However, as long as $H_2O$ and CO molecules do not decompose into radicals and atoms, the oxygen isotope fractionation in each molecule is probably preserved.

**Link to meteorites:** Here we examine how such isotopic heterogeneity in a molecular cloud may cause the variations of oxygen isotope compositions observed in our solar system. Taking relative oxygen abundances of silicates, ice, and gas to be 1 : 2 : 3 in molecular clouds, we assume that $\delta^{17\text{ and }18}O_{MC}$ = 0‰ for silicates, +120‰ for ice, and –80‰ for gas. The $\delta^{17\text{ and }18}O_{MC}$ values for $H_2O$ ice and CO gas are chosen to be within the simulated ranges and to conserve the mean isotope composition of the bulk molecular cloud. The $^{16}O$-depleted nature of ice relative to silicates is consistent with the evidence that the most $^{16}O$-depleted known component formed in the solar system is the product of aqueous alteration of Fe,Ni-metal by $H_2O$ in the most primitive (LL3.0) ordinary chondrite Semarkona.

A protoplanetary disk is formed by collapse of a molecular cloud core. In the outer region of the disk, because of low temperatures, the primordial oxygen isotope compositions of the molecular cloud components are preserved. CO sublimes while preserving its own oxygen isotope composition outside the orbits of outer planets even in the case of frozen CO. In the inner region of the disk, $H_2O$ ice evaporates. During an early stage of disk evolution accompanied by vigorous gas accretion, gas-dust fractionation is probably minor, and the mean oxygen isotope composition of the inner disk gas is reset to the value of the bulk molecular cloud $\delta^{17\text{ and }18}O_{MC}$ =0‰. Because transient heating events, such as formation of refractory inclusions and chondrules, were common in the inner solar nebula, the silicate grains would equilibrate with such gas and have similar oxygen isotope compositions.

As the gas accretion rate decreases, dust-gas fractionation processes begin to proceed in the disk. One such fractionation process is the dust sedimentation toward the disk midplane. In addition, dust particles may preferentially migrate toward the central star and ice in the dust evaporates after passing the snowline releasing $^{16}O$-depleted water vapor into the inner disk gas. This increases the mean $\delta^{17\text{ and }18}O_{MC}$ of disk gas along the mixing line between oxygen isotope composition of CO and that of $H_2O$ ice, correlating with the degree of $H_2O$ enrichment relative to $H_2O$/CO ratio in the parent molecular cloud. Although enrichment of $H_2O$ by a factor of ten is justified in the solar nebula, even moderate enrichment can produce significant $^{17\text{ and }18}O$-enrichment of the disk gas. For example, if 3 times $H_2O$ enrichment (i.e., relative oxygen abundances of ice:gas = 2:1) occurs, the mean $\delta^{17\text{ and }18}O_{MC}$ of the inner disk gas are calculated to be about +50‰. Therefore, oxygen isotope compositions of the disk gas are expected to have been changed easily by dust-gas fractionation processes. Silicate grains equilibrated with such $H_2O$ enriched gas during transient heating events would acquire isotope compositions with high $\delta^{17\text{ and }18}O_{MC}$ values.

The proposed scenario [2] can reproduce oxygen isotope heterogeneity in the inner solar nebula with an $^{17}O$- and $^{18}O$-enriched gas, i.e., $^{16}O$-depleted gas, relative to silicate dust, consistent with the conventional O isotope reservoirs inferred from meteorite studies. Under such an environment, the silicate dust evolves into an $^{16}O$-depleted composition through isotope exchange with the surrounding gas due to transient heating events in the nebula. Therefore, the average O isotope composition of the solar nebula normalized to the standard mean ocean water (SMOW) may be $\delta^{17,18}O_{SMOW} \cong -50$‰ or smaller.

We showed that even small mass fractionation for CO and atomic O in the molecular cloud, can explain the formation of $^{16}O$-rich/poor reservoirs observed for the solar nebula. The explanation becomes easier if we use larger mass fractionation factors as expected by chemical models and observations of molecular clouds. Thus, the $^{16}O$ isotope variations may not be unique to our solar system but ubiquitous in any planetary system. A direct test of this scenario is to measure the O isotope compositions of cometary ices and that of solar wind. We predict the O isotope values as $\delta^{17,18}O_{SMOW} \cong +50$ to +200‰, -100 to -450‰, and -50‰ for cometary $H_2O$, cometary CO and solar wind, respectively.

**References:** [1] R. N. Clayton, *Annu. Rev. Earth Planet. Sci.* **21**, 115 (1993), [2] H. Yurimoto & K. Kuramoto, *Science*, in press (2004) and references given therein.